



INSTITUTO  
DE DISEÑO Y  
FABRICACIÓN



UNIVERSITAT  
POLITÈCNICA  
DE VALÈNCIA

**DOCTORAL THESIS**

**Different approaches for improving  
the Stability of Hybrid Perovskites**

**Ph.D Candidate**

Júlia Marí Guaita

**Supervisors**

Dr. Bernabé Marí Soucase

Dr. Amal Bouich

València, December 2022



*Know, first, who you are, and then adorn yourself accordingly - **Epictetus***



En primer lugar, me gustaría agradecer a la Universitat Politècnica de València, y en especial a mi padre y mentor, Dr. Bernabé Marí Soucase, por darme la oportunidad de desarrollar este grato trabajo de investigación. A continuación, me gustaría agradecer a todas las personas que han hecho posible que mi labor como doctoranda resulte exitosa y satisfactoria;

Doy las gracias a todo mi equipo de trabajo por el apoyo y la colaboración en la investigación desarrollada. Entre ellos, se encuentra mi mentora y amiga, la doctora Amal Bouich, que ha hecho lo posible por allanar este tedioso camino de la disertación doctoral y me ha apoyado día tras días, tanto en lo personal como en lo académico.

También agradezco a todos los colaboradores del equipo de trabajo, que desde el lugar donde se encuentran y a pesar de las dificultades, han hecho un gran esfuerzo por mejorar mi trabajo y el de mi departamento, ayudándome a comprender la importancia de colaborar y compartir en la ciencia.

Además, me gustaría dar las gracias a mi madre Inmaculada, por su constante apoyo y persistencia haciéndome entender que el trabajo duro da sus frutos. A mi pareja Rubén, por hacerme crecer, enseñarme a saber valorar las oportunidades y a ver las cosas siempre desde el lado bueno.

Por último, doy las gracias a toda mi familia, amigos, y a todos aquellos que posiblemente sin saberlo, me han proporcionado inspiración y motivación para tener la disciplina y la constancia de trabajar día tras día por esto, a pesar de todos los obstáculos presentes en el camino.



## TABLE OF CONTENTS

ABSTRACT.....	VII
RESUMEN .....	IX
RESUM.....	XIII
<b>CHAPTER 1: INTRODUCTION.....</b>	<b>1</b>
1.1 GLOBAL ENERGY DEMAND .....	1
1.2 WORKING PRINCIPLE OF SOLAR CELLS .....	3
1.3 DIFFERENT GENERATIONS OF SOLAR CELLS .....	7
<b>CHAPTER 2: MOTIVATION AND OBJECTIVES.....</b>	<b>11</b>
2.1 HYBRID ORGANIC-INORGANIC PEROVSKITE MATERIALS AND SOLAR CELLS.....	11
2.2 OBJECTIVES .....	14
2.3 MOTIVATION .....	14
2.4 THESIS STRUCTURE .....	15
<b>CHAPTER 3: STABILITY IMPROVEMENT OF METHYLAMMONIUM LEAD IODIDE PEROVSKITE THIN FILMS BY BISMUTH DOPING .....</b>	<b>19</b>
1. INTRODUCTION .....	19
2. EXPERIMENTAL PROCEDURE.....	21
3. RESULTS AND DISCUSSION.....	23
4. DEGRADATION STUDY.....	28
5. CONCLUSION .....	28
<b>CHAPTER 4: TETRABUTYLAMMONIUM (TBA)-DOPED METHYLAMMONIUM LEAD IODIDE: HIGH QUALITY AND STABLE PEROVSKITE THIN FILMS .....</b>	<b>33</b>
1. INTRODUCTION .....	33
2. MATERIALS AND EXPERIMENTAL PROCEDURE.....	34
3. CHARACTERIZATION TECHNIQUES.....	34
4. RESULTS AND DISCUSSION.....	35
5. OPTICAL AND PHOTOLUMINESCENCE STUDY .....	39
6. DEGRADATION STUDY .....	42
7. DEVICE SPIRO/MAPBI <sub>3</sub> /TiO <sub>2</sub> /F.T.O SIMULATION.....	44
8. CONCLUSION .....	45
<b>CHAPTER 5: MANUFACTURE OF HIGH-EFFICIENCY AND STABLE-LEAD FREE SOLAR CELLS THROUGH ANTISOLVENT QUENCHING ENGINEERING .....</b>	<b>51</b>
1. INTRODUCTION .....	52
2. EXPERIMENTAL PROCEDURE .....	52
3. RESULTS AND DISCUSSION.....	53
4. DEGRADATION STUDY .....	56
5. DEVICE PERFORMANCE.....	57
6. DEVICE MANUFACTURE SPIRO-OMeTAD/MASnI <sub>3</sub> /TiO <sub>2</sub> /FTO.....	61
7. CONCLUSION .....	63
<b>CHAPTER 6: INVESTIGATION ON THE STABILITY AND EFFICIENCY OF MAPBI<sub>3</sub> AND MASNI<sub>3</sub> THIN FILMS FOR SOLAR CELLS.....</b>	<b>69</b>
1. INTRODUCTION .....	69
2. PEROVSKITE MANUFACTURE .....	70
3. CHARACTERIZATION TECHNIQUES.....	71
4. RESULTS AND DISCUSSION.....	71

5. DEGRADATION STUDY .....	75
6. DEVICE MANUFACTURE AND NUMERICAL SIMULATION .....	77
7. CONCLUSION .....	79
<b>CHAPTER 7: CONCLUSION.....</b>	<b>85</b>
GENERAL CONCLUSION .....	85
SUGGESTED FURTHER STUDIES.....	85
<b>ANNEX: DETAILED PUBLICATIONS AND CONFERENCES DURING PHD PERIOD.....</b>	<b>87</b>



## Abstract

Halide Organic-Inorganic Perovskites (HOIPs) are a solid family of materials that have been in the spotlight of the scientific community of solar photovoltaics due to their potential for building high-efficiency and low-cost solar cells. In recent years, they have experienced exponential growth in the efficiency obtained at lab conditions, going from 3% of PCE in 2009 to over 25% in 2021. But still, there are numerous challenges to overcome in these types of materials for solar cell applications, such as stability.

The purpose of this Doctoral Thesis is to study in deep different kinds of HOIPs for solar cell applications, including the optimization of the manufacturing process and the complete characterization of the films, such as X-ray-diffraction analysis, Field Emission Scanning Electron Microscopy analysis, Atomic Force Microscopy analysis, photoluminescence study, UV-visible absorption analysis, band-gap calculation, Transmittance electron microscopy, theoretical simulation with SCAPS-1D, and deep degradation study of the films. The objective of all this characterization analysis is supported to obtain proper crystallinity, morphology, topography, optical properties, PCE, and stability of the thin layers without increasing the manufacture of the devices.

Different strategies and techniques were used to fulfil the goal of the current work. Such strategies include doping with different compounds, antisolvent quenching engineering, and, changing the cation “B” in the general formula of perovskites;  $ABX_3$ , where A and B are two cations and X is the anion, frequently a halide (I, Br or Cl).

The focus of the present dissertation is the methylammonium lead iodide III ( $CH_3NH_3I_3$ ), which is known for exhibiting direct bandgap absorption from the top of the valence band to the bottom of the conduction band. The bandgap can be easily modified by varying A, B, and X and modulated by the suitable selection of mixed cations. Among the possible combinations, MA cation and metal  $Pb^{2+}$  have exhibited excellent optoelectronic properties, low-temperature solution-processable films, and potential for appropriate stability, due to very high charge-carrier mobility, large electron and hole diffusion length, large absorption coefficients, and low nonradiative recombination rates.

Specifically, four complete and published papers are shown in this book for furthering the aim of the PhD:

- Stability Improvement of Methylammonium Lead Iodide Perovskite Thin Films by Bismuth Doping
- Tetraabutylammonium (TBA)-Doped Methylammonium Lead Iodide: High Quality and Stable Perovskite Thin Films
- Manufacture of High-Efficiency and Stable Lead-Free Solar Cells through Antisolvent Quenching Engineering

- Investigation on the Stability and Efficiency of MAPbI<sub>3</sub> and MASnI<sub>3</sub> Thin Films for Solar Cells

The summary and general conclusions of the work are described in the following paragraphs.

Bismuth doping has improved the crystalline structure of the absorbent layer of MAPbI<sub>3</sub>, which leads to a significant improvement in the optoelectronic properties, the morphology of the surface of the layers, and even improves the stability of the devices. Bismuth doping was studied, introducing variable amounts of bismuth between 1 and 8% in the initial solution. The best results were obtained in the samples where 2% bismuth was introduced in the initial solution.

Doping with tetrabutylammonium (TBA) was also analysed by introducing different proportions of TBA in the initial mixture for the synthesis of MAPbI<sub>3</sub> layers. We observed that adding 5% TBA to the initial solution reduces the density of pinholes in the layers and improves crystallinity, which leads to a considerable improvement in the stability of the MAPbI<sub>3</sub> layers. With the optimal proportion of TBA, it is possible to increase the grain size and the intensity of the photoluminescence, basically due to the decrease in recombination centres. This set of property improvements achieved with TBA doping leads to increased device performance.

Since lead is a polluting element, we have made layers substituting Pb for Sn to obtain MASnI<sub>3</sub> layers. Substituting lead for tin increases grain size and has a positive effect on the light absorption coefficient. However, MASnI<sub>3</sub> shells are more unstable than MAPbI<sub>3</sub> shells and to overcome this problem different anti-solvents were used in the synthesis of MASnI<sub>3</sub> shells.

This approach is known as antisolvent engineering, and we have used it to improve MASnI<sub>3</sub> layers. Among the various antisolvents studied, toluene is the one that has managed to improve the stability of the MASnI<sub>3</sub> layers.

Using a numerical approach using SCAPS-1D, we have calculated that the efficiency of photovoltaic devices (PCE) based on MASnI<sub>3</sub> increases by 9.5% compared to devices based on MAPbI<sub>3</sub>.

## Resumen

Las perovskitas orgánicas-inorgánicas de haluros (HOIP) son una familia de materiales sólidos que están en el punto de mira de la comunidad científica debido a su potencial para producir células solares de alta eficiencia y bajo costo. En los últimos años han experimentado un crecimiento exponencial en la eficiencia obtenida en condiciones de laboratorio, pasando del 3% de PCE en 2009 a más del 25% en 2021. Pero aún quedan numerosos retos por superar en este tipo de materiales para aplicaciones en células solares, como son la estabilidad y durabilidad de los dispositivos.

El propósito de esta Tesis Doctoral es estudiar en profundidad diferentes tipos de HOIPs para aplicaciones de células solares, incluyendo la optimización del proceso de fabricación y la caracterización completa de las películas delgadas, tales como análisis de difracción de rayos X, análisis de microscopía electrónica de barrido de emisión de campo, análisis de microscopía de fuerza atómica, estudio de fotoluminiscencia, análisis de absorción de UV-visible, cálculo de banda prohibida, microscopía electrónica de transmitancia, simulación teórica con SCAPS-1D y estudio de la degradación de las películas. El objetivo de todo este análisis de caracterización se sustenta en obtener la adecuada cristalinidad, morfología, topografía, propiedades ópticas, eficiencia y estabilidad de las capas delgadas sin incrementar el coste de fabricación de los dispositivos.

Se utilizaron diferentes estrategias y técnicas para cumplir con los objetivos del presente trabajo. Dichas estrategias incluyen el dopaje con diferentes compuestos, la ingeniería de antisolventes y el cambio del catión "B" en la fórmula general de las perovskitas;  $ABX_3$ , donde A y B son los cationes y X es el anión, generalmente haluro (I, Br o Cl)

El enfoque de la presente disertación es el metilamonio de yoduro de plomo III (MAPI ó  $CH_3NH_3PbI_3$ ), que es conocido por exhibir un elevado coeficiente de absorción directa y una elevada longitud de difusión de los portadores de carga. La banda prohibida puede modificarse fácilmente variando los componentes A, B y X y modularse mediante la selección adecuada de haluros y cationes mixtos. Entre las posibles combinaciones, el catión MA y el metal  $Pb^{2+}$  han demostrado poseer excelentes propiedades optoelectrónicas, películas procesables en disoluciones a baja temperatura y potencial para una estabilidad adecuada debido a la muy alta movilidad del portador de carga, la gran longitud de difusión de electrones y huecos, a los altos coeficientes de absorción, la baja radiación no radiactiva y las altas tasas de recombinación.

Específicamente, en esta tesis se basa en cuatro artículos completos y ya publicados, cuyos títulos son:

- Stability Improvement of Methylammonium Lead Iodide Perovskite Thin Films by Bismuth Doping
- Tetrabutylammonium (TBA)-Doped Methylammonium Lead Iodide: High Quality and Stable Perovskite Thin Films
- Manufacture of High-Efficiency and Stable Lead-Free Solar Cells through Antisolvent Quenching Engineering
- Investigation on the Stability and Efficiency of MAPbI<sub>3</sub> and MASnI<sub>3</sub> Thin Films for Solar Cells

Las conclusiones generales de la investigación desarrollada en los trabajos mencionados han sido:

El dopado con bismuto ha permitido mejorar la estructura cristalina de la capa absorbente de MAPbI<sub>3</sub> lo cual lleva a una mejora importante de las propiedades optoelectrónicas, la morfología de la superficie de las capas e incluso se mejora la estabilidad de los dispositivos. Se estudió el dopado con bismuto, introduciendo cantidades variables de bismuto entre el 1 y 8% en la disolución inicial y los mejores resultados se obtuvieron en las muestras donde se introdujo un 2% de bismuto en la disolución inicial.

También se analizó el dopado con tetrabutylamonio (TBA) introduciendo distintas proporciones de TBA en la mezcla inicial para la síntesis de capas de MAPbI<sub>3</sub>. Observamos que añadiendo un 5% de TBA a la disolución inicial se consigue disminuir la densidad de ‘pinholes’ en las capas y se mejora la cristalinidad, lo que lleva a una mejora considerable de la estabilidad de las capas de MAPbI<sub>3</sub>. Con la proporción óptima de TBA, se logra incrementar el tamaño de grano y la intensidad de la fotoluminiscencia, básicamente debido a la disminución de centros de recombinación. Este conjunto de mejoras de las propiedades conseguidas con el dopado con TBA lleva a incrementar el rendimiento de los dispositivos.

Dado que el plomo es un elemento contaminante hemos realizado capas sustituyendo el Pb por Sn para obtener capas de MASnI<sub>3</sub>. La sustitución del plomo por estaño aumenta el tamaño de los granos y tiene un efecto positivo sobre el coeficiente de absorción de la luz. Sin embargo, las capas de MASnI<sub>3</sub> son más inestables que las de MAPbI<sub>3</sub> y para solucionar este problema se usaron diferentes antisolventes en la síntesis de las capas de MASnI<sub>3</sub>.

Esta aproximación se conoce como ingeniería de antisolventes y la hemos usado para mejorar las capas de MASnI<sub>3</sub>. Entre los varios antisolventes estudiados, el tolueno es el que ha conseguido mejorar la estabilidad de las capas de MASnI<sub>3</sub>.

Usando una aproximación numérica mediante el SCAPS-1D hemos calculado que la eficiencia de los dispositivos fotovoltaicos (PCE) basados en  $\text{MASnI}_3$  aumenta un 9,5% respecto a los dispositivos basados en  $\text{MAPbI}_3$ .



## Resum

Les perovskites orgàniques-inorgàniques d'halurs (HOIP) són una família sòlida de materials que han estat al punt de mira de la comunitat científica de l'energia solar fotovoltaica a causa del seu potencial per construir cèl·lules solars d'alta eficiència i de baix cost. En els darrers anys han experimentat un creixement exponencial en l'eficiència obtinguda en condicions de laboratori, passant del 3% de PCE el 2009 a més del 25% el 2021. Però encara queden nombrosos reptes per superar en aquest tipus de materials per a cèl·lules solars. aplicacions, com ara l'estabilitat.

El propòsit d'aquesta Tesi Doctoral és estudiar en profunditat diferents tipus de HOIPs per a aplicacions de cel·les solars, incloent-hi l'optimització del procés de fabricació i la caracterització completa de les pel·lícules, com ara anàlisi de difracció de raigs X, anàlisi de microscòpia electrònica d'escombrada d'emissió de camp, anàlisi atòmica Anàlisi de microscòpia de força, estudi de fotoluminescència, anàlisi d'absorció UV-visible, càlcul de banda prohibida, microscòpia electrònica de transmissió, simulació teòrica amb SCAPS-1D i estudi de degradació profunda de les pel·lícules. L'objectiu de tota aquesta anàlisi de caracterització se sustenta a obtenir la cristal·linitat adequada, morfologia, topografia, propietats òptiques, PCE i estabilitat de les capes primes sense incrementar la fabricació dels dispositius.

Es van fer servir diferents estratègies i tècniques per complir l'objectiu del present treball. Aquestes estratègies inclouen el dopatge amb diferents compostos, l'enginyeria d'extinció amb antisolvents i el canvi del catió "B" a la fórmula general de les perovskites;  $ABX_3$ , on A i B són dues cations i X és l'anió, sovint un halur (I, Br o Cl).

L'enfocament de la present dissertació és el iodur de plom III de metilamoni ( $CH_3NH_3I_3$ ), que és conegut per exhibir una absorció de banda prohibida directa des de la part superior de la banda de valència fins a la part inferior de la banda de conducció. La banda prohibida es pot modificar fàcilment variant A, B i X i modular-se mitjançant la selecció adequada de cations mixtes. Entre les possibles combinacions, el catió MA i el metall  $Pb^{2+}$  han exhibit excel·lents propietats optoelectròniques, pel·lícules processables en solució a baixa temperatura i potencial per a una estabilitat adequada, a causa de la molt alta mobilitat del portador de càrrega, gran longitud de difusió d'electrons i buits, grans coeficients d'absorció i baixa radiació no radioactiva taxes de recombinació.

Específicament, en aquest document es mostren quatre articles complets i publicats en els que està basat el treball desenvolupat en aquesta tesi.

- Stability Improvement of Methylammonium Lead Iodide Perovskite Thin Films by Bismuth Doping

- Tetrabutylammonium (TBA)-Doped Methylammonium Lead Iodide: High Quality and Stable Perovskite Thin Films
- Manufacture of High-Efficiency and Stable Lead-Free Solar Cells through Antisolvent Quenching Engineering
- Investigation on the Stability and Efficiency of MAPbI<sub>3</sub> and MASnI<sub>3</sub> Thin Films for Solar Cells

Les conclusions generals de la investigació duta a terme en esta tesi i en els treballs mencionats abans han sigut:

El dopat amb bismut ha permès millorar l'estructura cristal·lina de la capa absorbent de MAPbI<sub>3</sub>, produint una millora important de les propietats optoelectròniques, la morfologia de la superfície de les capes i fins i tot es millora l'estabilitat dels dispositius. Es va estudiar el dopat amb bismut, introduint quantitats variables de bismut entre l'1 i el 8% en la dissolució inicial. Els millors resultats es van obtenir a les mostres on es va introduir un 2% de bismut a la dissolució inicial.

També es va analitzar en dopat amb tetrabutylamoni (TBA) introduint diferents proporcions de TBA a la barreja inicial per a la síntesi de capes de MAPbI<sub>3</sub>. Observem que afegint un 5% de TBA a la dissolució inicial s'aconsegueix disminuir la densitat de pinholes a les capes i es millora la cristal·linitat, cosa que porta a una millora considerable de l'estabilitat de les capes de MAPbI<sub>3</sub>. Amb la proporció òptima de TBA, s'aconsegueix incrementar el tamany de gra i la intensitat de la fotoluminescència, bàsicament a causa de la disminució de centres de recombinació. Aquest conjunt de millores de les propietats aconseguides amb el dopatge amb TBA porta a incrementar el rendiment dels dispositius.

Atès que el plom és un element contaminant hem fet capes substituint el Pb per Sn per obtenir capes de MASnI<sub>3</sub>. La substitució del plom per estany augmenta el tamany dels grans i té un efecte positiu sobre el coeficient d'absorció de la llum. Tot i això, les capes de MASnI<sub>3</sub> són més inestables que les de MAPbI<sub>3</sub> i per solucionar aquest problema es van usar diferents antisolvents en la síntesi de les capes de MASnI<sub>3</sub>.

Aquesta aproximació es coneix com a enginyeria d'antisolvents i l'hem fet servir per millorar les capes de MASnI<sub>3</sub>. Entre els antisolvents estudiats, el toluè és el que ha aconseguit millorar l'estabilitat de les capes de MASnI<sub>3</sub>.

Usant una aproximació numèrica mitjançant el SCAPS-1D hem calculat que l'eficiència dels dispositius fotovoltaics (PCE) basats en MASnI<sub>3</sub> augmenta un 9,5% respecte dels dispositius basats en MAPbI<sub>3</sub>.



# Chapter 1: Introduction

## 1.1 Global energy demand

Global electricity demand is growing rapidly across the world, resulting in a maximum increase in history in absolute terms; 1414 TWh from 2020 to 2021 [1]. This growth has its main cause in the economic development of Asian countries, that are consequently, rapidly increasing their need for electricity. As a result, an environmental crisis is taking place in a World already undergoing a dreaded climate change. The result is that CO<sub>2</sub> emissions in energetic sector increased a 7% (778 million tonnes) in 2021, which means a new record in emissions from energy [2].

CO<sub>2</sub> and gas emissions to atmosphere are causing an increase in the temperature of the Earth (Figure 1), which is known as Global Warming. Global Warming has devastating consequences for life in planter Earth causing among others:

- Drought, that can harm food production and human health
- Flooding, that leads to disease spread and severe damages to ecosystems and infrastructure
- Snow is melting, causing survival difficulties for animals
- It is increasing the frequency of heavy precipitation events
- The sea levels are rising, which has many consequences such as destructive erosion, aquifer, and agricultural soil contamination, and lost habitat for animals

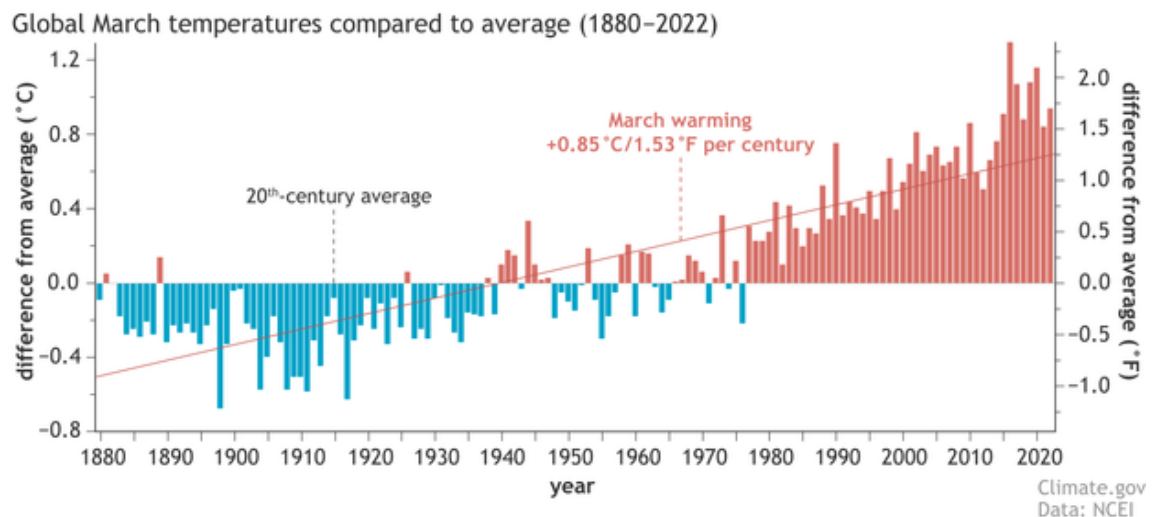
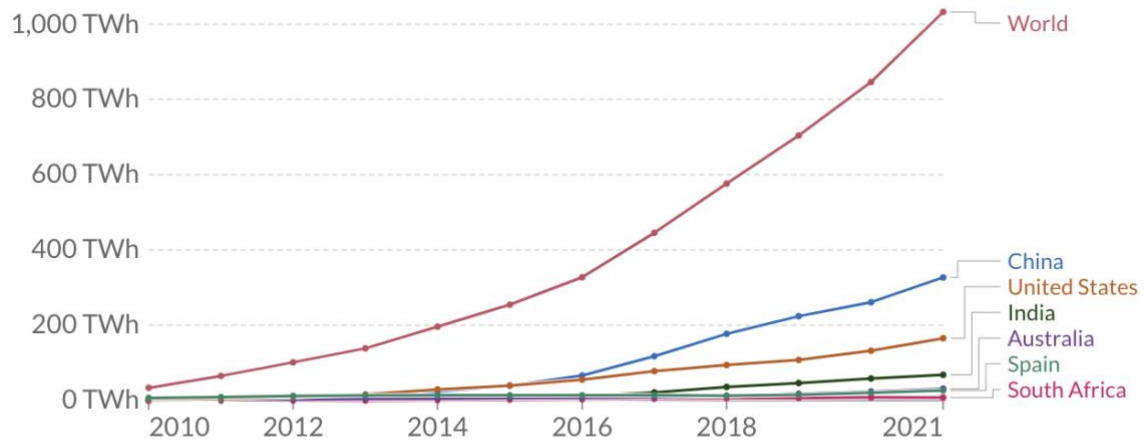


**Figure 1.** Global surface temperature compared to the 20<sup>th</sup>-century average each March from 1880 through 2022. Cooler-than-average Marches are coloured blue; warmer-than-average Marches are red. March temperatures have warmed by 1.53 degrees Fahrenheit (0.85 degrees Celsius) per century. The last time Earth had a cooler-than-average March was 1976 [3].

To overcome this exponential growth of emissions, the International Energy Agency has created a roadmap to achieve Net-Zero emissions by 2050, where the objective is to transform global energy consumption from using mostly fossil fuels to being predominated by renewable energy sources such as sun and wind, which together may contribute to the 50% of the transition for renewable energy supply [4].

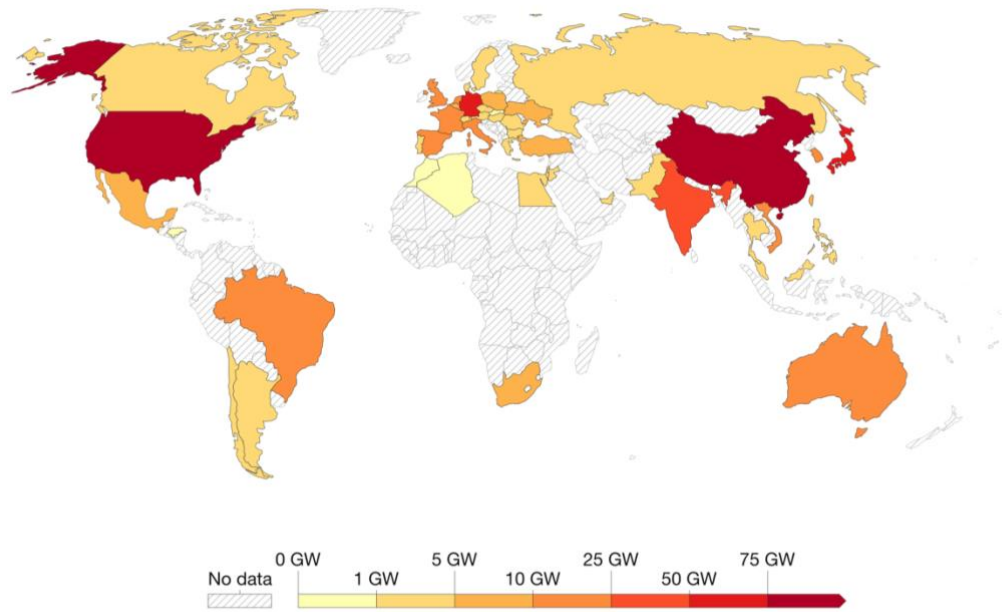
In the last decade, solar energy demand has increased exponentially worldwide (Figure 2), and the cost of PV installation has declined, which is a precursor for the proliferation of solar photovoltaics. Specifically, the price of installed solar has lowered 70%. This reduction is the aftermath of upgraded technology in solar cells and panel designs, the decline in manufacturing and production costs, diminished installation process, etc.



Source: Our World in Data based on BP Statistical Review of World Energy & Ember  
 OurWorldInData.org/renewable-energy • CC BY

**Figure 2.** Electricity generation from solar, measured in terawatt-hours (TWh) per year [5].

In 2021, solar power global installation broke the record for the 9th consecutive year with 168 GW of new solar photovoltaics, and in 2022 the increase is expected to continue and break the record again installing more than 200 GW.



Source: Statistical Review of World Energy - BP (2022)

OurWorldInData.org/renewable-energy • CC BY

**Figure 3.** Installed solar energy in 2021, measured in gigawatts (GW) [6].

Nowadays, we are all very aware of the power of solar energy. The compromise and commitment of governments that recognise the potential of the sun as an energy source makes solar the fastest growing renewable energy, being over the half of renewable capacity installed in the world in 2021, when Europe already reached the solar Terawatt age [7], China keeps the market leadership in 2021 with a 14% annual growth rate, Latin America experienced a promising growth in annual solar installations by 44%, and the US solar market installed a record of 23.6 GW of solar capacity [8].

### 1.2 Working principle of Solar Cells

A solar cell is a p-n junction diode constructed slightly different from a conventional junction diode. Solar cells are made by specific semiconducting materials which have certain properties for the proper conversion of electricity from solar radiation. The schematic device of a solar cell is shown in Figure 4.

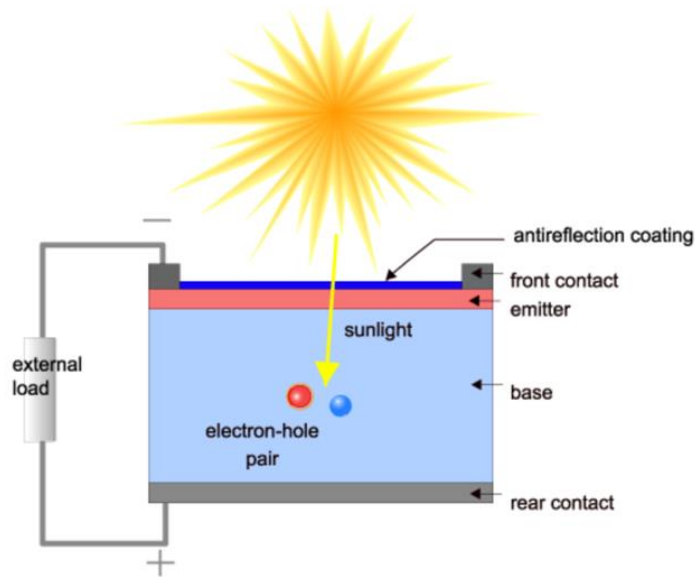


**Figure 4.** Schematic of p-n junction of a solar cell [9].

The structure of the solar cell consists of three parts:

- a) Absorption of photons
- b) Separation of charge carriers
- c) Collection of carriers across the electrode

When light reaches the p-n junction (absorbing material), the light photons enter the junction through the p-type layer generating the electron and hole pair inside the device. The absorption of energy photons depends on the bandgap of the absorbing material. The diffusion of charge carriers makes the donor ions and acceptor ions present in the junction of the solar cell, building an electric field inside the depletion layer. Due to this electric field, it is created a drift current, and the electrons are forced to move in the n-type region and holes to the p-type region. Then, the charge carriers will be collected towards the electrode as it is seen in Figure 5.

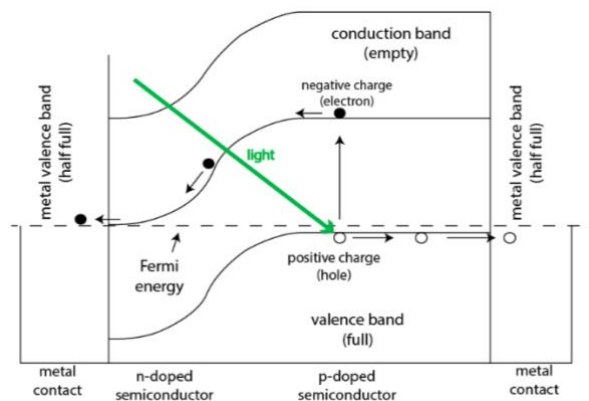


**Figure 5.** Band diagram of p-n junction in a standard solar cell [10].

## Fundamental Parameters of Solar Cells

The fundamental parameters associated with the solar cell are critical for the efficiency of solar cell. These parameters are described below:

### *Open circuit voltage*

The open-circuit voltage,  $V_{oc}$ , is the maximum voltage available from a solar cell, and occurs at zero current. The  $V_{oc}$  can be determined from the I-V graph of the solar cell (Figure 6), being the intercept of the I-V curve at the voltage axis. The equation for  $V_{oc}$  is found by setting the net current equal to zero (Equation 1):

$$V_{oc} = \frac{KT}{q} \ln \left( \frac{I_L}{I_0} + 1 \right)$$

*Equation 1*

Equation 1 shows that  $V_{oc}$  depends on the current measured in light condition,  $I_L$ , and on the dark reverse current,  $I_0$ , which depends on the recombination in the solar cell.

### *Short circuit current ( $I_{sc}$ )*

The short-circuit current,  $I_{sc}$ , is defined as the maximum current that flows when the voltage across the device is zero (Figure 5). The short circuit current density depends on the photon flux incident on the solar cell, on the area of the solar cell, the optical properties of the solar cell, and on the minority-carrier collection probability.

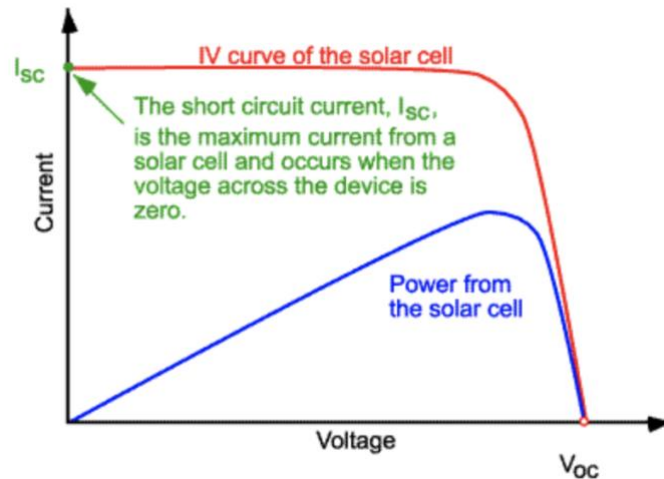


**Figure 6.** I-V curve of a solar cell showing the short-circuit current [11].

### Fill Factor (FF)

The fill factor defines the ratio between the maximum power generated by the solar cell ( $P_{max} = I_{mpp} V_{mpp}$ ) and the product of  $V_{oc}$  with  $J_{sc}$  (Equation 2).

$$FF = \frac{I_{mpp} V_{mpp}}{J_{sc} V_{oc}}$$

Equation 2

The subscript “mpp” denotes the maximum power point (MPP) of the solar cell, meaning the point on the I-V curve characteristic of the solar cell at which the solar cell has the maximum power output. To optimise the performance of solar devices, it is mandatory to operate the solar cells at the MPP.

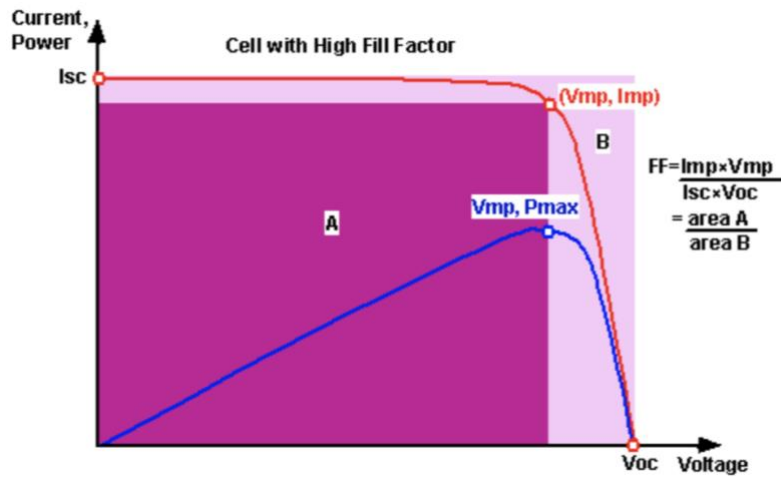


**Figure 7.** Graph of solar cell output current and power as a function of voltage. The FF is the area of the largest rectangle which will fit in the I-V curve [12].

### Power conversion efficiency (PCE)

Power conversion efficiency is the parameter defined to compare the performance of solar cell devices. PCE is the ratio between the output power from the solar cell to input power from sun and it is obtained with the following equation (Equation 3):

$$PCE = \frac{P_{max}}{I_{in}} = \frac{J_{sc} V_{oc} FF}{I_{in}}$$

Equation 3

The PCE of the solar cells, as well as reflecting the performance of the solar device, also depends on the spectrum and intensity of the incident light and the temperature of the solar cell, which makes critical the conditions for measuring the PCE when comparing different solar devices.

### Quantum efficiency (QE)

The quantum efficiency of a solar cell is defined as the ratio of the number of electrons that are collected at the solar cell to the total number of the incident photons of the solar cell. The QE is either represented in photon wavelength as shown in Figure 8, for an ideal solar cell.

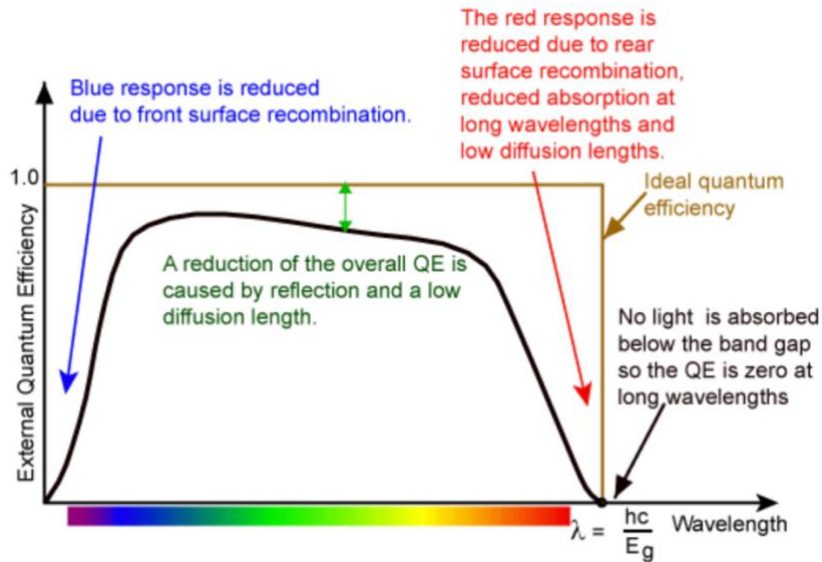


**Figure 8.** Quantum efficiency of a solar cell [13].

Quantum efficiency ideally has the square shape shown in the figure above, but most of solar cell's QE is reduced due to the recombination effects that take place.

### 1.3 Different Generations of Solar Cells

Research on solar cells has been growing fast since the beginning due to the motivation of researchers for developing this noteworthy and powerful invention. Figure 9 (released on 06-30-2022) shows the progress of the best research-cell efficiencies from 1976 to the present.

PV technology can be divided into three generations of solar cells, though research is ongoing for developing new technologies. The three generations are known as first, second, and third, and each of them differs the cost and efficiency.

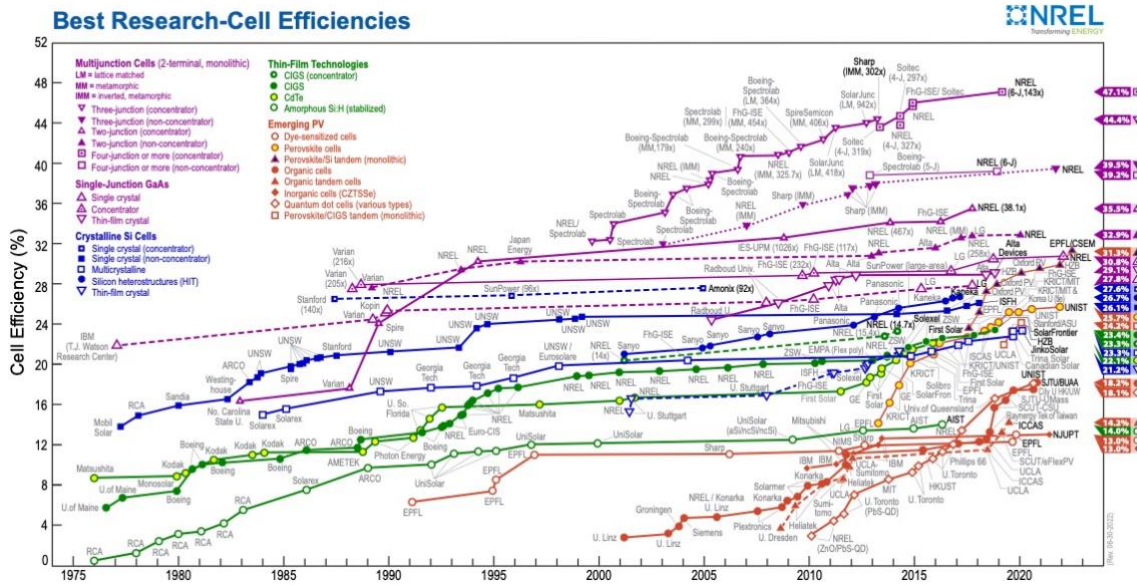


Figure 9. Best Research-Cell Efficiencies chart [14].

### First generation

The first generation of solar cells is mainly based in crystalline silicon or GaAs wafers. The solar cells of this generation are, nowadays, dominating the PV market and own a well-matured technology. This high-efficiency and high stability solar cells Silicon-based solar cells have reached a PCE of 26.33% [15] approaching their theoretical efficiency maximum of 29% in 2016. However, the manufacturing process of crystalline silicon solar cells demands lots of energy and requires extremely pure silicon using a single junction for extracting energy from photons. In 2007, first-generation devices stand for 89.6% of commercial production, though the market share has declined since. Regarding the disadvantages of first-generation solar cells, especially the high-cost production, researchers have focused on c-Si heterojunction technology, which consists of c-Si as an absorber layer, with thin-film Si for the selective-contacts of both polarities, reporting a 26.7% of PCE [16]. The aim of this heterojunction technology is to increase the PCE of solar devices and significantly reduce the cost of production which consequently reduces the levelized cost of electricity (LCOE).

### Second generation

The second generation has been under deep research during the 1990s and early 2000s to overcome the main issue of the first generation; the cost of production. This issue has been achieved using thin-film technologies and reducing the material present in the device and boosting its quality. The second generation of solar cells is based in materials with



good PV properties such as, amorphous silicon, CdTe, CdS, CIGS and CZTS and, cells are manufactured with cheap fabrication process. The second-generation of solar cells constitutes the second largest market share because of its advantages in cost production, nevertheless, solar cells of this generation have lower PCE, only 20% reported for CIGS [17], fast degradation when exposed to light and poor availability of the raw materials.

### *Third generation*

Research towards low-cost and high-efficiency solar cells, finally gave birth to the third-generation solar cells, which is significantly wide and under continuous deep research, but it remains an emerging technology and it is the generation with the less market share. Despite that, third generation has a promising future in the PV market with excellent potential for large-scale solar electricity generation [18]. The manufacture process for 3<sup>rd</sup> solar cells generation is based in solution processing techniques.

The 3<sup>rd</sup> generation of solar cells includes organic and inorganic semiconductors, nanostructured SCs, quantum dot SCs, dye-sensitized solar cells, multi-junction solar cells and hybrid materials. In this last category, there are included the organic-inorganic hybrid perovskites, the topic of this dissertation. Hybrid organic-inorganic perovskite SCs will be described in the following chapter.

Indeed, research in the 3<sup>rd</sup> generation has borne its fruits and the improvement in efficiencies for the emerging solar cells has known a spectacular growth in the recent years. In Figure 10, the advances in the emerging 3<sup>rd</sup> generation solar cell have been highlighted.

As can be seen, perovskite solar cells have already reached a record of 25.7 % and when combined with silicon through tandem Perovskite / Silicon solar cells the efficiency growth up to 31.3%.

Other approaches, like Perovskite/CIGS tandem solar cells declare record efficiencies of 24.2 % while maximum efficiencies for quantum dots-based solar cells and organic cells are about 18.2%.



## Chapter 2: Motivation and Objectives

This is a paper-based doctoral thesis that considers four publications about hybrid perovskites. In this chapter, there is an introduction of hybrid perovskites, and next, objectives, motivation, and the structure of the book is described.

### 2.1 Hybrid Organic-Inorganic Perovskite materials and Solar Cells

#### Introduction

The mineral perovskite, named after the Russian mineralogist Count Lev Perovski, was used in solar cells for the first time in 2009. Since then, scientists have been deeply studying the material considering its potential in the PV technology. The actual record for single junction perovskite solar cells was set in 2021 by Korean researchers from South Korea's Ulsan National Institute of Science and Technology (UNIST) reaching a 25.8% of PCE [19]. The record for the emerging HOIPSCs technology was set by CSEM and EPLF in July 2022 achieving a 31.25% of PCE, smashing the barrier of 30% efficiency [20]. This record was established using tandem-type perovskite-silicon solar cells, combination expected to deliver cost-effective solar cells. But, even with this high-efficient and low-cost technology, the theoretical limit is still far from reality, taking into account that Perovskite/Silicon tandems could achieve a maximum PCE of 45% under standard test conditions [21].

#### Structure

The typical structure of hybrid perovskites consists of a simple formula:  $ABX_3$ , described in Figure 11, where A cation is confined in a caged formed by B cations and X anions. The hybrid perovskite forms a unique crystal formed by monovalent organic A-site cation ( $A = CH_3NH_3$  and  $HC(NH_2)^{2+}$ ), divalent B-site group IV cations ( $B = Pb^{2+}$  and  $Sn^{2+}$ ), and X-site halide anions ( $X = I^-$ ,  $Br^-$ , and  $Cl^-$ ).

When A-site cation is  $MA^+$ , studied in this PhD, the unit cell consists of 12 atoms. For hybrid perovskites, optoelectronic properties including bandgap and mobility of charge carriers vary significantly with the choice of the A cation. Also, hybrid perovskites manifest strong phase variation with temperature. Further to this,  $MAPbI_3$  is set into three different crystal symmetries (cubic, tetragonal, and orthorhombic) depending on the temperature.

Besides, the  $MASn$ -based perovskite compounds  $MASn_xPb_{1-x}I_3$  are reported to show pseudo-cubic structures when  $x \geq 0.5$ , while the beta phase is observed at  $x < 0.5$ .

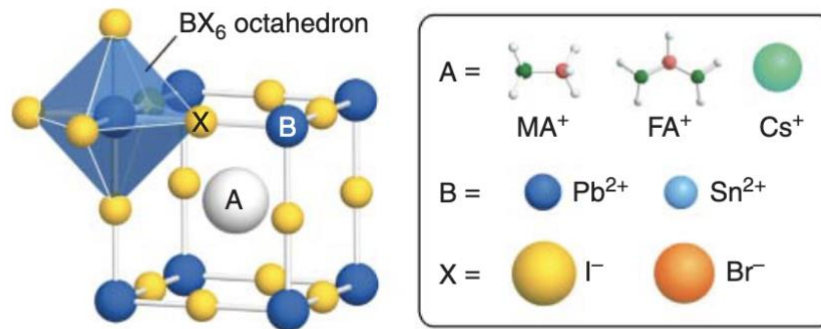


**Figure 11.** Schematic structure of a cubic  $ABX_3$  perovskite [22].

### Perovskite materials

Today, research made possible that many compounds adopted perovskite structure, giving hybrid perovskite solar cells a wide spectrum of structural phases and chemical and structural properties. All materials that perovskites regard are able to experience phase transitions with accessible cubic, tetragonal, orthorhombic, trigonal and monoclinic polymorphs depending on the combination of the typical  $ABX_3$  perovskite formula.

Examples of metal oxide perovskites ( $ABO_3$ ) are  $KTaO_3$ ,  $SrTiO_3$  and,  $GdFeO_3$ , and by the partial substitution of the anion, sublattice broadens the possibilities of the combination.

In halide perovskite, the oxidation states of both cations must be three. This results in only ternary combinations possible, such as  $CsSnI_3$ . However, hybrid halide perovskites consist of a divalent inorganic cation and an inorganic cation of equal charge.  $CH_3NH_3PbI_3$ , aka MAPI, is an example of hybrid halide perovskites. For the case of hybrid halide perovskite, any molecular cation that fits the perovskite network can be used for the compound. Cations that are reported to give the solar devices the highest PCE are Rb, Cs,  $CH_3NH_3$ , and formaminidium ( $HC(NH_2)_2$ ), separated or mixed.

### Working Principle of Perovskite Solar Cells

Perovskite solar cells bring distinct properties over conventional solar cells not only due to materials. The working principle of perovskite solar cells is described in the following paragraph.

The structure of the perovskite solar cell is formed by a transparent electrode that make light reach the absorber material of the device as it is represented in Figure 12. Both electron and hole transport layers facilitate the proper transportation of electrons and holes. In the solar cell, perovskite layer works as light absorber and thus, makes photons get absorbed, which creates the electron and hole pair. The electron and hole transport layers, ETL and HTL, respectively, allow the transport of electrons and block the holes.

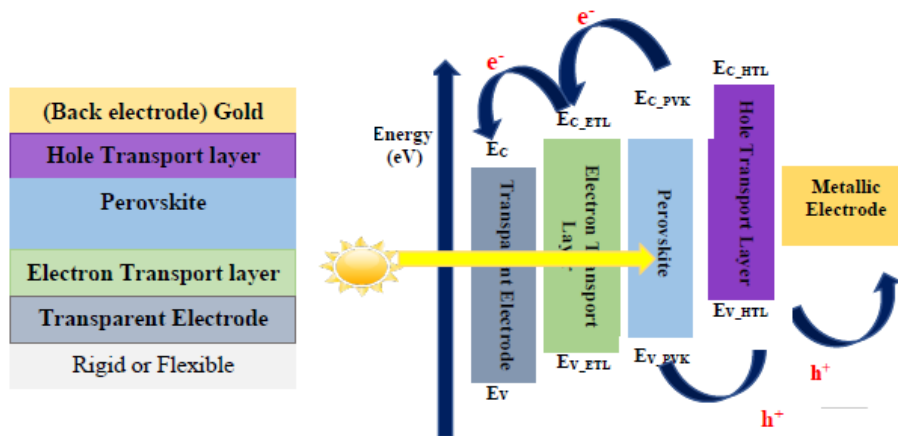


**Figure 12.** Schematic of perovskite solar cell working principle [23].

When light reaches the perovskite layer, photons are absorbed with an energy greater than the bandgap of the perovskite material. This phenomenon generates the before-mentioned electron and hole pairs that afterwards are excited onto their lowest unoccupied molecular level and highest occupied molecular level. ETL and HTL creation separates electrons and holes accordingly to later be collected by their respective back and front electrodes.

## Properties

Hybrid perovskites own multifunctional behaviour and exceptional optoelectronic properties for photovoltaic applications. Optoelectronic properties deserve special interest, making the electronic structure of the materials fundamental for understanding the perovskites band structure and density of states. The optoelectronic properties include excited state lifetime, recombination mechanisms, mobility of charge carriers, and intrinsic carrier concentration. Halide perovskites are considered a special class of semiconductors. They exhibit inverted electronic structure relative to conventional III-V compounds like GaAs, which has a substantial As 4p character in the upper valence band and Ga and As 4s character in the lower conduction band [24]. The electronic structure also has remarkable consequences for the structural properties, giving perovskites high distortion rate that results in high ionic conductivity observed in the cubic phase of perovskites [25].

Also, light absorption is fundamental for proper performance in PV applications. Hybrid perovskites are very efficient absorbing light due to its direct bandgap. In particular, the absorption coefficient of  $\text{MAPbI}_3$  is higher than  $3.0 \times 10^4 \text{ cm}^{-1}$  in the visible region, which is more than one order of magnitude larger than conventional silicon solar cells [26] fact

that makes possible to manufacture high-efficient perovskite layers with a thickness of 0.3-0.6  $\mu\text{m}$ . On the contrary, silicon layers thickness is usually about 300  $\mu\text{m}$ . This significant difference results in less raw material required and thus, lower cost.

## **Challenges**

Despite the potential of hybrid perovskites for optoelectronic applications, further research is required to fulfill the manufacture of a high-efficiency and high-stable solar device. Stability and efficiency are two important parameters for the commercialization of the devices. In recent years, the main studies on HOIPSCs focused in enhancing the efficiency of the devices, and the increase in PCE has experienced a substantial growth. However, stability is still a limiting factor, imperative for the commercial viability of the mentioned devices. Degradation rapid decreases the lifetime of the perovskite solar cells. Studies report that degradation is a consequence of exposure to humidity, oxygen, ultraviolet radiations, and temperatures [27]. In this work, the aim is to mitigate the stability issues of hybrid perovskites by implementing several techniques in the manufacture perovskite layers and related devices [28].

## **2.2 Objectives**

Regarding the literature review, the following thesis general objectives were suggested and, then carried out for the elaboration and scientific research thereof:

- Design and manufacture of several thin layers for solar cells using different materials MA-based
- Configuration of different perovskite materials for improving the properties of the solar cells
- Characterization and simulation of the devices made in the experimental part

The specific objectives of all the investigations carried out in the dissertation work go towards high-stable and high-efficiency hybrid perovskite solar cells and are listed below:

- *Doping to reduce lead quantity of the solar cell and boost the stability*
- *Study the influence of the antisolvent in the properties of the device*

## **2.3 Motivation**

The straightforward motivation of the presented thesis comes from the well-known energy and environmental crises that is taking place nowadays. All horrific consequences global warming has in planet Earth, makes scientific investigation a must to mitigate such

effects. Regarding the world needs for deep research in the field of energy and technology in general and my personal interest, I considered convenient to contribute to the research in the photovoltaic field.

I am grateful and motivated to investigate in specific the materials for hybrid perovskite solar cells, guided by both of my supervisors. Dedicated time and effort were put in this investigation to develop the technology of the HOIP solar cells and therefore, improve the stability, efficiency, optoelectronic properties, and non-toxic characteristics.

All my knowledge was focused during three years in the fourth papers that complete this dissertation and other relevant studies based in the same topic. The literature review was mandatory to decide the thread of the work and the objectives of the Ph.D.

## 2.4 Thesis Structure

The thesis book structure is described into the following chapters, each of them summarized for facilitating the understanding of the reader:

- Chapter 1 includes general introduction and a short state of the art.
- Chapter 2 deals with the perovskite materials and define the motivation and objectives of this work.
- Chapter 3 presents the first paper of the work: **Stability Improvement of Methylammonium Lead Iodide Perovskite Thin Films by Bismuth Doping**
- Chapter 4 is about the second publication of the thesis dissertation: **Tetrabutylammonium (Tba)-Doped Methylammonium Lead Iodide: High Quality and Stable Perovskite Thin Films**
- Chapter 5 exposes the third work of the PhD: **Manufacture of High-Efficiency and Stable-Lead Free Solar Cells Through Antisolvent Quenching Engineering**
- Chapter 6 presents the fourth paper of the thesis: **Investigation on The Stability and Efficiency of  $\text{MaPbI}_3$  and  $\text{MaSnI}_3$  Thin Films for Solar Cells**
- Chapter 7 presents the summary and conclusion of the work and suggested further studies
- Annex includes a list of publications and conferences attended during the period of my thesis.

## References chapters 1 and 2

[1] International Energy Agency (15 July 2021) *Global electricity demand is growing faster than renewables, driving strong increase in generation from fossil fuels.*

<https://www.iea.org/news/global-electricity-demand-is-growing-faster-than-renewables-driving-strong-increase-in-generation-from-fossil-fuels>

[2] Ember (30 March 2022) Global electricity review. <https://ember-climate.org/insights/research/global-electricity-review-2022/>

[3] NOAA Climate.gov (22 June 2022) Climate Change: Global Temperature. <https://www.climate.gov/news-features/understanding-climate/climate-change-global-temperature>.

[4] International Energy Agency (May 2021) Net Zero by 2050. <https://www.iea.org/reports/net-zero-by-2050>.

[5] Our world in data (2022) Electricity generation. <https://ourworldindata.org/grapher/electricity-generation?tab=chart>

[6] Our world in data (2022) Installed solar energy capacity. <https://ourworldindata.org/grapher/installed-solar-pv-capacity?tab=map>

[7] Solar Power Europe (10 May 2022). World Installs a Record 168 GW of Solar Power in 2021, enters Solar Terawatt Age. [solarpowereurope.org](http://solarpowereurope.org)

[8] Solar Energy Industries Association (8 September 2022) U.S. Solar Market Insight. <https://www.seia.org/us-solar-market-insight>

[9] PV Education <https://www.pveducation.org/pvcdrom/solar-cell-operation/solar-cell-structure>

[10] Wikipedia. Schottky junction solar cell. [https://en.wikipedia.org/wiki/Schottky\\_junction\\_solar\\_cell](https://en.wikipedia.org/wiki/Schottky_junction_solar_cell)

[11] PV Education <https://www.pveducation.org/pvcdrom/solar-cell-operation/short-circuit-current>

[12] PV Education <https://www.pveducation.org/pvcdrom/solar-cell-operation/fill-factor>

[13] PV Education <https://www.pveducation.org/pvcdrom/solar-cell-operation/quantum-efficiency>

[14] National Renewable Energy Laboratory (NREL) <https://www.nrel.gov/pv/cell-efficiency.html>

[15] Kaneka Coporation (14 September 2016) [https://www.kaneka.co.jp/en/images/topics/1473811995/1473811995\\_101.pdf](https://www.kaneka.co.jp/en/images/topics/1473811995/1473811995_101.pdf)



- [16] Liu, Y., Li, Y., Wu, Y., Yang, G., Mazzarella, L., Procel-Moya, P., ... & Sun, B. (2020). High-efficiency silicon heterojunction solar cells: materials, devices and applications. *Materials Science and Engineering: R: Reports*, 142, 100579.
- [17] Iqbal, M. A., Malik, M., Shahid, W., Din, S. Z. U., Anwar, N., Ikram, M., & Idrees, F. (2022). Materials for Photovoltaics: Overview, Generations, Recent Advancements and Future Prospects. *Thin Films Photovoltaics*, 5(10.5772).
- [18] Conibeer, G. (2007). Third-generation photovoltaics. *Materials today*, 10(11), 42-50.
- [19] Aju Business Daily (25 October 2021)  
<https://www.ajudaily.com/view/20211025093115151>
- [20] CSEM and EPLF (7 July 2022) <https://www.csem.ch/press/new-world-records-perovskite-on-silicon-tandem-solar?pid=172296>
- [21] Futscher, M. H., & Ehrler, B. (2016). Efficiency limit of perovskite/Si tandem solar cells. *ACS Energy Letters*, 1(4), 863-868.
- [22] Fujiwara, H. (Ed.). (2022). *Hybrid Perovskite Solar Cells: Characteristics and Operation*. John Wiley & Sons.
- [23] Singh N. (2021). *Design and Simulation of Electron and Hole Transport Layer for Lead-Free Perovskite Solar Cell Application* –Doctoral dissertation, Thapar Institute Of Engineering and Technology.
- [24] Manser, J. S., Christians, J. A., & Kamat, P. V. (2016). Intriguing optoelectronic properties of metal halide perovskites. *Chemical reviews*, 116(21), 12956-13008.
- [25] Yamada, K., Isobe, K., Tsuyama, E., Okuda, T., & Furukawa, Y. (1995). Chloride ion conductor CH<sub>3</sub>NH<sub>3</sub>GeCl<sub>3</sub> studied by Rietveld analysis of X-ray diffraction and <sup>35</sup>Cl NMR. *Solid State Ionics*, 79, 152-157.
- [26] Huang, J., Yuan, Y., Shao, Y., & Yan, Y. (2017). Understanding the physical properties of hybrid perovskites for photovoltaic applications. *Nature Reviews Materials*, 2(7), 1-19.
- [27] Ahmed, M. I., Habib, A., & Javaid, S. S. (2015). Perovskite solar cells: potentials, challenges, and opportunities. *International Journal of Photoenergy*, 2015.
- [28] Rong, Y., Hu, Y., Mei, A., Tan, H., Saidaminov, M. I., Seok, S. I., ... & Han, H. (2018). Challenges for commercializing perovskite solar cells. *Science*, 361(6408), eaat8235.



# Chapter 3: Stability Improvement of Methylammonium Lead Iodide Perovskite Thin Films by Bismuth Doping

Authors: Júlia Marí Guaita<sup>a</sup>, Amal Bouich<sup>a</sup> and Bernabé Marí<sup>a</sup>

<sup>a</sup>Institut de Disseny per a la Fabricació i Producció Automatitzada, Universitat Politècnica de València.

## Abstract

Perovskites have been in the spotlight in the field of solar cells due to their high efficiency and their low cost of materials and fabrication processes. The PSCs have shown an efficiency of up to 25%. Nevertheless, PSCs have some drawbacks such as rapid degradation in ambient conditions. In order to improve PSCs stability, lead is usually replaced with Bismuth. In this article, we report the results when doping the Methylammonium lead iodide (CH<sub>3</sub>NH<sub>3</sub>)PbI<sub>3</sub> aka MAPbI<sub>3</sub> with different Bismuth quantities. The incorporation of bismuth into the lattice leads to a remarkable change in optoelectronics and morphological structure. Substituting lead atoms with 2% of bismuth results in removing pinholes, increasing the crystallite size and the optical absorption, and the MAPbI<sub>3</sub>. We also report that Bismuth showed improvement in the stability of MAPbI<sub>3</sub> pure that started showing degradation after four weeks compared to the sample of 2%, 4%, and 8% of Bismuth that kept under the dark remained stable.

## 1. Introduction

It is worldwide known that Solar Power is experiencing remarkable growth as it is an excellent source of renewable energy. Solar Power has the potential to offer a significant supply of globally demanded energy. Every hour of Sun radiation that the Earth receives could be enough to produce enough electricity for a whole year of the world requirements.

Perovskites, used as absorbers in Solar Cells, have shown exceptional optical and electronic properties as well as substantial reductions in the manufacturing costs and ease of fabrication. However, Perovskites have some drawbacks when used in solar cells and they experience rapid degradation when exposed to UV radiation. The new generation of mixed organic-inorganic halide perovskites is promising. They have successfully shown efficiency of over 25% when used as absorbers in solar cells [1].

Solar Cell performance depends highly on the perovskite layer, which is responsible for the light absorption and generation of photoinduced carriers. Therefore, perovskite layers need delicate and critical deposition when fabricating the Solar Cell. Perovskites, described with the formula ABX<sub>3</sub> (where A is a cation such as Cs or CH<sub>3</sub>NH<sub>3</sub>, B is usually lead, and X halide) can be fabricated by different methods; one-step and two-step spin-

coating are the most used solution processes for the perovskite's layers. One-step spin-coating deposition stands out over two-step for its ease of fabrication.

Among all hybrid-organic-inorganic-perovskites, methylammonium lead iodide  $\text{CH}_3\text{NH}_3\text{PbI}_3$  (MAPbI<sub>3</sub>) seems to be one the best options for solar cells due to its outstanding ferroelectric, pyroelectric, fibroelastic, and piezoelectric properties and they have also been reported to be marvellous as absorber layers in solar cells with an increase of efficiency of a 15% in only four years [2].

Bismuth Bi dopant was used to overcome the inconvenience of toxicity and degradation of MAPbI<sub>3</sub> solar cells. It demonstrated to enhance the rate of degradation of hybrid organic-inorganic perovskites by the partial substitution of Pb by Bi [3]. In addition, recent studies about Bi-doped MAPbI<sub>3</sub> perovskite reported high defect tolerance, improved Seebeck coefficient, and higher electrical conductivity [4].

In other research work, Cs cation has been used to substitute MA in the MAPbI<sub>3</sub> structure to investigate its potential for solar cells. XRD (x-ray diffraction) showed that when incorporating Cs in the MAPbI<sub>3</sub>, the tetragonal structure is transformed into an orthorhombic phase. Also, when adding Cs, the connectivity of the grains increases and with 40 and 50% of Cs doping, the inter-grain voids are improved in the films. In conclusion, in this study, they report better performance and major PCE of the device when doping with 30% of Cs. [5].

Many studies focused on the doping of the MAPbI<sub>3</sub> to improve the efficiency of the Perovskite Solar Cells (PCSs). But few studies use Mg as a doping agent. It is known that Mg could be interesting to incorporate into the MAPbI<sub>3</sub> perovskites because it affects the energy band structure and morphology [6].

Calcium was also used as a doping agent for the MAPbI<sub>3</sub>. Adding Ca might enlarge bandgap structures by concurrent up-shifting. Besides, the electronegativity of Ca is smaller than that of Pb, and the stronger antibonding character Ca-I bonding ends in a larger bandgap of Ca<sup>2+</sup> perovskite. Moreover, *Lu et al.* concluded that ~~that~~ doping the MAPbI<sub>3</sub> with Ca is a highly effective strategy to improve the photovoltaic performance of the solar cells [7].

Recent studies reported that Cl-doped MAPbI<sub>3</sub> improves substantially the charge transport within the perovskite layer. This may be essential for obtaining PV efficiencies. [8].

When doping the MAPbI<sub>3</sub> with Rb, the conductivity of the perovskite could be significantly tuned from n-type to p-type. The carrier concentration and mobility can be controlled by the dopant concentration. In addition, a slight blue shift of the PL

(photoluminescence) peak was reported with the increase of Rb, and at the concentration range of 1.5-1.8M, the dominant crystal structure can go from cubic to orthorhombic [9].

In this work, we doped MAPbI<sub>3</sub> perovskites with different Bismuth percentages to explore how doping with Bismuth affects the properties of the perovskite solar cell. Bismuth ions incorporated in MAPbI<sub>3</sub> thin films improve the crystallinity of MAPbI<sub>3</sub> layers and enhance the electrical properties of the device. Further, as the Bi atom has a similar radius to Pb it is relatively easy to incorporate Bi into the MAPbI<sub>3</sub> lattice by substituting the Pb atom [10]. The synthesis of the Bi-doped MAPbI<sub>3</sub> samples was performed by the one-step spin method. After the synthesis, the samples prepared were characterized with different techniques such as XRD, FESEM (field emission scanning electron microscope), AFM (atomic force microscopy), PL, and optical absorbance to measure the crucial parameters for great performance in perovskite-based devices. We report that bismuth doping intensifies the properties of MAPbI<sub>3</sub> making better electrical performance and improving the stability of the devices.

## **2. Experimental procedure**

### **Materials**

All chemicals used were bought from Sigma-Aldrich and used as received. Methylammonium iodide (MAI), Lead iodide (PbI<sub>2</sub>, 99%), and Bismuth (III) iodide (BiI<sub>3</sub>, 99%) were used as precursor materials and Dimethylformamide (DMF 99.9%) and Dimethyl sulfoxide (DMSO 99.9%) as solvents.

### **Elaboration of thin films**

The MAPbI<sub>3</sub> thin films were deposited on FTO (fluorine tin oxide)-coated glass substrates. The FTO substrates were cleaned for 15 minutes in detergent Hellmanex, ethanol, acetone, and isopropanol in an ultrasonic bath and subsequently exposed for 15 minutes to UV-Ozone ambient.

MAPbI<sub>3</sub> precursor solution was prepared by completely dissolving MAI and Lead Iodide in DMSO (0,095 mL) and DMF 1ml, at room temperature. To dope MAPbI<sub>3</sub> with Bismuth, a variable amount (x%) of Bismuth iodide was added, where x is the percentage of Bismuth present in the precursor solution. The solution prepared was left to heat overnight at 75°C in the glovebox. FTO-substrates were statically spin-coated at 4500 RPM for 50 seconds, after which they were annealed for 5 minutes at 50 degrees and then 10 minutes for 100 degrees. Samples were kept in an inert N<sub>2</sub> atmosphere until used.

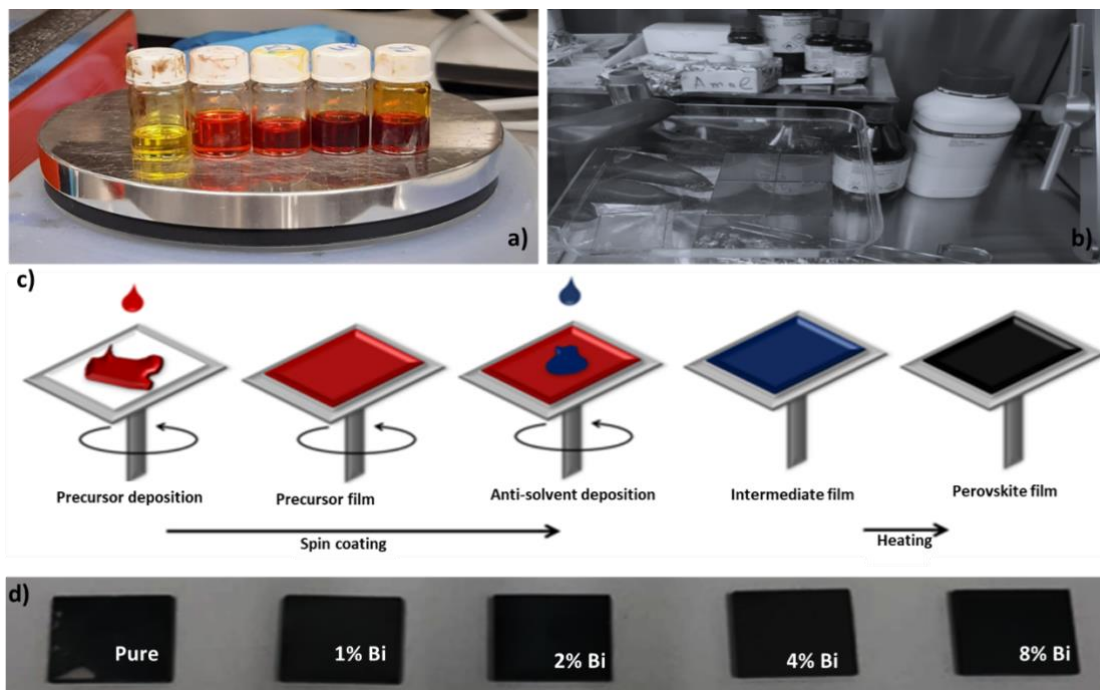


**Figure 1.** Scheme of the one-step spin-coating procedure for thin films MAPbI<sub>3</sub> perovskites.

**Figure 1** displays the preparation process of the samples. In a) the solutions with different quantities of bismuth are placed over the plate to be completely dissolved. In b) we can see the substrates of FTO (2.5cm x 2.5cm) where we will deposit the different solutions. In c) there is the scheme of how we deposit the solution on the substrate in the spin-coating machine. And finally, d) shows pictures of the samples prepared after the annealing treatment.

### Characterization techniques

The samples studied for this work, MAPbI<sub>3</sub> thin films and doped with Bismuth with different quantities (0 %, 1 %, 2 %, 4 %, and 8 %) were characterized by XRD using a RIGAKU Ultima IV diffractometer with Cu  $\kappa\alpha$  radiation ( $\lambda = 1.5418 \text{ \AA}$ ). Morphology images were taken FESEM Quanta 200-FEI at applied voltage 1.5 kV, AFM measurements were performed by a Nano Surf Mobile S microscope scanning by tapping mode, Optical properties were performed with Ocean Optics HR4000 spectrophotometer by a Si-CCD and PL emission source was a semiconductor laser at 405 nm.

### 3. Results and discussion

The different samples MAPbI<sub>3</sub> undoped and doped with the different Bismuth (Bi) doping percentages  $x\%$  where ( $x=0,1,2,4,8$ ), were scanned with XRD analysis as shown in Fig. 2 a). The diffraction peaks located at 14.0, 24.0, 28.0, and 32.0 correspond to the planes of (110), (211), (220), (222), (400), and (303) respectively, that belong to the characteristic peaks of MAPbI<sub>3</sub>. The peaks reported correspond to the same diffraction peaks previously reported [9,10]. Furthermore, the incorporation of Bi contents from (0–8%) shows an improvement in the MAPbI<sub>3</sub> peaks intensity where 2%Bi sample shows slightly higher intensity than the rest of the samples, and a decrease was observed for PbI<sub>2</sub> peaks which indicated the enhanced stability of MAPbI<sub>3</sub> doped. These results are well-matched with the previously reported pure MAPbI<sub>3</sub> crystalline phase, As indicated by XRD, the Bi-doped MAPbI<sub>3</sub> single crystals maintain a perfect cubic perovskite structure ( $Pm-3m$ ) [11].

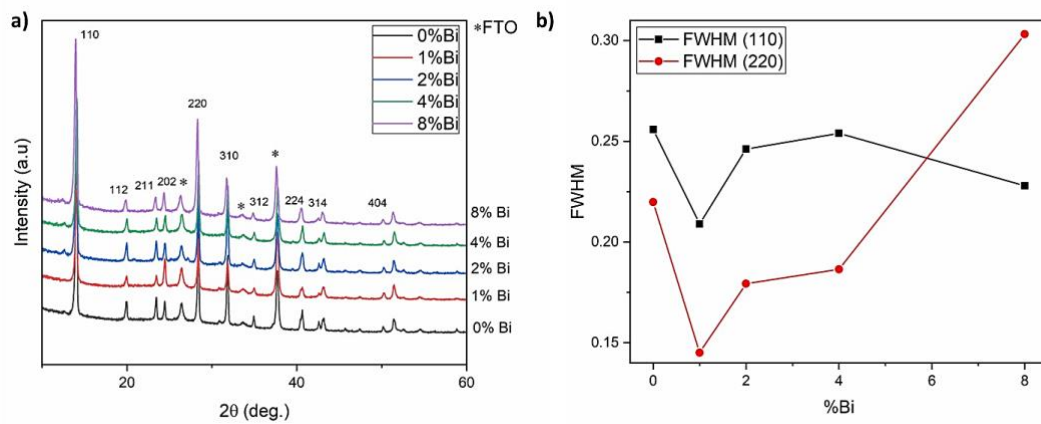


**Figure 2.** a) XRD patterns of MAPbI<sub>3</sub> pure and doped  $x\%$  Bi where  $x$  (0, 1, 2, 4, 8). b) FWHM of characteristic 110 and 220 XRD peaks for different amounts of Bi.

**Figure 2 b)** shows the calculated FWHM values for (110) and (220) XRD peaks. The (110) peak FWHM increases with the Bismuth percentage, however, it decreases when the Bismuth content in the perovskite rises to 8%. For the (220) peak, the FWHM increases with the Bismuth content. The FWHM is affected by the composition and the annealing temperature, indicating that these parameters influence the crystallinity of the film, concerning that smaller FWHM means higher crystallinity, so in this case, 1% Bismuth sample shows the lower value of FWHM.

The surface morphology and roughness vary with the different quantities of Bismuth in the perovskite thin films. These parameters are shown in **Table I** Effective lattice strain has been calculated to know about the deformations of the grains in the surface of the film. Equation 1 was used to obtain the effective lattice strain ( $\epsilon$ ).

$$\beta \cos(\theta) = \frac{k\lambda}{D} + 4\epsilon \sin(\theta) \quad (1)$$

where  $\theta$  is the Bragg angle,  $k$  is a constant (0.94),  $\beta$  is the FWHM, and  $\lambda$  is the wavelength of the x-ray. The dislocation density of the crystal was calculated using equation 2.

$$\delta = \frac{1}{D^2} \quad (2)$$

**Table I.** Grain size, dislocation density, and lattice strain of XRD of MAPbI<sub>3</sub> thin films.

Sample ID	Grain size (nm)	Roughness (nm)	Dislocation density (nm <sup>-1</sup> )	Lattice strain ( $\epsilon \times 10^{-3}$ )
Pure MAPbI <sub>3</sub>	333	41	0.90x10 <sup>-5</sup>	9.05
2% Bi	345	275	0.84x10 <sup>-5</sup>	8.71
8% Bi	293	125	1.16x10 <sup>-5</sup>	8.13

To verify how the morphology changes of MaPbI<sub>3</sub>, pure films are observed by doping with Bismuth, FESEM analysis of MaPbI<sub>3</sub> pure and doped x% Bi, where x (0,1,2,4,8) was performed. **Figure 3** shows top-view FESEM images of the different samples analysed in the work. The surface of the 1% Bismuth sample looks quite like the pure MAPbI<sub>3</sub>. According to the grain size, we report a bigger grain size when the percentage of Bismuth in the sample is higher. Also, 4% Bismuth sample and 8% Bismuth sample have dark surfaces and are not as smooth as 1% and 2% samples. The FESEM image of the MAPbI<sub>3</sub> coincides with the work of Chen et al. where they report the morphology of the MAPbI<sub>3</sub> [14,15]. Also, mapping analysis it is showing that lead and iodide were distributed homogenously in the surface of pure MaPbI<sub>3</sub> (Figure 3 f-h).

The MAPbI<sub>3</sub> surface contained the irregular size of the grain boundaries, the 1% Bi-doped makes the film surface homogenous with the reduction of the size of the grain boundary. Moreover, the crystal and grain sizes are noticeably increased with 2% of Bi.

The surface morphology and roughness vary with the different quantities of Bismuth in the perovskite thin films. These parameters are shown in **Table I** Effective lattice strain has been calculated to know about the deformations of the grains in the surface of the film. Equation 1 was used to obtain the effective lattice strain ( $\epsilon$ ).

$$\beta \cos(\theta) = \frac{k\lambda}{D} + 4\epsilon \sin(\theta) \quad (1)$$



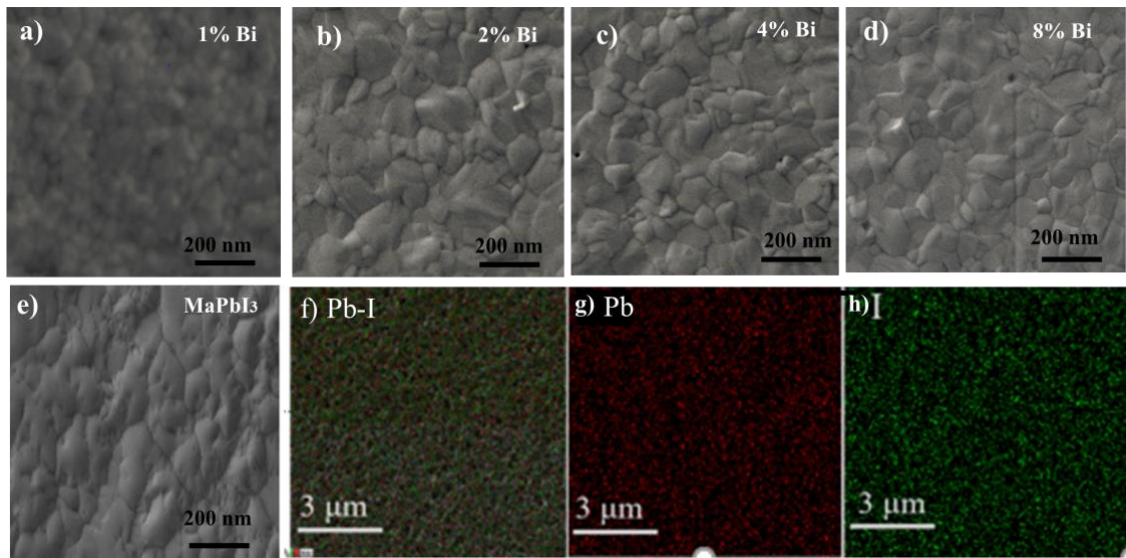


**Figure 3.** (a-e) FESEM images of  $\text{MaPbI}_3$  thin films doped with different percentage of Bi ( $x = 0, 1, 2, 4, 8$ ). (f-h) Mapping of Pb and I components in halide perovskite  $\text{MAPbI}_3$ .

The absorption study was performed in order to understand the impact of the Bismuth in the optical properties of  $\text{MaPbI}_3$ . All the samples prepared show good absorption with a small difference between the samples by increasing the percentage of Bi dopant, as well as the absorption of the pure sample ( $\text{MaPbI}_3$ ) agrees with the previous paper reported [16]. In **Figure 4 (a)** we can observe that the rest of the samples doped with different percentages of Bi from 1% to 8% have absorption at the same wavelength range. 2% Bi sample shows slightly higher absorption than the rest of the samples matching also with FESEM results above, this indicates better performance of the perovskite film.

The calculated value of the bandgap from the UV visible technique is from 1.78 eV to 2.2 eV as shown in Table I where the samples  $\text{MaPbI}_3$  doped 2% Bismuth have the optimal bandgap around 1.78eV.

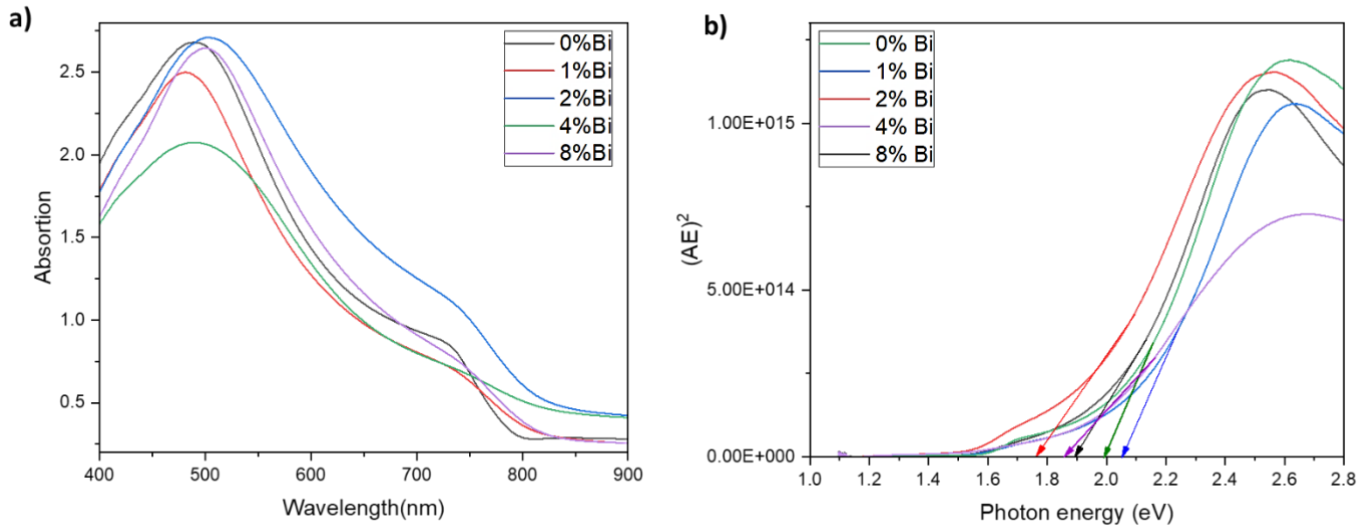


**Figure 4.** (a) UV-Visible absorption of  $\text{MaPbI}_3$  thin films doped with different percentage of Bi ( $x = 0, 1, 2, 4, 8$ ). (b) Optical bandgap of  $\text{MaPbI}_3$  thin films doped with different percentage of Bi ( $x = 0, 1, 2, 4, 8$ ).

**Table II. The bandgap of  $\text{MaPbI}_3$  thin films doped with different percentages of Bi ( $x = 0, 1, 2, 4, 8$ ).**

Sample ID	Bandgap Absorption		Bandgap PL		Stokes shift
	$\lambda(\text{nm})$	$E_g(\text{eV})$	$\lambda(\text{nm})$	$E_g(\text{eV})$	(meV)
Pure $\text{MaPbI}_3$	619.98	2.00	678	1.82	171
2% Bi	695.43	1.78	685	1.81	30
8% Bi	652.15	1.9	686	1.80	92

The photoluminescence measurements shown in **Figure 5** were recorded at ambient temperature. We report that the PL peak intensity for the different Bismuth percentages is in the range of 700-850 nm. Also, we report the highest PL peak intensity is in the 2% of Bismuth sample, compared to the PL peak of  $\text{MaPbI}_3$  pure and  $\text{MaPbI}_3$  doped with 8% of Bismuth. The higher intensity of PL indicates good photoluminescent properties of the films prepared.

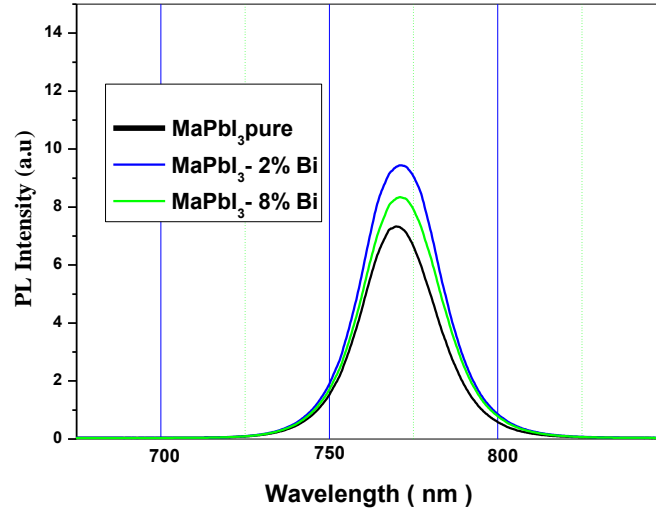


**Figure 5.** Room temperature photoluminescence of perovskite thin films; pure  $\text{MaPbI}_3$  and  $\text{BMAPbI}_3\text{-Bi}$ , with 2%, and 8% of Bismuth.

**Figure 6** shows the AFM analysis of the perovskite thin films of  $\text{MaPbI}_3$  pure,  $\text{MAPbI}_3$  doped with 2% Bi, and  $\text{MaPbI}_3$  doped with 8% Bi in an area of  $2\mu\text{m} \times 2\mu\text{m}$ . According to the experimental analysis carried out at the AFM, roughness and surface morphology of the different samples vary with the amount of Bismuth present in the absorber layer, showing that 2% of the Bismuth sample has  $R_{\text{rms}}$  of 275 nm and grain size of 345 nm (see **Table II**) which is greater compared with pure  $\text{MaPbI}_3$  and 8% of Bismuth sample.

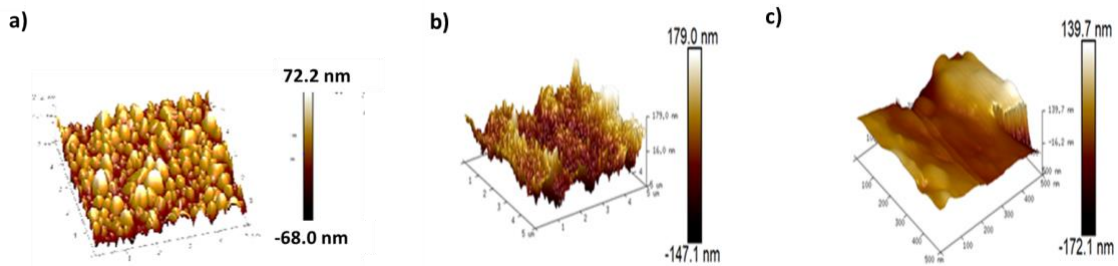


**Figure 6.** (a) AFM images of  $\text{MaPbI}_3$  thin films, (b) AFM images of  $\text{MaPbI}_3$  thin films doped with 2% Bi and (c) AFM images of  $\text{MaPbI}_3$  thin films doped with 8% Bi.

According to **Table II**, the dislocation density of these 3 samples was studied deeply because they show better characterization, varies between  $0.84 \times 10^{-5} \text{ nm}^{-1}$  and  $1.16 \times 10^{-5} \text{ nm}^{-1}$ . Lower dislocation density means better performance, which means that in this case, the 2% of Bismuth sample is the better option although it does not show the higher effective lattice strain.

## 4. Degradation Study

Perovskite solar cells are vulnerable to oxygen and humidity. In this study, Bismuth is used to overcome this rapid degradation. The samples prepared were kept in dark ambient for 1 week. It is seen that when samples were kept in dark ambient, they did not experience degradation at all for 1 week. Like this, we can confirm that the Bismuth improves the stability of the samples that started showing degradation after week 4. After 5 weeks, the sample of 2%, 4%, and 8% of Bismuth kept under dark remained stable (see **Figure 7 b**).

As mentioned before, the sample that showed better performance in all the characterization parts was the one prepared with 2% of Bismuth. In **Figure 7 a**), we can see an evolution of the optical bandgap of the 2%Bi sample where the bandgap of the aged Bi sample remains good after 4 weeks. This means this quantity of Bismuth is good to enhance the performance and the stability of the film. To sum up, we report that the bismuth shows an important role to slow down the degradation of  $\text{MaPbI}_3$  thin films.

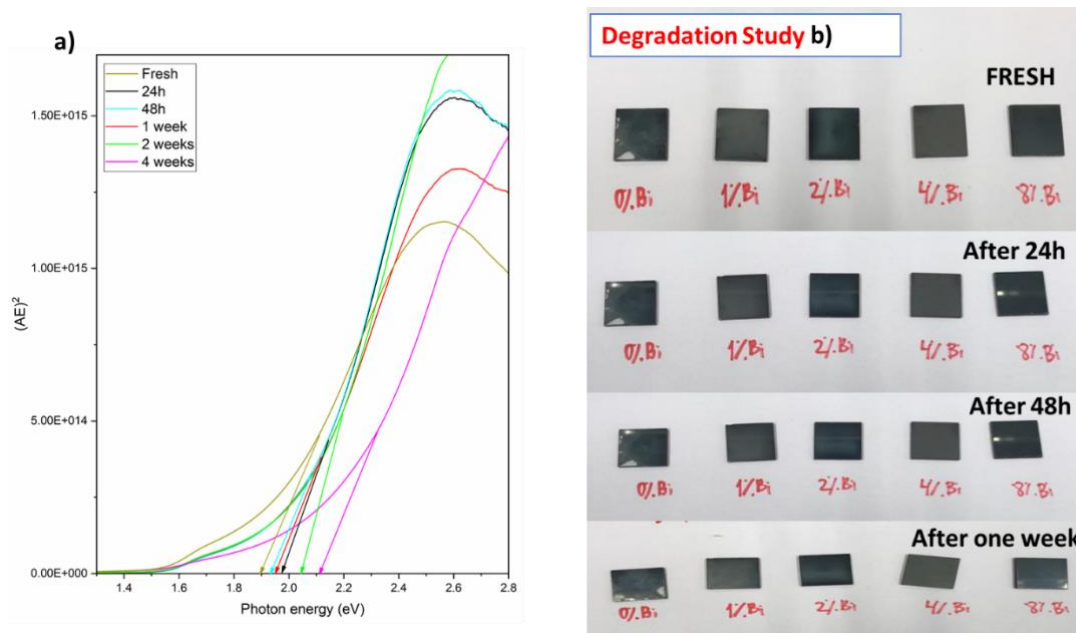


**Figure 7.** a) Optical bandgap of  $\text{MaPbI}_3$  thin films doped 2% of Bismuth for different periods after the deposition. b) Degradation study of samples with different Bismuth percentages along the time.

## 5. Conclusion

In this study, we present the result of different perovskite absorbers with different quantities of Bismuth as a doping agent for the purpose of improving the stability and the performance of optoelectronic devices. The different samples were prepared inside a glovebox through a one-step spin coating method and subsequently characterized by XRD, FESEM, optical absorption, and photoluminescence. XRD study indicates that the

addition of Bi increases the intensity of the  $\text{MAPbI}_3$  diffraction peaks, being the 2%Bi specimen the sample with the highest XRD intensity and the lowest presence of  $\text{PbI}_2$  peaks, which is a signal of the improved stability of Bi-doped  $\text{MAPbI}_3$  thin films. The FWHM graph reveals that 1% Bismuth sample shows the lowest value of FWHM which means the highest crystallite size. FESEM images show grain sizes are notably improved when adding 2% of Bismuth to the  $\text{MAPbI}_3$  which means better performance in photovoltaic devices.


## References

- [1] Yoo, J. J., Seo, G., Chua, M. R., Park, T. G., Lu, Y., Rotermund, F., ... & Seo, J. (2021). Efficient perovskite solar cells via improved carrier management. *Nature*, 590(7847), 587-593.
- [2] Chen, L. C., Lee, K. L., Wu, W. T., Hsu, C. F., Tseng, Z. L., Sun, X. H., & Kao, Y. T. (2018). Effect of different  $\text{CH}_3\text{NH}_3\text{PbI}_3$  morphologies on photovoltaic properties of perovskite solar cells. *Nanoscale research letters*, 13(1), 1-9.
- [3] Siegler, T. D., Houck, D. W., Cho, S. H., Milliron, D. J., & Korgel, B. A. (2018). Bismuth Enhances the Stability of  $\text{CH}_3\text{NH}_3\text{PbI}_3$  (MAPI) perovskite under high humidity. *The Journal of Physical Chemistry C*, 123(1), 963-970.
- [4] Xiong, Y., Xu, L., Wu, P., Sun, L., Xie, G., & Hu, B. (2019). Bismuth doping-induced stable Seebeck effect based on  $\text{MAPbI}_3$  polycrystalline thin films. *Advanced Functional Materials*, 29(16), 1900615.
- [5] Imran, M., Saleem, A., Khan, N. A., & Kamboh, A. H. (2019). Enhanced efficiency and stability of perovskite solar cells by partial replacement of  $\text{CH}_3\text{NH}_3^+$  with inorganic  $\text{Cs}^+$  in  $\text{CH}_3\text{NH}_3\text{PbI}_3$  perovskite absorber layer. *Physica B: Condensed Matter*, 572, 1-11.
- [6] Yang, F., Kamarudin, M. A., Kapil, G., Hirotnani, D., Zhang, P., Ng, C. H., ... & Hayase, S. (2018). Magnesium-doped  $\text{MAPbI}_3$  perovskite layers for enhanced photovoltaic performance in humid air atmosphere. *ACS applied materials & interfaces*, 10(29), 24543-24548.
- [7] Lu, C., Zhang, J., Hou, D., Gan, X., Sun, H., Zeng, Z., ... & Zhu, Y. (2018). Calcium doped  $\text{MAPbI}_3$  with better energy state alignment in perovskite solar cells. *Applied Physics Letters*, 112(19), 193901.
- [8] Colella, S., Mosconi, E., Fedeli, P., Listorti, A., Gazza, F., Orlandi, F., ... & Mosca, R. (2013).  $\text{MAPbI}_{3-x}\text{Cl}_x$  mixed halide perovskite for hybrid solar cells: the role of chloride as dopant on the transport and structural properties. *Chemistry of Materials*, 25(22), 4613-4618.

- [9] Bai, X., Zou, X., Zhu, J., Pei, Y., Yang, Y., Jin, W., & Chen, D. (2018). Effect of Rb doping on modulating grain shape and semiconductor properties of MAPbI<sub>3</sub> perovskite layer. *Materials Letters*, 211, 328-330.
- [10] Li, C., Chen, X., Li, N., Liu, J., Yuan, B., Li, Y., ... & Cao, B. (2020). Highly conductive n-type CH<sub>3</sub>NH<sub>3</sub>PbI<sub>3</sub> single crystals doped with bismuth donors. *Journal of Materials Chemistry C*, 8(11), 3694-3704.
- [11] Guo, X., McCleese, C., Kolodziej, C., Samia, A. C., Zhao, Y., & Burda, C. (2016). Identification and characterization of the intermediate phase in hybrid organic–inorganic MAPbI<sub>3</sub> perovskite. *Dalton Transactions*, 45(9), 3806-3813.
- [12] Bahtiar, A., Rahmanita, S., & Inayat, Y. D. (2017). Pin-hole free perovskite film for solar cells application prepared by controlled two-step spin-coating method. In *IOP Conference Series: Materials Science and Engineering* (Vol. 196, No. 1, p. 012037). IOP Publishing.
- [13] Li, C., Chen, X., Li, N., Liu, J., Yuan, B., Li, Y., ... & Cao, B. (2020). Highly conductive n-type CH<sub>3</sub>NH<sub>3</sub>PbI<sub>3</sub> single crystals doped with bismuth donors. *Journal of Materials Chemistry C*, 8(11), 3694-3704.
- [14] Chen, L. C., Lee, K. L., Wu, W. T., Hsu, C. F., Tseng, Z. L., Sun, X. H., & Kao, Y. T. (2018). Effect of different CH<sub>3</sub>NH<sub>3</sub>PbI<sub>3</sub> morphologies on photovoltaic properties of perovskite solar cells. *Nanoscale research letters*, 13(1), 1-9.
- [15] Xiong, Y., Xu, L., Wu, P., Sun, L., Xie, G., & Hu, B. (2019). Bismuth doping–induced stable Seebeck effect based on MAPbI<sub>3</sub> polycrystalline thin films. *Advanced Functional Materials*, 29(16), 1900615.
- [16] Bi, C., Shao, Y., Yuan, Y., Xiao, Z., Wang, C., Gao, Y., & Huang, J. (2014). Understanding the formation and evolution of interdiffusion grown organolead halide perovskite thin films by thermal annealing. *Journal of Materials Chemistry A*, 2(43), 18508-18514.
- [17] Bartolomé, J., Climent-Pascual, E., Redondo-Obispo, C., Zaldo, C., Álvarez, A. L., de Andrés, A., & Coya, C. (2019). Huge photostability enhancement in bismuth-doped methylammonium lead iodide hybrid perovskites by light-induced transformation. *Chemistry of Materials*, 31(10), 3662-3671.



# Stability Improvement of Methylammonium Lead Iodide Perovskite Thin Films by Bismuth Doping

JULIA MARÍ-GUAITA,<sup>1</sup> AMAL BOUICH <sup>1,2</sup> and BERNABÉ MARÍ<sup>1</sup>

1.—Institut de Disseny per a la Fabricació i Producció Automatitzada, Universitat Politècnica de València, Valencia, Spain. 2.—e-mail: bouich.amal@gmail.com

Perovskites have been in the spotlight in the field of solar cells due to their high efficiency and their low cost of materials and fabrication processes. Perovskite solar cells (PSCs) have shown an efficiency of up to 25%. Nevertheless, PSCs have some drawbacks such as rapid degradation in ambient conditions. To improve PSC stability, lead is usually replaced with bismuth. In this article, we report the results when doping the methylammonium lead iodide ( $\text{CH}_3\text{NH}_3\text{PbI}_3$ , aka  $\text{MAPbI}_3$ ), with different bismuth quantities. The incorporation of bismuth into the lattice leads to a remarkable change in optoelectronics and morphological structure. Substituting lead atoms with 2% bismuth improves some characteristics of  $\text{MAPbI}_3$  layers, such as removing pinholes and increasing crystallite size and optical absorption. Furthermore, bismuth doping improves the stability of pure  $\text{MAPbI}_3$  layers, which after 4 weeks exhibits higher degradation compared to bismuth-doped  $\text{MAPbI}_3$  samples, which remain stable after that period.

## INTRODUCTION

It is known worldwide that photovoltaic solar energy (PSE) is experiencing remarkable growth as it is an excellent source of renewable energy. PSE has the potential to offer a significant supply of globally demanded energy. Every hour of sun radiation that the Earth receives could be enough to produce enough electricity for a whole year of the world requirements.

Perovskites, used as absorbers in photovoltaic solar cells, have shown exceptional optical and electronic properties as well as substantial reductions in the manufacturing costs and ease of fabrication. However, perovskites have some drawbacks when used in solar cells, and they experience rapid degradation when exposed to UV radiation. The new generation of mixed organic-inorganic halide perovskites is promising in PSE because they have successfully shown efficiencies over 25% when using perovskite absorbers in solar cells.<sup>1</sup>

Solar cell performance depends highly on the perovskite layer, which is responsible for the light absorption and generation of photoinduced carriers. Therefore, perovskite layers need delicate and critical deposition when fabricating the solar cell. Hybrid perovskites, described with the formula  $\text{ABX}_3$  (where A is a cation such as Cs or  $\text{CH}_3\text{NH}_3$ , B is usually lead, and X is halide) can be fabricated by different methods; one-step and two-step spin-coatings are the most used solution processes for the perovskite layers. One-step spin-coating deposition stands out over two-step for its ease of fabrication.

Among all hybrid-organic-inorganic-perovskites, methylammonium lead iodide  $\text{CH}_3\text{NH}_3\text{PbI}_3$  ( $\text{MAPbI}_3$ ) seems to be one the best options for solar cells due to its outstanding ferroelectric, pyroelectric, fibroelastic, and piezoelectric properties, and they have also been reported to be excellent absorber layers in solar cells with a 15% increase of efficiency in only 4 years.<sup>2</sup>

Bismuth (Bi) doping was used to overcome the inconvenience of toxicity and degradation of  $\text{MAPbI}_3$  solar cells. It enhanced the rate of degradation of hybrid organic-inorganic perovskites by the partial substitution of Pb by Bi.<sup>3</sup> In addition,

(Received January 1, 2022; accepted May 16, 2022)

Published online: 08 June 2022





# Chapter 4: Tetrabutylammonium (TBA)-Doped Methylammonium Lead Iodide: High Quality and Stable Perovskite Thin Films

Authors: Amal Bouich<sup>a,b\*</sup>, Julia Mari-Guaita<sup>a</sup>, Bouchta Sahraoui<sup>c</sup>, Pablo Palacios<sup>b</sup>, Bernabé Mari<sup>a</sup>.

<sup>a</sup>Institut de Disseny i Fabricació, Universitat Politècnica, València, Spain

<sup>b</sup>Física Aplicada a las Ingenierías Aeronáutica y Naval & Instituto de Energía Solar, Universitat Politècnica, Madrid, Spain

<sup>c</sup>University of Angers, France

## Abstract

This work reported the successive incorporation of tetrabutylammonium (TBA) into Methylammonium lead Iodide (MAPbI<sub>3</sub>) perovskite. The thin films were characterized by X-Ray diffraction (XRD), Scanning electron microscopy (SEM), Transmittance electron microscopy (TEM), Atomic force microscopy (AFM), and UV-Visible spectroscopy. It was shown that introducing TBA increases the crystallinity, grain size, surface morphology without pin-hole, and roughness of the MAPbI<sub>3</sub> thin films. Moreover, the MA<sub>(1-x)</sub>TBA<sub>x</sub> PbI<sub>3</sub> thin film shows better stability in a relative humidity of ~60% after 15 days than the pure MAPbI<sub>3</sub> thin film. The obtained results are hoped to be helpful for stability and improvement of the performance of the MAPbI<sub>3</sub> thin films by doping TBA cations under ambient conditions.

## 1. Introduction

To begin with, nowadays, the Perovskites with formula ABX<sub>3</sub> (A = cation (Formamidinium (FA), Methylammonium (MA)..), B= metal cation and X is a halogen anion VII halides (Br<sup>-</sup>, Cl<sup>-</sup>, I<sup>-</sup>)), have been demonstrated good absorbers properties for solar cells with higher photovoltaic conversion efficiency (PCE) [1,4]. Methylammonium lead triiodide (MAPbI<sub>3</sub>) solar cells show good optoelectronic properties with a bandgap between 1.4 eV and 1.5 eV [5], a high absorption coefficient around 10<sup>5</sup>cm<sup>-1</sup> [6,7] with amazing PCE = 25 % [8,9]. To manufacture MAPbI<sub>3</sub> Solar cells, low-cost and simple techniques have been used to deposit the MAPbI<sub>3</sub> film: thermal vapor deposition, two-step vapor-assisted deposition, two-step solution deposition, and one-step solution deposition [10,13]. Despite the outstanding PCE reported of MAPbI<sub>3</sub> solar cells, the problem of MAPbI<sub>3</sub> degradation by the loss of MAI and formation of lead iodide PbI<sub>2</sub> under humid conditions and higher temperatures makes use of MAPbI<sub>3</sub> difficult. Concerning to improve the stability of MAPbI<sub>3</sub>, MAPbI<sub>3</sub> was doped by cesium and

showed the potential to enhance the stability of  $\text{MAPbI}_3$  solar cell under UV irradiance conditions [14]; also on the road for stable  $\text{MAPbI}_3$ , the divalent anion  $\text{Se}^{2-}$  was incorporated in  $\text{MAPbI}_3$  structure to increase the atomic interactions between the inorganic and the organic cations [15,16]. Considering the ongoing discussion, some researchers have demonstrated that the  $\text{MAPbBr}_3$  absorber is more stable than  $\text{MAPbI}_3$ ; the  $\text{MAPbBr}_3$  optical absorption is not appropriate for solar cell production [17].

In this research work, the tetrabutylammonium iodide (TBA) was incorporated into  $\text{MAPbI}_3$  solution in the form of  $\text{MA}_{(1-x)}\text{TBA}_{(x)}\text{PbI}_3$  thin film to study the effect on the structure-property of the  $\text{MAPbI}_3$  when TBA was incorporated in different percentages. As a result, significant improvement was found in the crystallinity, morphology, optical properties, and stability of the  $\text{MA}_{(1-x)}\text{TBA}_{(x)}\text{PbI}_3$  thin film. The obtained results are hoped to help delay the degradation and to enhance the performance of the  $\text{MAPbI}_3$  thin film by doping TBA cations under ambient conditions.

## 2. Materials and Experimental Procedure

Methylammonium iodide (MAI), Lead (II) iodide ( $\text{PbI}_2$ ), Chlorobenzene (CBZ), Methylammonium iodide (MAI) and Tetrabutylammonium iodide (TBAI), anhydrous N,N-dimethylformamide (DMF) and Dimethyl Sulfoxide (DMSO). All compounds were purchased from Sigma-Aldrich, and they were used without any additional purification. The  $\text{MA}_{1-x}\text{TBA}_x\text{PbI}_3$  solution was prepared in a glovebox by dissolving  $\text{PbI}_2$ , TBAI, and MAI in the solvent of DMF and DMSO; the solution was agitated at 60 °C for 3 hours.

## 3. Characterization techniques

X-ray diffraction (XRD) was employed to characterize the crystallinity of the films using RIGAKU Ultima IV diffractometer the range of  $2\theta = 10^\circ$  to  $60^\circ$  using CuK $\alpha$  radiation ( $\lambda = 1.5418 \text{ \AA}$ ) at room temperature. The morphology characteristic of thin films was constantly observed by scanning electron microscopy (SEM) model (Quanta 200 - FEI) under 1.5 kV accelerated potential in several magnifications. In addition, the films were examined by atomic force microscopy (AFM) with 0.5Hz a scan rate. The fringes crystallinity was confirmed by Transmission electron microscopy with 2.5 KV. Also, UV-VIS and PL spectra were characterized using Ocean Optics HR4000 spectrophotometer in the range of 300 to 850 nm and He-Cd laser source Si-CCD detector Hamamatsu for PL analysis, respectively.

#### 4. Results and discussion

In the present work, thin films perovskite  $MA_{1-x}TBA_xPbI_3$  were successfully deposited on FTO back contact using a simple spin-coating technique. Figure 1 shows the XRD results of the  $MA_{1-x}TBA_xPbI_3$  where  $X = (0, 1, 2.5, 5, 10)$ . The characteristic peaks located at  $14^\circ$  and  $28^\circ$  match to XRD planes of (110) and (220) respectively in agreement with  $MAPbI_3$  structure [18-19] without any  $PbI_2$  binary phase. Thus, a significant increase was found in the main XRD peaks (110) and (220) intensities and crystallinity by incorporating the TBA amount. Figure 2 represents the zoomed XRD peak in the range of  $13^\circ$  to  $15^\circ$ ; the small shift was observed towards a lower  $2\theta$  degree after the incorporation of TBA compared to the  $MAPbI_3$  thin film. Furthermore, the increase in the crystal lattice could be related to a bigger radius TBA ( $4.70 \text{ \AA}$ ) than a small radius of MA ( $1.8 \text{ \AA}$ ).

The  $MAPbI_3$  thin film with a tetragonal structure where  $a = b = 8.90 \text{ \AA}$ ,  $c = 11.12 \text{ \AA}$  and with insignificant changes due to TBA incorporation where  $a = b = 8.91 \text{ \AA}$ ,  $c = 11.11 \text{ \AA}$ . The crystal parameters details of  $MA_{1-x}TBA_xPbI_3$  and the grain size were calculated using the Pawley method summarized in Table 1. Moreover, FWHM of peaks (110) and (220) values gradually decrease an agreement of good crystallinity of the films with increasing the amount of TBA from 0 to 5% in Figure 1(c). In this respect, the stability of the  $MAPbI_3$  main (110) peak remains excellent after incorporating TBA amounts. Especially many studies have been reported that the inorganized Pb atoms affect the surface imperfections of the film, which leads to a decrease in the performance of perovskite devices. In the current work, the TBA arguably shows a significant improvement of  $MAPbI_3$  stability that degrades quickly into  $PbI_2$  in external conditions [20].

**Table 1.** Lattice parameters of  $MA_{1-x}TBA_xPbI_3$  via the Pawley method.

Sample. ID	a = b (Å)	c (Å)	Grain Size (nm)	Roughness (nm)	Dislocation density (nm <sup>-1</sup> )	Lattice strain (ε)
<b>MAPbI<sub>3</sub></b>	8.90	11.12	184.7	147.7	$1.04 \times 10^{-05}$	0.38
<b>5% TBA</b>	8.91	11.11	249.1	198.5	$0.52 \times 10^{-05}$	0.39
<b>10% TBA</b>	8.99	11.13	209.8	158.0	$0.61 \times 10^{-05}$	0.37

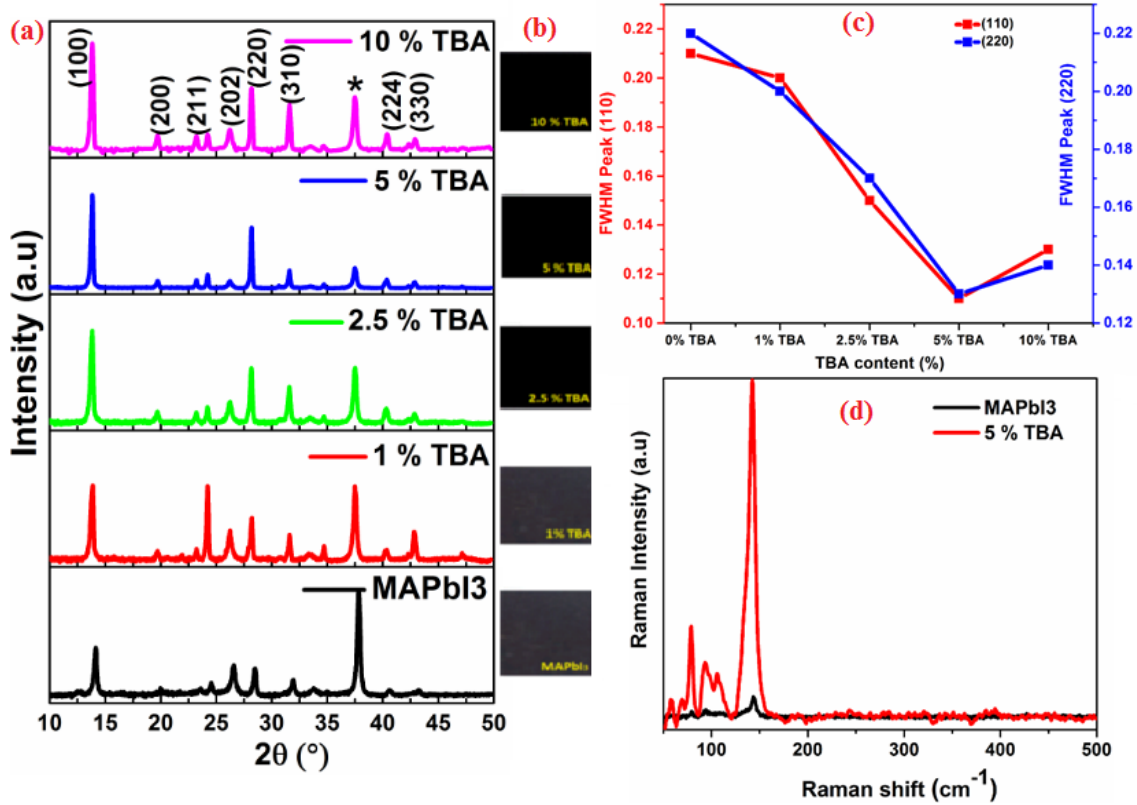


**Figure 1.** a) XRD pattern of MA<sub>1-x</sub>TBA<sub>x</sub>PbI<sub>3</sub> where X% = (0, 1, 2.5, 5 and 10), b) MA<sub>1-x</sub>TBA<sub>x</sub>PbI<sub>3</sub> photographs c) FWHM of (011) and (022) peaks of MA<sub>1-x</sub>TBA<sub>x</sub>PbI<sub>3</sub> c) Raman spectra of MAPbI<sub>3</sub> undoped and doped with 5% TBA.

Here, the Raman spectroscopy analysis was used to verify the phase identification of pure MAPbI<sub>3</sub> and 5% doped TBA Figure 1(d). The dominant two vibrational modes were identified for MAPbI<sub>3</sub> approximately at 68 cm<sup>-1</sup> and 142 cm<sup>-1</sup>. The intensities of the same vibrational mode increased after incorporating 5% TBA content. The 68 and 142 cm<sup>-1</sup> bands matched with the obtained results from XRD that confirmed the incorporation of TBA, which plays a vital role in the formation of crystallinity [21].

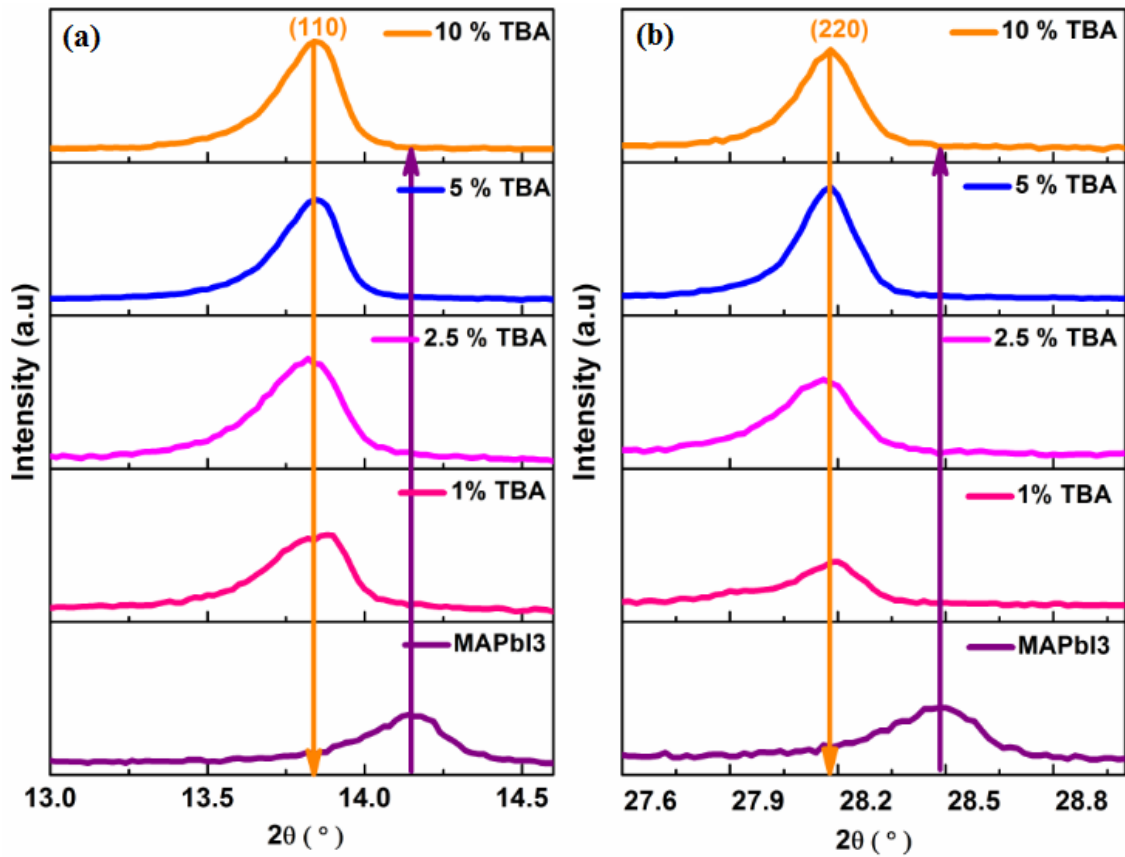


**Figure 2.** The zoomed XRD peaks, a) (110) and, b) (220) of  $MA_{1-x}TBA_xPbI_3$  where  $X$  % = (0 %, 1 %, 2.5 %, 5 %, and 10 %).

Figure 3 illustrates the SEM images of  $MA_{1-x}TBA_xPbI_3$  where  $X$  % (0 %, 1 %, 2.5 %, 5 %, 10 %). The undoped  $MAPbI_3$  shows a small grain size with a smooth surface and good distribution of lead and iodide [22]. In the same way, the TBA incorporation increase gradually grain size of 210 nm for pure  $MAPbI_3$ , 290 nm for the doped  $MAPbI_3$  with 1.0 % TBA, 490 nm for 2.50 % TBA as well as with a higher value of 500 nm for 5.0 % TBA figure (a-d). This improvement of the grain size of doped  $MAPbI_3$  can be due to the crystal growth by decreasing crystal nucleation and lead to good surface coverage and higher crystallinity, as shown by the XRD analysis [23,24]. In this connection, the enhanced crystallinity and grain size could be attributed to fewer defects in the trap state, decreasing the non-radiative recombination in the  $MAPbI_3$  surface [25].

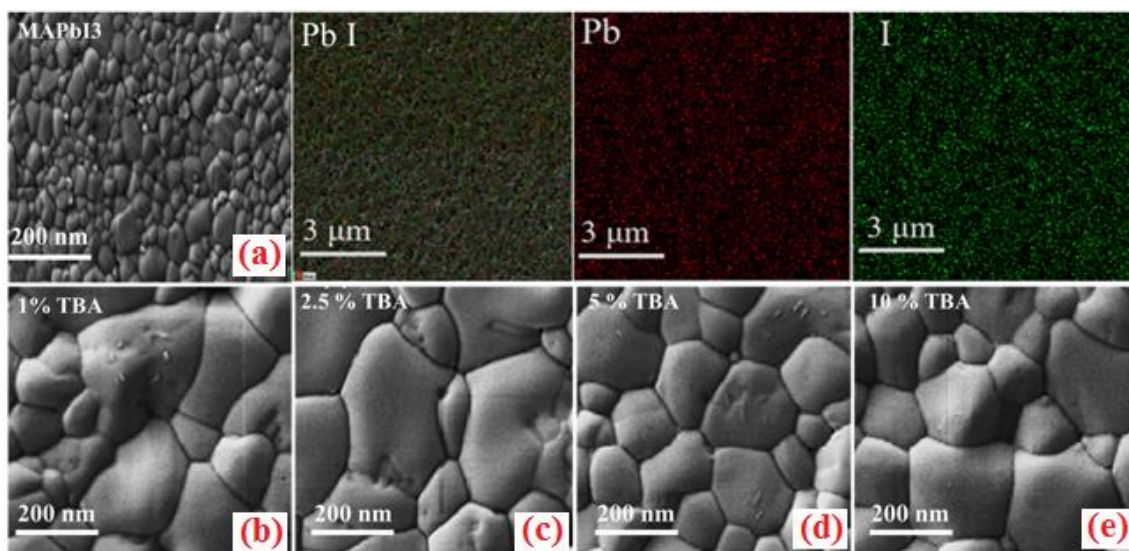


**Figure 3.** a) EDS Mapping of MAPbI<sub>3</sub> (b-e) SEM images of pure and doped MAPbI<sub>3</sub>.

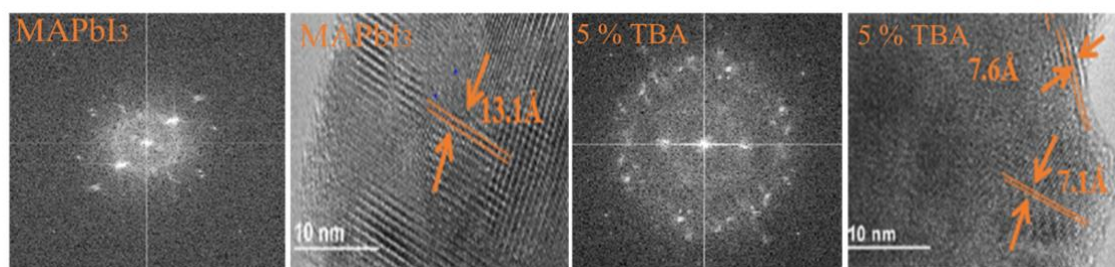


**Figure 4.** HRTEM Images of undoped and 5 % TBA doped MAPbI<sub>3</sub>.

The specimen preparation technique used for perovskite samples prepared is tripod polishing for perovskite for high-resolution TEM investigation, scratching the perovskite film prepared and putting it in the special grid of aluminium to characterize the samples with TEM analysis, Figure 4 displays TEM analysis of pure MAPbI<sub>3</sub> and doped with 5 % TBA expose the scattered through lattice fringes spacing of 13.10 Å correspond to [110] crystallographic plan as well as 7.60 Å match with [220] crystallographic respectively. The selected portion of the electron diffraction spectrum shows that pure and 5% TBA doped MAPbI<sub>3</sub> films are polycrystalline, where is in good agreement with XRD results [26-27].

Figure 5 shows AFM images with 2 and 3 Dimension of undoped and doped MAPbI<sub>3</sub>, where the measured roughness is varying, that offers a change compared to doped and undoped MAPbI<sub>3</sub> where RMS= (147.7 nm, 198 nm, and 168 nm ) calculated for the x% TBA where x = (0, 5 and 10) respectively which is measured by the root-mean-square (RMS) (Table 1). Moreover, the RMS value of 10% TBA doped MAPbI<sub>3</sub> shows a slight decrease than the incorporation of 5% of TBA, showing the optimum level for large grain size and high roughness in the AFM analysis [28].

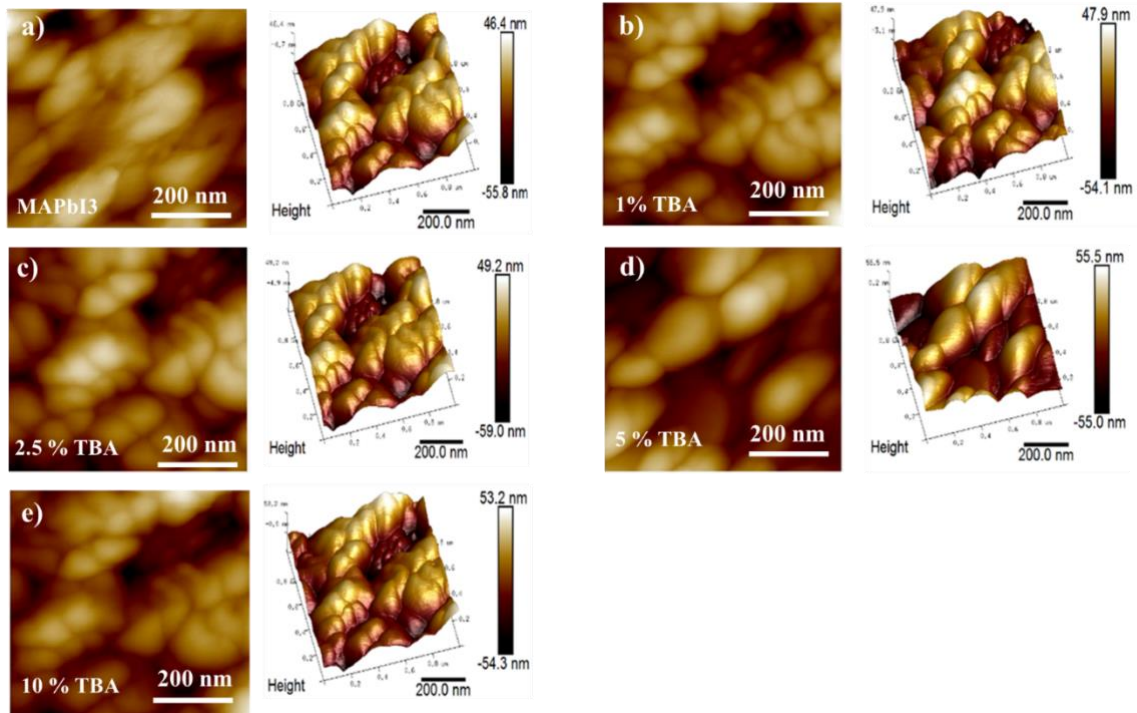


**Figure 5.** AFM images 2 and 3 Dimensional of pure and doped MAPbI<sub>3</sub>.

## 5. Optical and photoluminescence study

This experiment performed the optical absorption and photoluminescence measurements for MAPbI<sub>3</sub> thin film doped TBA to analyse the optoelectronic properties. Here, Figure 6 (a) illustrates the optical absorption of MAPbI<sub>3</sub> pure and doped TBA from 400 nm to 900 nm wavelength, where the optical bandgap was estimated around 1.55 to 1.59 eV. Upon monitoring carefully, the variation in the optical bandgap was observed by incorporating the TBA amount. This significant improvement could be related to pinhole-free TBA doped MAPbI<sub>3</sub> films, as shown in SEM analysis [29].

Besides, Figure 7 shows the photoluminescence spectrum of undoped MAPbI<sub>3</sub> and doped TBA, where the FWHM intensity progressively increases with the increase of TBA content. Doped 5% TBA represents a significantly higher red emission around 55 nm. This emission is three times higher than undoped MAPbI<sub>3</sub> thin film. The results could be attributed to reducing trap density states with decreased charge recombination, which improved the thin film's optoelectronic properties [30,31].

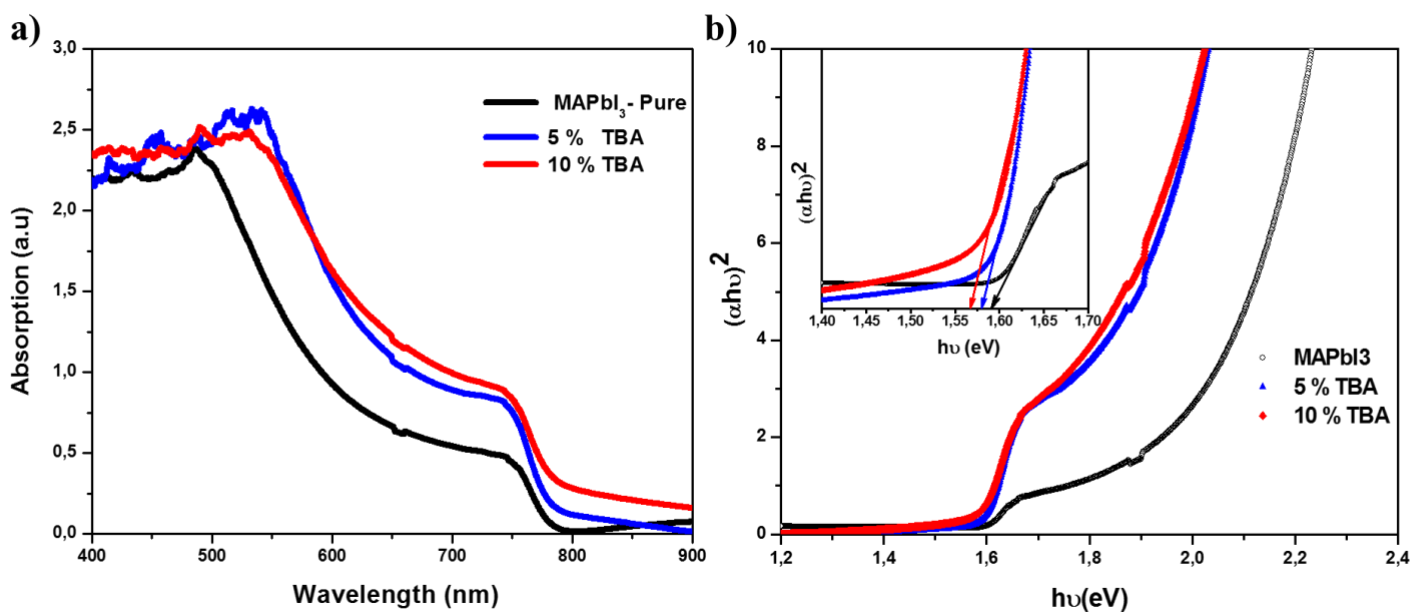


**Figure 6.** a) Optical absorption, b) calculated bandgap of MA<sub>1-x</sub>TBA<sub>x</sub>PbI<sub>3</sub> where X % = (0 %, 5 %, and 10 %).

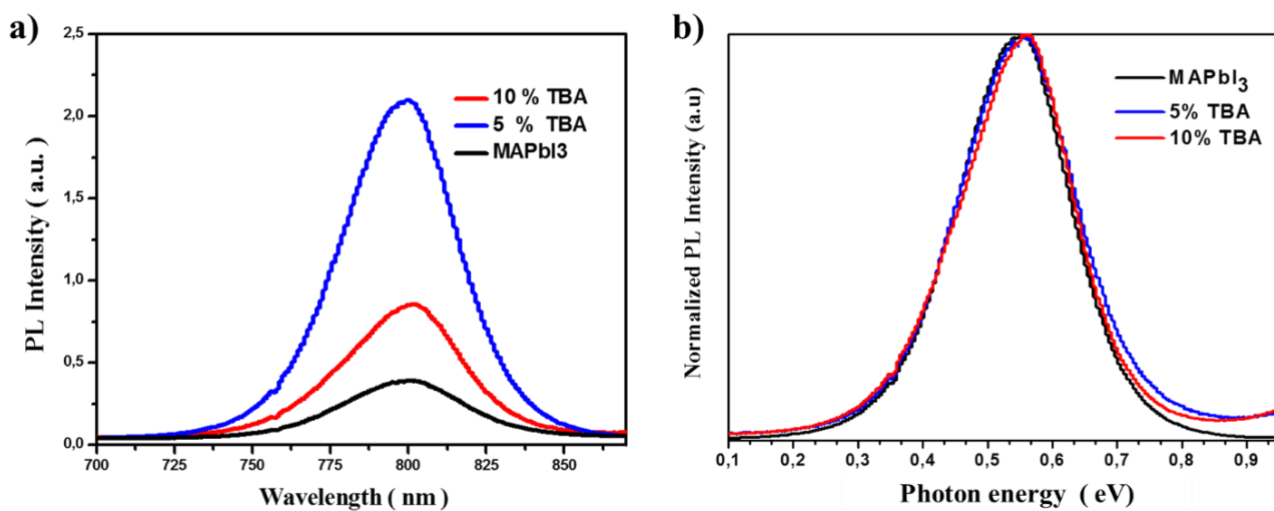


**Figure 7.** a) PL spectra and b) is the normalized PL spectra of MA<sub>1-x</sub>TBA<sub>x</sub>PbI<sub>3</sub> where X % = (0 %, 5 %, and 10 %) thin film.



In this context, one of the essential parameters of semiconductor materials is the Stokes shift. This shift was observed between the optical absorption edge and PL peak. The comparison of Stokes shift values is summarized in Table 2. The Stokes shift describes the reduction of lattice parameters in the crystals. The low value of the Stokes shift indicates the good photophysical properties of MAPbI<sub>3</sub> [32,33].

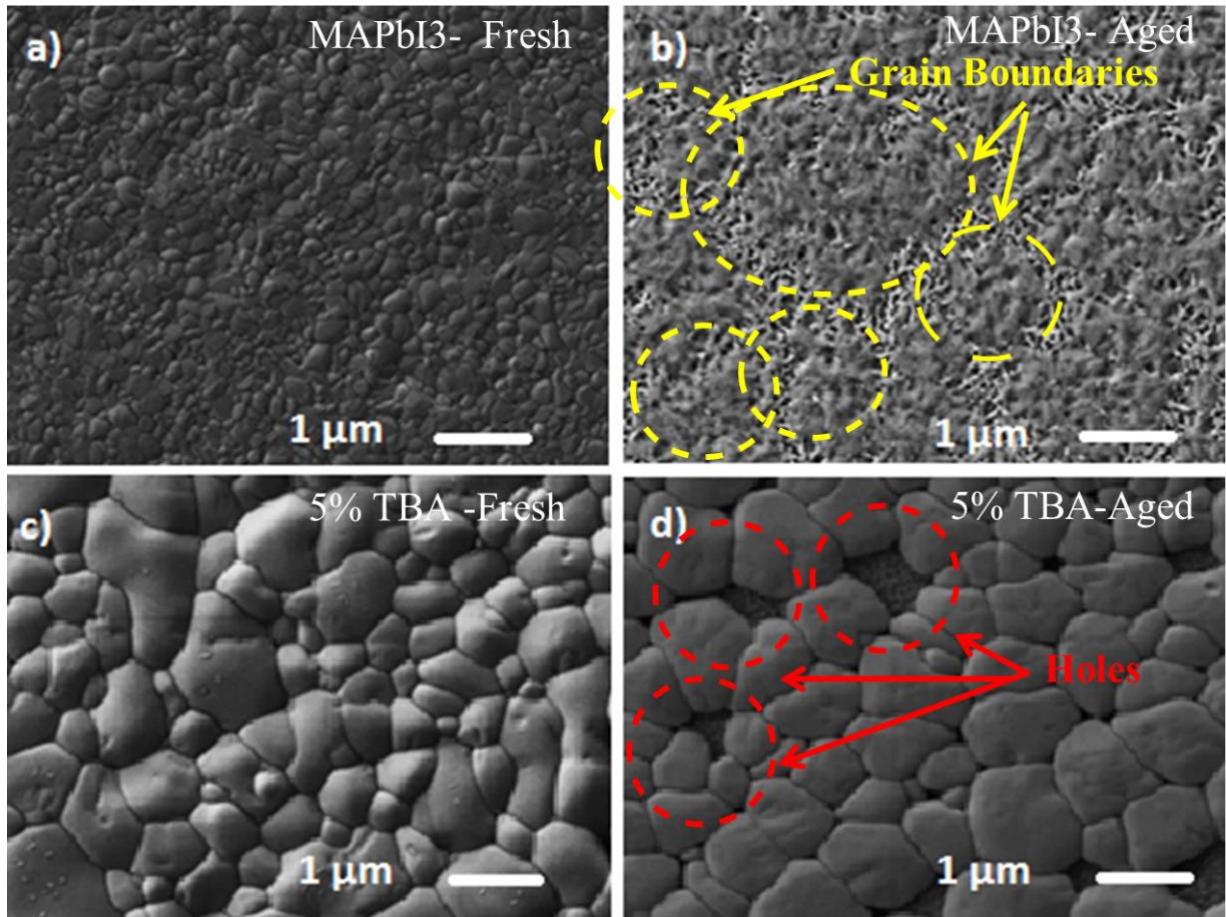
**Table 2.** Band gap variation of MA<sub>1-x</sub>TBA<sub>x</sub>PbI<sub>3</sub> where X % = (0 %, 5 %, and 10 %).

Sample	Eg from PL		Eg from UV		Stokes shift
	$\lambda$ (nm)	Eg(eV)	$\lambda$ (nm)	Eg(eV)	meV
<b>MAPbI<sub>3</sub> Pure</b>	778	1.59	752	1.6	220
<b>5% TBA doped</b>	785	1.57	761	1.58	220
<b>10% TBA doped</b>	786	1.56	763	1.56	200

## 6. Degradation study

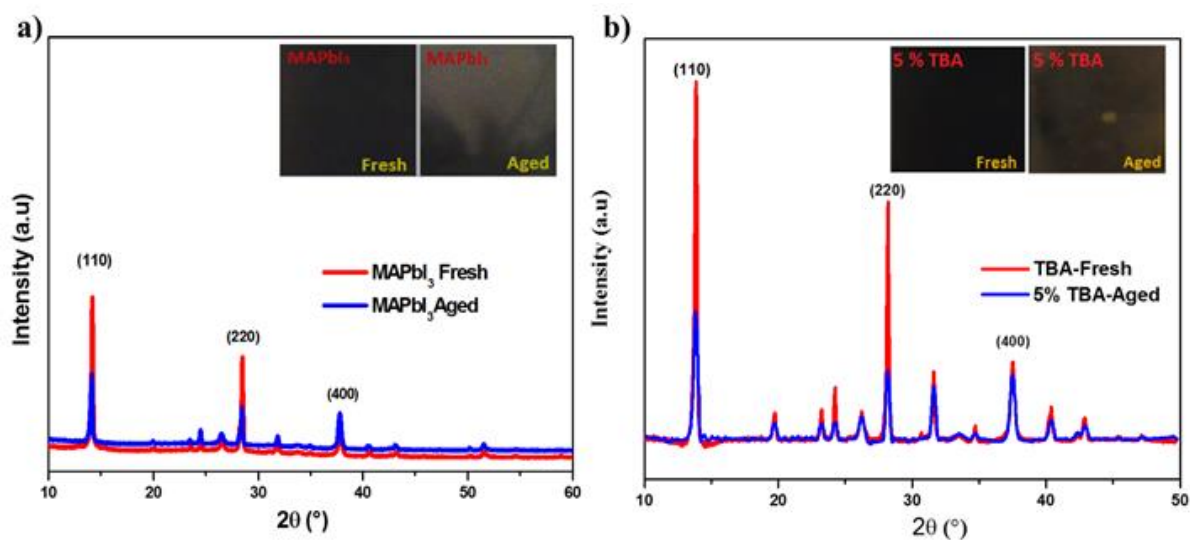
The degradation of pure MAPbI<sub>3</sub> and 5% doped TBA samples were examined under a dark relative 60% humidity environment where samples were stored for 15 days. Consequently, a significant transformation from the black color to the yellow color was observed for the pure MAPbI<sub>3</sub> aged sample after two weeks which indicated the dissociation of MAPbI<sub>3</sub> to PbI<sub>2</sub> confirmed by yellow color compared to 5% doped TBA aged sample was less affected (figure 9).

Figure 8 illustrates the SEM images of the MAPbI<sub>3</sub> surface were affected by humidity and the water molecules over the grain boundaries, which led to the degradation of MAPbI<sub>3</sub> and the formation of PbI<sub>2</sub> and MAI. The TBA cation reduced the grain boundaries to prevent the access of humidity into the film. Furthermore, the 5% TBA doped MAPbI<sub>3</sub> has shown a slight crystal structure distortion than the pure MAPbI<sub>3</sub> [34,35].



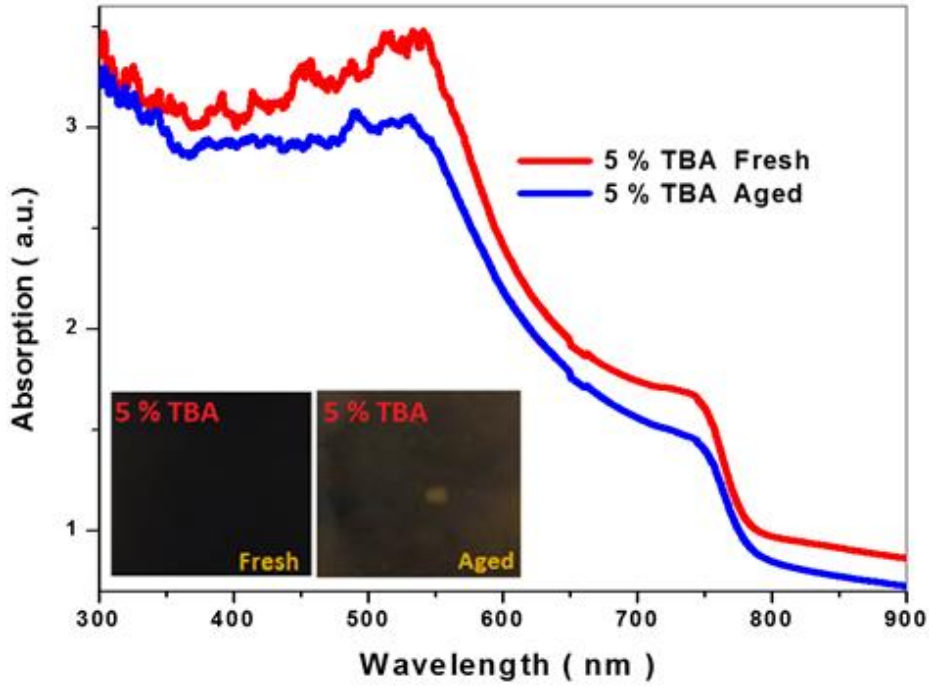
**Figure 8.** SEM images of Fresh and aged pure and 5% TBA doped MAPbI<sub>3</sub> layers.

Figure 9 displays the XRD patterns and the structural variations through the degradation of the doped and undoped MAPbI<sub>3</sub> with the characteristic peak (110) of pure MAPbI<sub>3</sub> shows dramatically reduced; however, the 5% TBA doped MAPbI<sub>3</sub> thin film observed less affected by the environment as compared to pure MAPbI<sub>3</sub>.



**Figure 9.** The XRD pattern of fresh and aged MAPbI<sub>3</sub> and 5 % TBA samples.

Furthermore, the environmental effect was studied from the UV-Visible analysis of the 5% TBA doped MAPbI<sub>3</sub>; Figure. 10 shows a slow-down variation in the absorption edge, and the colour changed from dark to brown of the sample after two weeks in relative humidity (60%). The obtained results confirm that incorporating TBA into the MAPbI<sub>3</sub> could decrease the degradation of the methylammonium lead triiodide absorber for photovoltaic application.



**Figure 10.** The absorbance of fresh and aged 5% TBA sample.

### 7. Device Spiro/MAPbI<sub>3</sub>/TiO<sub>2</sub>/F.T.O Simulation

As we noticed a change in the bandgap of doped with 5 % TBA and undoped MAPbI<sub>3</sub> has been observed. The effect of thickness and bandgap variation of the absorber layer has a more significant impact on the performance of solar cells. We simulate a proposed solar cell having a model “Gold/SpiroOmTAD/MAPbI<sub>3</sub>/TiO<sub>2</sub>/FTO/Glass” to keep this impact on the cell's performance. Here Gold is used as a front contact, OmTAD as ETL, MAPbI<sub>3</sub> as an absorber layer, TiO<sub>2</sub> as HTL, F.T.O is working as a back contact, and glass is a substrate [35,36].

**Table.3:** Characteristic Parameters of doped and undoped MAPbI<sub>3</sub> based solar cell by Scaps 1D.

Solar Cell	V <sub>oc</sub>	J <sub>sc</sub>	FF	E.T.A
	V	mA/cm <sup>2</sup>	%	%
<b>Spiro/MAPbI<sub>3</sub>/TiO<sub>2</sub>/F.T.O</b>	0.95	22.4	87.1	18.01
<b>Spiro/MAPbI<sub>3</sub>:TBA/TiO<sub>2</sub>/F.T.O</b>	0.85	25.7	86.1	20.1

Figures 11 c) show the J-V characteristics curve and clearly show the effect of doped and undoped MAPbI<sub>3</sub>, Voc was 0.95V, Jsc of 22.4 mA/cm<sup>2</sup>, FF of 87.1%, and Eta of 18.01% recorded. Here we note that undoped is giving less performance, Voc, Jsc, FF, and Eta

were registered as 0.85V, 25.7 mA/cm<sup>2</sup>, 86.1%, and 20.42%, respectively, which was good as compared to the results of the film growth and crystallinity.

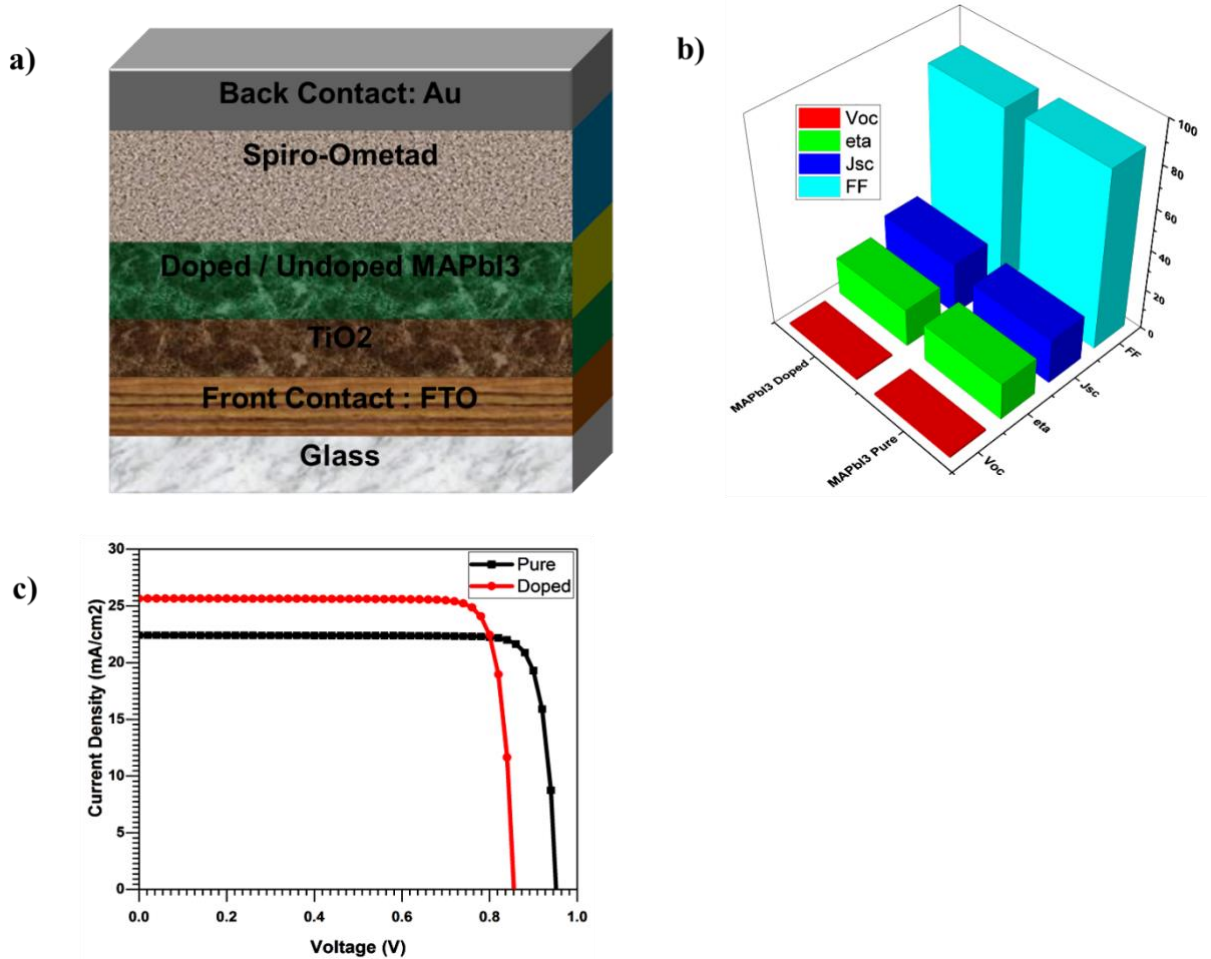


**Figure 11** a) diagram of MAPbI<sub>3</sub> based solar cell b) Characteristics Parameters Comparison of MAPbI<sub>3</sub> based solar cell c) JV characteristic curves of MAPbI<sub>3</sub> based solar cell simulated.

## 8. Conclusion

To sum up, from the preceding discussion, it appears that the doped with a small amount of TBA significantly increases the morphology and stability of MAPbI<sub>3</sub> thin film for photovoltaic applications. The XRD analysis revealed that the crystallinity of MAPbI<sub>3</sub> thin film enhanced with TBA, the TBA affects leading MAPbI<sub>3</sub> film with a homogenous, highly rough surface and large grain size, which could cause trap more light in the surface. Similarly, the MA<sub>(1-x)</sub>TBA<sub>x</sub>PbI<sub>3</sub> thin film shows better stability in a relative humidity of ~60% after 15 days than pure MAPbI<sub>3</sub> thin film. The obtained results are hoped to help

delay the degradation and to enhance the performance of the MAPbI<sub>3</sub> thin film by doping TBA cations under ambient conditions.

## References

- [1] Weidman, M. C., Seitz, M., & Tisdale, W. A. (2019). U.S. Patent No. 10,273,405. Washington, DC: U.S. Patent and Trademark Office.
- [2] Smith, M. D., Connor, B. A., & Karunadasa, H. I. (2019). Tuning the luminescence of layered halide perovskites. *Chemical Reviews*, 119(5), 3104-3139.
- [3] Quan, L. N., Rand, B. P., Friend, R. H., Mhaisalkar, S. G., Lee, T. W., & Sargent, E. H. (2019). Perovskites for Next-Generation Optical Sources. *Chemical Reviews*, 119(12), 7444-7477.
- [4] Fakharuddin, A., Shabbir, U., Qiu, W., Iqbal, T., Sultan, M., Heremans, P., & Schmidt-Mende, L. (2019). Inorganic and Layered Perovskites for Optoelectronic Devices. *Advanced Materials*, 1807095.
- [5] Wang, Y., Fang, W. H., Long, R., & Prezhdo, O. V. (2019). Symmetry Breaking at MAPbI<sub>3</sub> Perovskite Grain Boundaries Suppresses Charge Recombination: Time-Domain ab Initio Analysis. *The journal of physical chemistry letters*, 10(7), 1617-1623.
- [6] Im, J. H., Lee, C. R., Lee, J. W., Park, S. W., & Park, N. G. (2011). 6.5% efficient perovskite quantum-dot-sensitized solar cell. *Nanoscale*, 3(10), 4088-4093.
- [7] De Roo, J., Ibáñez, M., Geiregat, P., Nedelcu, G., Walravens, W., Maes, J., ... & Hens, Z. (2016). Highly dynamic ligand binding and light absorption coefficient of cesium lead bromide perovskite nanocrystals. *ACS Nano*, 10(2), 2071-2081.
- [8] Park, N. G. (2015). Perovskite solar cells: an emerging photovoltaic technology. *Materials Today*, 18(2), 65-72.
- [9] Xiao, Z., Bi, C., Shao, Y., Dong, Q., Wang, Q., Yuan, Y., ... & Huang, J. (2014). Efficient, high yield perovskite photovoltaic devices have grown by integrating solution-processed precursor stacking layers. *Energy & Environmental Science*, 7(8), 2619-2623.
- [10] Yantara, N., Sabba, D., Yanan, F., Kadro, J. M., Moehl, T., Boix, P. P., & Grätzel, C. (2015). Loading of mesoporous titania films by CH<sub>3</sub>NH<sub>3</sub>PbI<sub>3</sub> perovskite, single-step vs. sequential deposition. *Chemical Communications*, 51(22), 4603-4606.
- [11] Ko, H. S., Lee, J. W., & Park, N. G. (2015). 15.76% efficiency perovskite solar cells prepared under high relative humidity: the importance of PbI<sub>2</sub> morphology in two-step deposition of CH<sub>3</sub>NH<sub>3</sub>PbI<sub>3</sub>. *Journal of Materials Chemistry A*, 3(16), 8808-8815.
- [12] Chen, Q., Zhou, H., Hong, Z., Luo, S., Duan, H. S., Wang, H. H., ... & Yang, Y. (2013). Planar heterojunction perovskite solar cells via vapor-assisted solution process. *Journal of the American Chemical Society*, 136(2), 622-625.

- [13] Patel, J. B., Wong-Leung, J., Van Reenen, S., Sakai, N., Wang, J. T. W., Parrott, E. S., ... & Johnston, M. B. (2017). Influence of Interface Morphology on Hysteresis in vapor-deposited Perovskite Solar Cells. *Advanced Electronic Materials*, 3(2), 1600470.
- [14] Niu, G., Yu, H., Li, J., Wang, D., & Wang, L. (2016). Controlled orientation of perovskite films through mixed cations toward high-performance perovskite solar cells. *Nano Energy*, 27, 87-94.
- [15] Li, J., Jiu, T., Duan, C., Wang, Y., Zhang, H., Jian, H., & Li, Y. (2018). Improved electron transport in MAPbI<sub>3</sub> perovskite solar cells based on dual doping graphdiyne. *Nano Energy*, 46, 331-337.
- [16] Gong, J., Yang, M., Rebollar, D., Rucinski, J., Liveris, Z., Zhu, K., & Xu, T. (2018). Divalent anionic doping in perovskite solar cells for enhanced chemical stability. *Advanced Materials*, 30(34), 1800973.
- [17] Ahmad, Z., Shikoh, A. S., Paek, S., Nazeeruddin, M. K., Al-Muhtaseb, S. A., Touati, F., ... & Al-Thani, N. J. (2019). Degradation analysis in mixed (MAPbI<sub>3</sub> and MAPbBr<sub>3</sub>) perovskite solar cells under thermal stress. *Journal of Materials Science: Materials in Electronics*, 30(2), 1354-1359.
- [18] Abdelmageed, G., Jewell, L., Hellier, K., Seymour, L., Luo, B., Bridges, F., & Carter, S. (2016). Mechanisms for light-induced degradation in MAPbI<sub>3</sub> perovskite thin films and solar cells. *Applied Physics Letters*, 109(23), 233905.
- [19] Ono, L. K., Raga, S. R., Remeika, M., Winchester, A. J., Gabe, A., & Qi, Y. (2015). Pinhole-free hole transport layers significantly improve the stability of MAPbI<sub>3</sub>-based perovskite solar cells under operating conditions. *Journal of Materials Chemistry A*, 3(30), 15451-15456.
- [20] Yu, W., Yu, S., Zhang, J., Liang, W., Wang, X., Guo, X., & Li, C. (2018). Two-in-one additive-engineering strategy for improved air stability of planar perovskite solar cells. *Nano Energy*, 45, 229-235.
- [21] Fateev, S. A., Petrov, A. A., Khrustalev, V. N., Dorovatovskii, P. V., Zubavichus, Y. V., Goodilin, E. A., & Tarasov, A. B. (2018). Solution processing of methylammonium lead iodide perovskite from  $\gamma$ -butyrolactone: crystallization mediated by solvation equilibrium. *Chemistry of Materials*, 30(15), 5237-5244.
- [22] Chen, L. C., Lee, K. L., Wu, W. T., Hsu, C. F., Tseng, Z. L., Sun, X. H., & Kao, Y. T. (2018). Effect of different CH<sub>3</sub> NH<sub>3</sub> PbI<sub>3</sub> morphologies on photovoltaic properties of perovskite solar cells. *Nanoscale research letters*, 13(1), 140.
- [23] Banerjee, D., & Chattopadhyay, K. K. (2018). Hybrid Inorganic Organic Perovskites: A Low-Cost-Efficient Optoelectronic Material. In *Perovskite Photovoltaics* (pp. 123-162). Academic Press.
- [24] Liu, C., Cheng, Y. B., & Ge, Z. (2020). Understanding of perovskite crystal growth and film formation in scalable deposition processes. *Chemical Society Reviews*, 49(6), 1653-1687.

- [25] Guo, P., Ye, Q., Yang, X., Zhang, J., Xu, F., Shchukin, D., ... & Wang, H. (2019). Surface & grain boundary co-passivation by fluorocarbon-based bifunctional molecules for perovskite solar cells efficiency over 21%. *Journal of materials chemistry A*, 7(6), 2497-2506.
- [26] Giesbrecht, N., Schlipf, J., Grill, I., Rieder, P., Dyakonov, V., Bein, T., ... & Docampo, P. (2018). Single-crystal-like optoelectronic properties of MAPbI<sub>3</sub> perovskite polycrystalline thin films. *Journal of Materials Chemistry A*, 6(11), 4822-4828.
- [27] Jones, T. W., Osherov, A., Ansari, M., Sponseller, M., Duck, B. C., Jung, Y. K., ... & Li, Y. (2019). Lattice strain causes non-radiative losses in halide perovskites. *Energy & Environmental Science*, 12(2), 596-606.
- [28] Tombe, S., Adam, G., Heilbrunner, H., Yumusak, C., Apaydin, D. H., Hailegnaw, B., ... & Sariciftci, N. S. (2018). The influence of perovskite precursor composition on the morphology and photovoltaic performance of mixed halide MAPbI<sub>3-x</sub>Cl<sub>x</sub> solar cells. *Solar Energy*, 163, 215-223.
- [29] Sun, C., Guo, Y., Fang, B., Guan, L., Duan, H., Chen, Y., ... & Liu, H. (2017). Facile preparation of high-quality perovskites for efficient solar cells via a fast conversion of wet PbI<sub>2</sub> precursor films. *RSC advances*, 7(36), 22492-22500.
- [30] Ngo, T. H., Gil, B., Shubina, T. V., Damilano, B., Vezian, S., Valvin, P., & Massies, J. (2018). Enhanced excitonic emission efficiency in porous GaN. *Scientific reports*, 8(1), 1-9.
- [31] Brennan, M. C., Zinna, J., & Kuno, M. (2017). Existence of a size-dependent Stokes shift in CsPbBr<sub>3</sub> perovskite nanocrystals. *ACS Energy Letters*, 2(7), 1487-1488.
- [32] Bouich, A., Ullah, S., Marí, B., Atourki, L., & Touhami, M. E. (2021). One-step synthesis of FA1-xGAXPbI<sub>3</sub> perovskites thin film with enhanced stability of alpha (α) phase. *Materials Chemistry and Physics*, 258, 123973.
- [33] Bouich, A., Mari, B., Atourki, L., Ullah, S., & Touhami, M. E. (2021). Shedding Light on the Effect of Diethyl Ether Antisolvent on the Growth of (CH<sub>3</sub>NH<sub>3</sub>)PbI<sub>3</sub> Thin Films. *JOM*, 73(2), 551-557. [34] Huang, J., Tan, S., Lund, P. D., & Zhou, H. (2017). Impact of H<sub>2</sub>O on organic-inorganic hybrid perovskite solar cells. *Energy & Environmental Science*, 10(11), 2284-2311.
- [35] Kundu, S., and Timothy L. K. In situ studies of the degradation mechanisms of perovskite solar cells. *EcoMat* 2, no. 2 (2020): e12025.
- [36] Mesbahi, O., Tlemçani, M., Janeiro, F. M., Hajjaji, A., & Kandoussi, K. (2021). Sensitivity analysis of a new approach to photovoltaic parameters extraction based on the total least squares method. *Metrology and Measurement Systems*, 751-765.





# Tetrabutylammonium (TBA)-Doped Methylammonium Lead Iodide: High Quality and Stable Perovskite Thin Films

Amal Bouich<sup>1,2\*</sup>, Júlia Mari-Guaita<sup>1</sup>, Bouchta Sahraoui<sup>3</sup>, Pablo Palacios<sup>2</sup> and Bernabé Mari<sup>1</sup>

<sup>1</sup>Institut de Disseny i Fabricació, Universitat Politècnica de València, València, Spain, <sup>2</sup>Física Aplicada a Las Ingenierías Aeronáutica y Naval and Instituto de Energía Solar, Universitat Politècnica de Madrid, Madrid, Spain, <sup>3</sup>Institut des Sciences et Technologies Moléculaires d'Angers, University of Angers, Angers, France

This work reported the successive incorporation of tetrabutylammonium (TBA) into Methylammonium lead iodide (MAPbI<sub>3</sub>) perovskite. The thin films were characterized by X-Ray diffraction (XRD), Scanning electron microscopy (SEM), Transmittance electron microscopy (TEM), Atomic force microscopy (AFM), and UV-Visible spectroscopy. It was shown that introducing TBA increases the crystallinity, grain size, surface morphology without pin-hole, and roughness of the MAPbI<sub>3</sub> thin films. Moreover, the MA<sub>(1-x)</sub>TBA<sub>x</sub>PbI<sub>3</sub> thin film shows better stability in a relative humidity of ~60% after 15 days than the pure MAPbI<sub>3</sub> thin film. The obtained results are hoped to be helpful for stability and improvement of the performance of the MAPbI<sub>3</sub> thin films by doping TBA cations under ambient conditions.

**Keywords:** MA<sub>(1-x)</sub>TBA<sub>x</sub>PbI<sub>3</sub>, XRD, SEM, TEM, PL, UV-visible spectroscopy

## HIGHLIGHTS

- The MA(1-X)TBAX PbI3 thin film crystallinity was enhanced with TBA incorporation.
- The morphology of MAPbI3 improved with a pinhole-free surface.
- Optical and PL properties were boosted with the TBA incorporation into MAPbI3 thin film.
- MA(1-X)TBAX PbI3 thin film shows better stability than pure MAPbI3 thin film.

## INTRODUCTION

To begin with, nowadays, the Perovskites with formula ABX<sub>3</sub> (A = cation (Formamidinium (FA), Methylammonium (MA)), B = metal cation and X is a halogen anion VII halides (Br<sup>-</sup>, Cl<sup>-</sup>, I<sup>-</sup>)), have been demonstrated good absorbers properties for solar cells with higher photovoltaic conversion efficiency (PCE) (Fakharuddin et al., 2019; Weidman et al., 2019). Methylammonium lead triiodide (MAPbI<sub>3</sub>) solar cells show good optoelectronic properties with a bandgap between 1.4 and 1.5 eV (Wang et al., 2019), a high absorption coefficient around 10<sup>5</sup>cm<sup>-1</sup> (Im et al., 2011; De Roo et al., 2016) with amazing PCE = 25% (Xiao et al., 2014; Park, 2015). To manufacture MAPbI<sub>3</sub> Solar cells, low-cost and simple techniques have been used to deposit the MAPbI<sub>3</sub> film: thermal vapor deposition, two-step vapor-assisted deposition (Chen et al., 2013), two-step solution deposition, and one-step solution deposition (Yantara et al., 2015; Patel et al., 2017). Despite the outstanding PCE reported of MAPbI<sub>3</sub> solar cells, the problem of MAPbI<sub>3</sub> degradation by the loss of MAI and formation of lead

## OPEN ACCESS

### Edited by:

Anurag Krishna,  
Swiss Federal Institute of Technology  
Lausanne, Switzerland

### Reviewed by:

Letian Dou,  
Purdue University, United States  
Nouredine El Messaoudi,  
Université Ibn Zohr, Morocco  
Mouhaydine Temrani,  
University of Evora, Portugal

### \*Correspondence:

Amal Bouich  
ambo1@doctor.upv.es

### Specialty section:

This article was submitted to  
Solar Energy,  
a section of the journal  
Frontiers in Energy Research

**Received:** 21 December 2021

**Accepted:** 13 January 2022

**Published:** 22 February 2022

### Citation:

Bouich A, Mari-Guaita JA, Sahraoui B,  
Palacios P and Mari B (2022)  
Tetrabutylammonium (TBA)-Doped  
Methylammonium Lead Iodide: High  
Quality and Stable Perovskite  
Thin Films.  
Front. Energy Res. 10:840817.  
doi: 10.3389/fenrg.2022.840817



# Chapter 5: Manufacture of High-Efficiency and Stable-Lead Free Solar Cells Through Antisolvent Quenching Engineering

Authors: Amal Bouich<sup>1,2,3\*</sup>, Julia Marí-Guaita<sup>1</sup>, Bernabé Marí Soucase<sup>1</sup>, Pablo Palacios<sup>2,3</sup>.

<sup>1</sup>Escuela Técnica Superior de Ingeniería del Diseño: Universitat Politècnica de València, València, Spain.

<sup>2</sup>Instituto de Energía Solar, ETSI Telecomunicación, Universidad Politécnica de Madrid, Ciudad Universitaria, s/n, Madrid, Spain

<sup>3</sup>Dept. Física Aplicada a las Ingenierías Aeronáutica y Naval. ETSI Aeronáutica y del Espacio, Universidad Politécnica de Madrid, Pz. Cardenal Cisneros, 3, 28040 Madrid, Spain

## Abstract

The antisolvent quenching has shown to significantly enhance several perovskite films used in solar cells; however, there have been no studies on its impact on MASnI<sub>3</sub>. Here, we investigate the role that different antisolvents such as diethyl ether, toluene, and chlorobenzene have on the growth of the MASnI<sub>3</sub> films. Crystallinity, morphology, topography, and optical properties of the obtained thin films were characterized by X-ray diffraction (XRD), scanning electron microscopy (SEM), photoluminescence (PL) measurements, and UV-visible spectroscopy. The impact of the different antisolvent treatments was evaluated based on the surface homogeneity as well as the structure of the MASnI<sub>3</sub> thin films. Also, the thermal annealing was optimized to control the crystallization. The antisolvent applied was modified to manage the supersaturation process better. The results support the use of chlorobenzene and toluene to reduce pinholes and increase grain size. Toluene was found to improve further the morphology and the stability of the thin films, as it showed less degradation after four weeks under dark with 60% humidity. Furthermore, we performed the simulation using SCAPS-1D software to observe the effect of these antisolvents on the performance of MASnI<sub>3</sub>-based solar cells. Additionally, we produced the device FTO/TiO<sub>2</sub>/MASnI<sub>3</sub>/Spiro-OMeTAD/Au, with a remarkable photoconversion efficiency (PCE) improvement from 5.11 % for the MASnI<sub>3</sub> Device by using chlorobenzene. While PCE 9.44% for MASnI<sub>3</sub> Device by using Toluene with better stability, the results here support antisolvent quenching as a reproducible method for improving perovskite devices under ambient conditions.

## 1. Introduction

Solar energy is considered a basis of clean and abundant energy, so it has become essential to take a lot more advantage of solar radiation as an energy source in the field of photovoltaics [1]; recently, organic, and inorganic perovskite technologies have become attractive and promising materials for researchers, especially those based on methylammonium halides. Perovskite devices showing power conversion efficiencies higher than 23% have been reported [2]. Also, perovskite materials have remarkable optical and electronic properties, such as broad light absorption coefficient, long charge carrier diffusion length, and small exciton binding energy, and they are able to generate electrons and hole pairs [3]. Furthermore, for perovskite thin-film fabrication, a variety of techniques have been used, such as one-step solution deposition [4,5], two-step solution deposition [6], vapor deposition [7], and thermal deposition [8]. One-step deposit carried out via spin-coating demonstrates an excellent capability to fabricate perovskite devices. Moreover, the device's efficiency reported homogeneous and compact thin films using the spin coating technique. It has been shown that the morphology of perovskite thin films plays a vital role in device performance. Many methods and treatments have been introduced to optimize product quality by improving the surface homogeneity and crystallinity of the films.

In this study, the thin films of  $\text{MASnI}_3$  were treated with different antisolvents to see how they affected the supersaturation of the solvent. We report that complex interactions between the solvent and antisolvent are related to the film's physicochemical properties; therefore, choosing the antisolvent type is critical for improving the perovskite film morphology and, in turn, boosting the device performance. The antisolvent effects were observed in the variation of morphology, structure, and composition of the thin films. Toluene (TOL), chlorobenzene (CBZ), and diethyl ether (DE) were the antisolvents used in this investigation. The obtained  $\text{MASnI}_3$  samples were further analyzed by other characterization techniques such as XRD, SEM, AFM, and optical and photoluminescence analysis. Additionally, we produced the device FTO/ $\text{TiO}_2$ / $\text{MASnI}_3$ /Spiro-OMeTAD/Au, with an amazing photoconversion efficiency (PCE).

## 2. Experimental Procedure

### Materials

Tin (II) iodide ( $\text{SnI}_2$ ), Methylammonium iodide (MAI), n n-dimethylformamide (DMF), and dimethyl sulfoxide (DMSO) were used for manufacturing the optoelectronic devices. Diethyl ether, chlorobenzene, and toluene were used as antisolvents. Fluorine tin oxide-coated glass (FTO) was used as a substrate.

### Sample preparation

The prepared solution of MASnI<sub>3</sub> was spin-coated onto the FTO substrate at 2000 rpm for 20 s. Different antisolvents were dripped to the MASnI<sub>3</sub> thin films, and subsequently, the as-prepared MASnI<sub>3</sub> samples were annealed in a vacuum for 20 minutes at 250 °C.

The perovskite thin film's crystal structure analysis was performed by the XRD RIGAKU Ultima IV diffractometer. The surface morphology was investigated through scanning emission microscopy (SEM) at different magnifications. The film's topography was characterized using atomic force microscopy (AFM). The absorption was measured using a UV-Visible wavelength range from 300 to 850 nm, and photoluminescence (PL) was performed using a He-Cd laser.

### 3. Results and discussion

The influence of antisolvent on the films' phase structure and microstructure was studied by X-ray diffraction. Figure 1 shows the X-ray diffraction patterns of MASnI<sub>3</sub> films treated with different antisolvents. The diffraction peaks that appear at: 14°, 28°, 31°, 38°, and 31° correspond to the (110), (220), (222), (224), and (314) respectively. These results are in good agreement with those found elsewhere [9, 10]. XRD results of MASnI<sub>3</sub> films prepared show good crystallinity, and the characteristic (110) peak intensity increases enormously by using toluene as an antisolvent compared to chlorobenzene and diethyl ether. The intensity decrement can be attributed to the excessive solubility of methylammonium iodide (MAI).

#### Lattice parameters

The lattice parameters were calculated using (1) and (2) with different diffraction two theta angles.

$$\frac{1}{d^2} = \frac{k^2}{a^2} + \frac{l^2}{c^2} \quad (1)$$

$$\eta\lambda = d_{hkl}\sin(\theta) \quad (2)$$

Where a, b, c are the lattice parameters, *hkl* are miller indices, *d<sub>hkl</sub>* is the interplanar distance, and *k* is the wavelength (0.154 nm). The obtained lattice parameters of the main (110) peak were a = b = 8 Å, c = 11.9 Å, corresponding to the tetragonal structure.

The lattice strain ( $\epsilon$ ) indicates the thin films crystals' deformation calculated from the equation (3). The obtained results are summarized between 340 nm and 400 nm in Table 1.

$$\beta\cos(\theta) = \frac{k\lambda}{D} + 4\epsilon\sin(\theta) \quad (3)$$

Where  $\beta$  is the FWHM value,  $k$  is the dielectric constant ( $k = 0.9$ ),  $\lambda$  is the wavelength of the X-ray ( $\lambda = 0.1540$  nm),  $\theta$  is the Bragg diffraction angle and  $D$  is the crystallite size (nm). Equation (4) below shows the estimated grain size dislocation density.

$$\gamma = \frac{1}{D^2} \quad (4)$$

Table 1 shows that the four samples have different grain sizes from 300 nm to 400 nm, with  $\text{MASnI}_3$  treated with different antisolvent. The larger grain size of 400 nm is for the toluene, and the lower effective lattice around 0.37 is explained by a lesser of deficiencies and distortions of the grains.

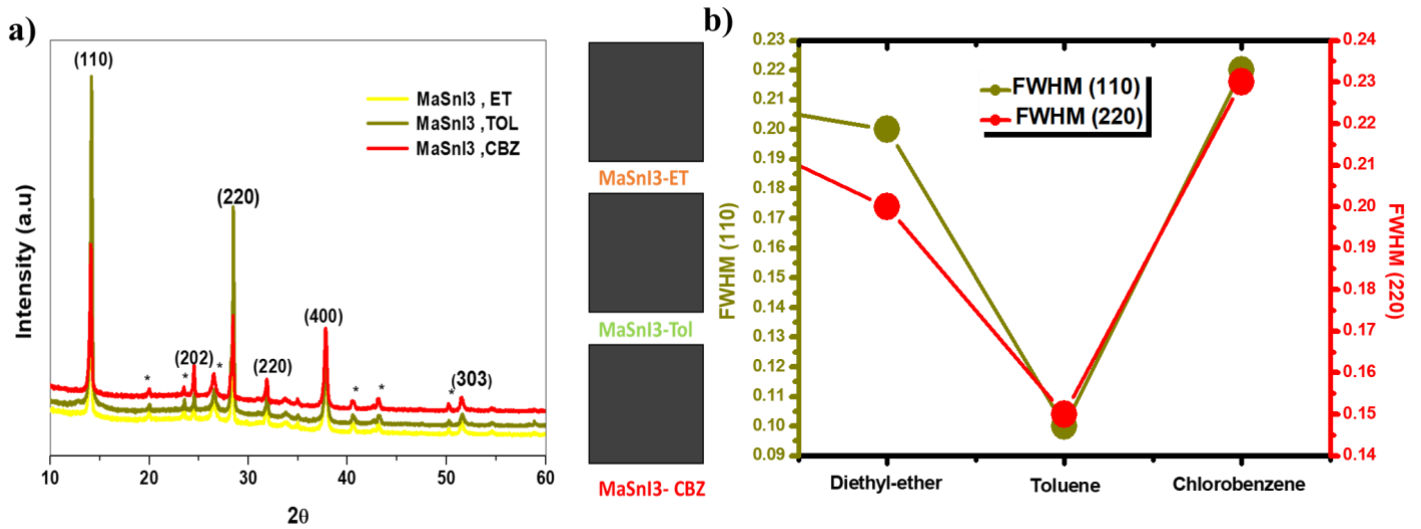


**Figure 1.** XRD patterns of  $\text{MASnI}_3$  Films treated with different antisolvents, toluene, chlorobenzene, and diethyl ether.

**Table 1.** Parameters of XRD spectra of  $\text{MASnI}_3$  films treated with different antisolvents, toluene, chlorobenzene, and diethyl ether.

Sample ID	Grain size (nm)	Dislocation density ( $\text{nm}^{-1}$ )	Lattice strain ( $\epsilon$ )
$\text{MASnI}_3$ - ET	340	$1.05 \times 10^{-5}$	0.38
$\text{MASnI}_3$ - CBZ	360	$0.90 \times 10^{-5}$	0.39
$\text{MASnI}_3$ - Tol	400	$0.62 \times 10^{-5}$	0.37

Figure 2 shows (SEM) images of  $\text{MASnI}_3$  treated with different antisolvents. The surface morphology of  $\text{MASnI}_3$  was examined with SEM. It is found that with diethyl ether the crystals are poorly formed. Even the chlorobenzene was not changing that much in the morphology of the film. However, toluene significantly altered the morphology, and the largest crystal size was obtained, further explaining the change in the morphology of  $\text{MASnI}_3$  related to the type of antisolvent [11, 12]. Besides, the addition of antisolvent

gave fine needles that agglomerate easily. This proves that supersaturation plays a vital role in a crystallization system and influences the crystals' size, shape, and degree of accumulation [13,14]. The remaining solvent is removed under 250 ° C during the annealing treatment. The conversion of forerunners to the perovskite phase is almost perfect in all cases, but we are introducing to affect the surface.

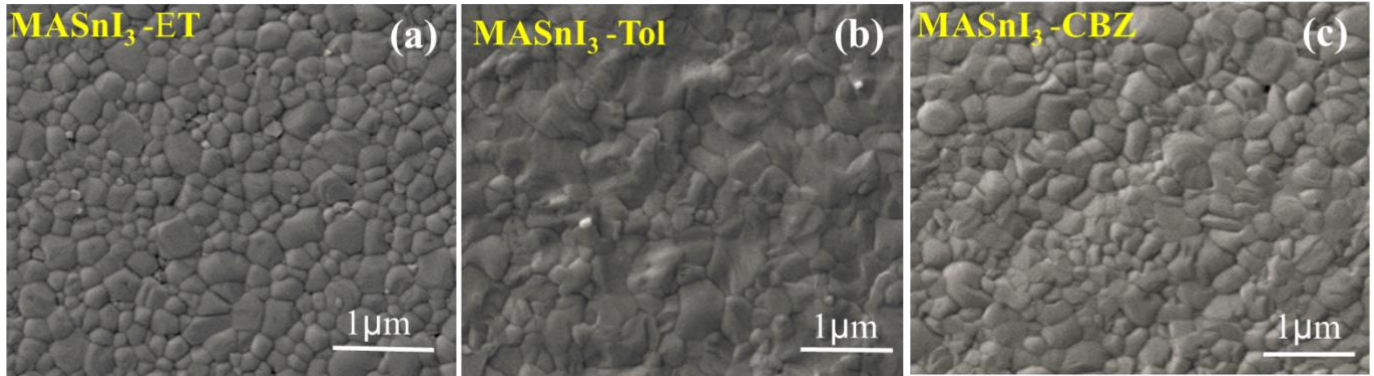


**Figure 2.** SEM images of MASnI<sub>3</sub> Films treated with different antisolvents: a) Diethyl ether, b) Toluene, c) Chlorobenzene.

Figure 3 shows the characteristic peak of PL of the three MASnI<sub>3</sub> samples for the three MASnI<sub>3</sub> with ET, TOL and CBZ applied as antisolvents in the range of 750 to 800 nm [16]. The PL peak of MASnI<sub>3</sub> treated with toluene shows a higher intensity than the MASnI<sub>3</sub> sample treated with diethyl ether or chlorobenzene. The MASnI<sub>3</sub> treated with TOL also shows the optimal bandgap around 1.75 eV. It can be related to phase transitions commonly found for halide perovskite [17,19].

**Table 2.** Optical Bandgap of the MASnI<sub>3</sub> treated with Toluene, Diethyl ether, and Chlorobenzene.

Sample	$\lambda$ (nm)	Eg-PL (eV)	$\lambda$ (nm)	Eg-UV (eV)	Shift stokes (meV)
MASnI <sub>3</sub> -ET	779	1.59	750	1.63	40
MASnI <sub>3</sub> -TOL	782	1.58	759	1.60	20
MASnI <sub>3</sub> -CBZ	787	1.57	760	1.62	50

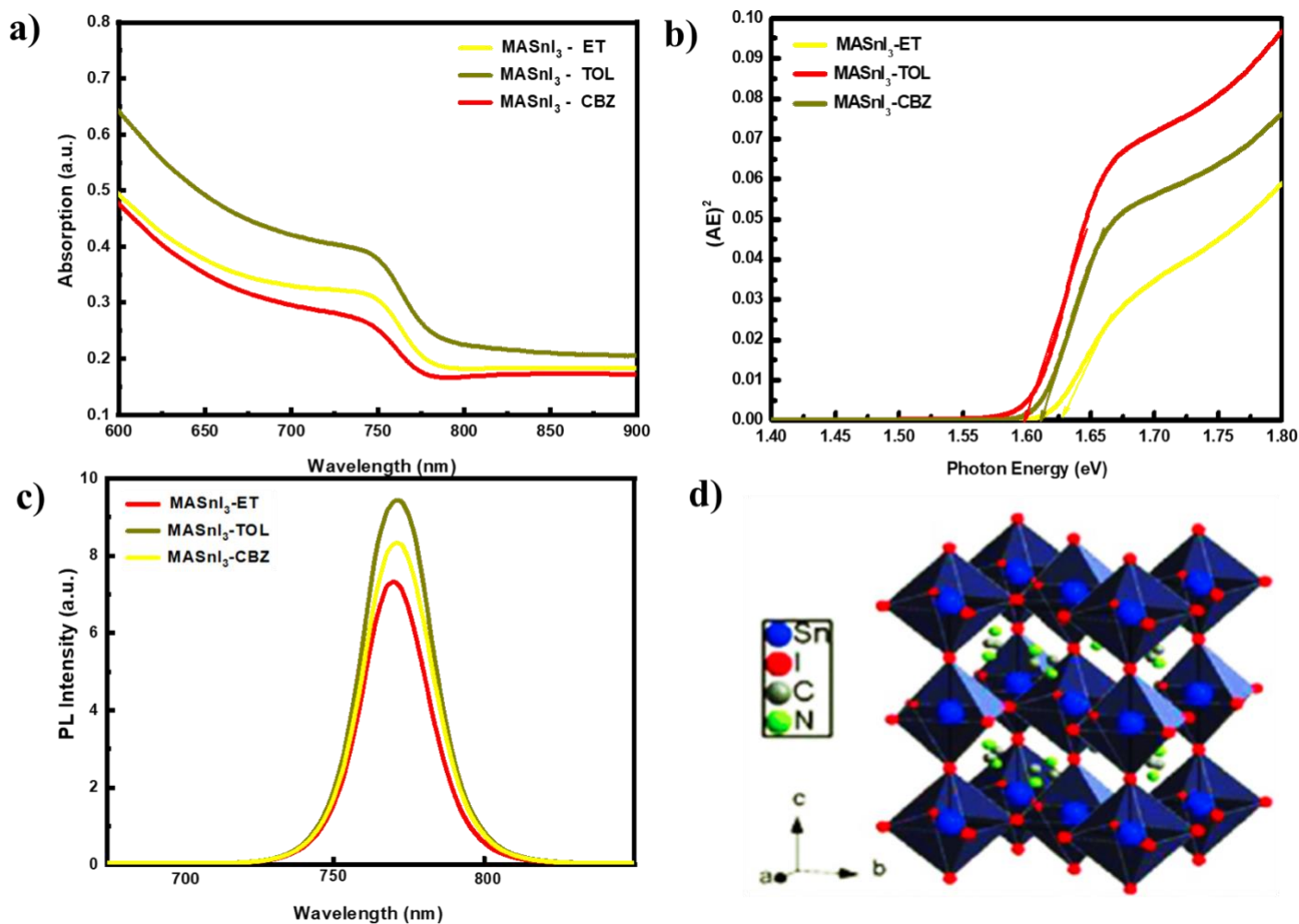


**Figure 3.** a) Absorption of MASnI<sub>3</sub> films, b) bandgap, c) photoluminescence (PL), d) Crystal structure of MASnI<sub>3</sub>.

#### 4. Degradation study

Oxygen and humidity significantly impact the stability of perovskite solar cells. Once the film is exposed to extreme conditions of the environment, the degradation mechanism of MASnI<sub>3</sub> film has been attributed to reducing these compounds to SnI<sub>2</sub>, MA, and HI. The stability of MASnI<sub>3</sub> films was examined after four weeks of being treated with the three antisolvents. To investigate the degree of degradation of MASnI<sub>3</sub> samples, we performed XRD and SEM measurements on both fresh and four-week-old MASnI<sub>3</sub> samples, kept under 60% humidity in a dark environment.



The XRD patterns for the four weeks aged MASnI<sub>3</sub> films treated with chlorobenzene and toluene antisolvents, there is a slightly reduced intensity of characteristic peaks (110) and (220) when compared to MASnI<sub>3</sub> films treated with diethyl-ether in which there is a dramatic increase in the intensity (Figure 4a, b, and c). In this regard, using the chlorobenzene and toluene as antisolvents enhances the stability of MASnI<sub>3</sub> films more than the samples treated with diethyl ether. Similar results have been reported [20, 24]. SEM images also support this finding (Figures 4d, e, and f). The surface morphology changes are observed in the SEM images of aged MASnI<sub>3</sub> films with new grain boundaries and new defects. Therefore, the degradation process differs between the antisolvent-treated films.

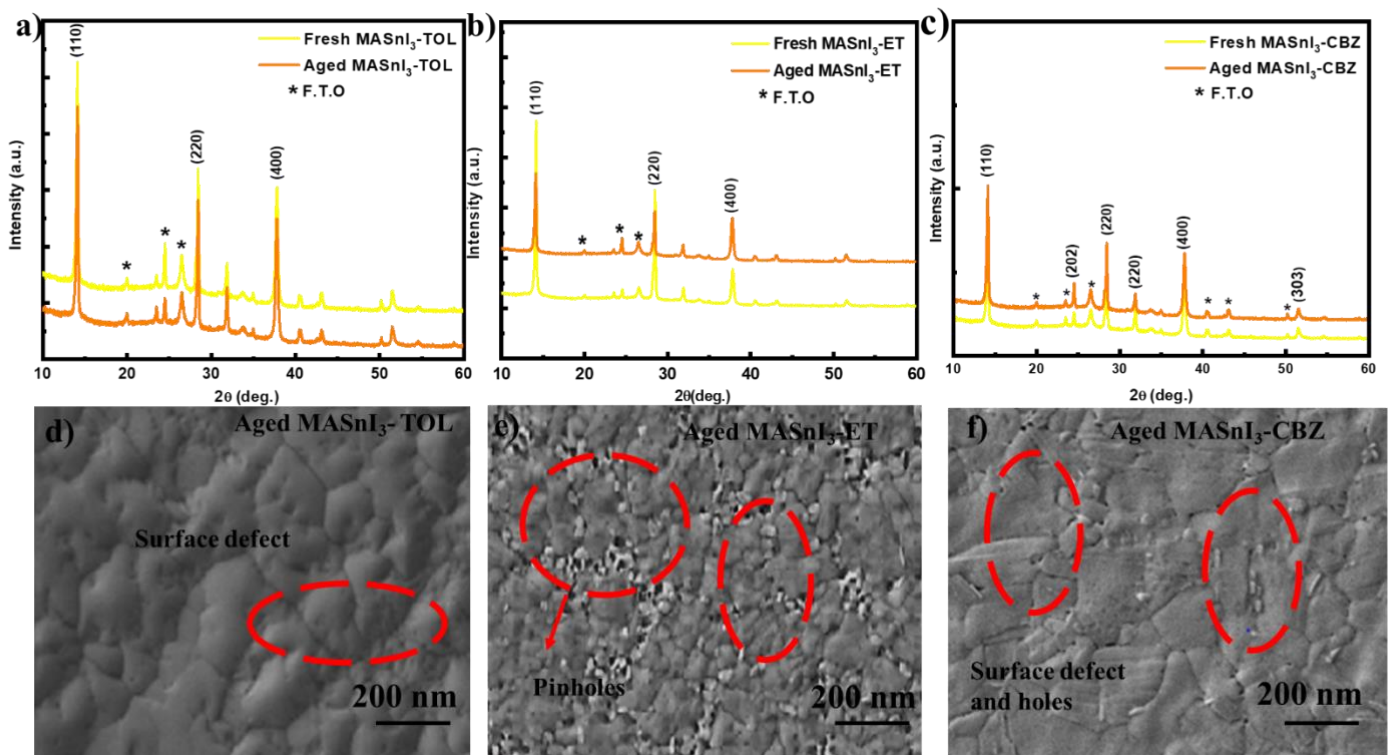


**Figure 4.** Degradation study of MASnI<sub>3</sub> treated with different antisolvents (a) XRD pattern fresh and aged MASnI<sub>3</sub> treated by toluene (b) XRD pattern fresh and aged MASnI<sub>3</sub> treated by diethyl ether (c) XRD pattern fresh and aged MASnI<sub>3</sub> treated by chlorobenzene (d) SEM image of Aged MASnI<sub>3</sub> treated by toluene (e) SEM image of Aged MASnI<sub>3</sub> treated by toluene (f) SEM image of aged MASnI<sub>3</sub> treated by chlorobenzene.

## 5. Device performance

We have seen that the thickness varies when different antisolvents are used, and similarly, the bandgap varies when MASnI<sub>3</sub> is used. Solar cells are more sensitive to variation in

thickness related to the bandgap of their absorbing layers. In order to keep this impact on the cell's performance, we simulate a proposed solar cell with a model "Gold/Spiro OmeTAD/MASnI<sub>3</sub>/TiO<sub>2</sub>/FTO/Glass". MASnI<sub>3</sub> is used as an absorbent layer, TiO<sub>2</sub> is used as a hole transfer layer, and glass is used as a substrate.

**Table 3.** Bandgap variation concerning diethyl ether, toluene, and chlorobenzene for MASnI<sub>3</sub>.

Sample	Thickness (nm)	Band gap-UV (eV)
MASnI <sub>3</sub> -ET	200	1.63
MASnI <sub>3</sub> - TOL	210	1.60
MASnI <sub>3</sub> -CBZ	210	1.62

The simulation parameters used in SCAPS-1D software are shown in Table 1 and Table 2. Table 1 shows our experimental-based calculations, which we use for Table 2. The work function for back and front contact are left as default in SCAPS-1D. The proposed solar cell used in SCAPS-1D is arranged according to the experimentally formed solar cell, as shown in Figure 5 and the layers of the cell can be seen in Figure 10.

**Table 4.** Simulation Parameters of MASnI<sub>3</sub>-based solar cell.

Parameters	Spiro	MASnI <sub>3</sub>	TiO <sub>2</sub>	FTO
Thickness ( <i>um</i> )	0.20	Variable	0.05	0.5
Bandgap (eV)	3.17	Variable	3.2	3.5
Electron affinity (eV)	2.05	3.49	3.9	4.0
Dielectric Permittivity	3.00	20.0	9.0	9.0
CB Effective Density of States (1/cm <sup>3</sup> )	2.2 x 10 <sup>18</sup>	1.0E+19	2.0E+17	2.2E+18
VB Effective Density of States (1/cm <sup>3</sup> )	1.8 x 10 <sup>19</sup>	1.0E+19	6.0E+17	1.8E+19
Electron Thermal Velocity (cm/s)	1.0E+7	1.0E+7	1.0E+7	1.0E+7
Hole Thermal Velocity (cm/s)	1.0E+7	1.0E+7	1.0E+7	1.0E+7
Electron Mobility (cm <sup>2</sup> /Vs)	2.0E-4	2.30E+3	1.00E+2	2.00E+1
Hole Mobility (cm <sup>2</sup> /Vs)	2.0E-4	3.20E+2	2.50E+1	1.00E+1
Donor Density ND (1/cm <sup>3</sup> )	0.0E+0	1.0E+9	1.0E+17	1.0E+17
Acceptor Density NA (1/cm <sup>3</sup> )	2.0E+19	1.0E+9	0.0E+0	0.0E+0

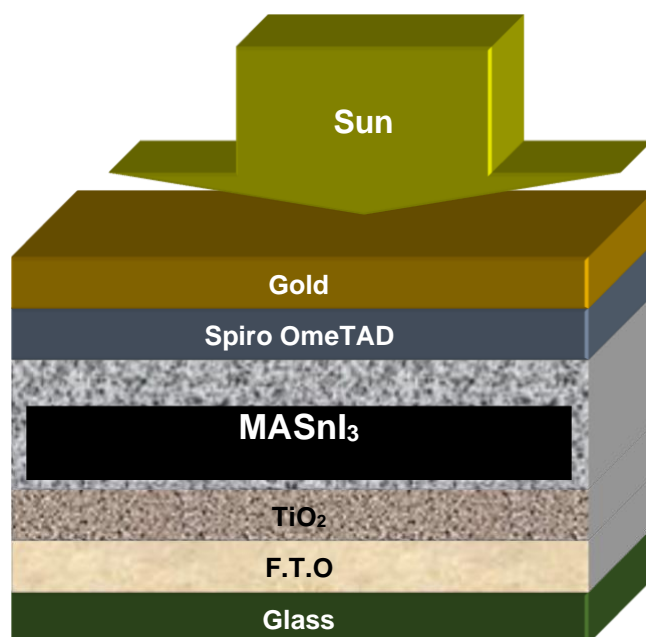


**Figure 5.** Schematic diagram of MASnI<sub>3</sub>-based solar cell.

The SCAPS-1D software was run under 1000 W/m<sup>2</sup> illumination and at ambient temperature (300 K). The series resistance and shunt resistances were kept negligible, and infinite, respectively, which are the ideal values that experimentally do not exist up to these limits. The bandgap and thickness of MASnI<sub>3</sub> were used according to Table 1.

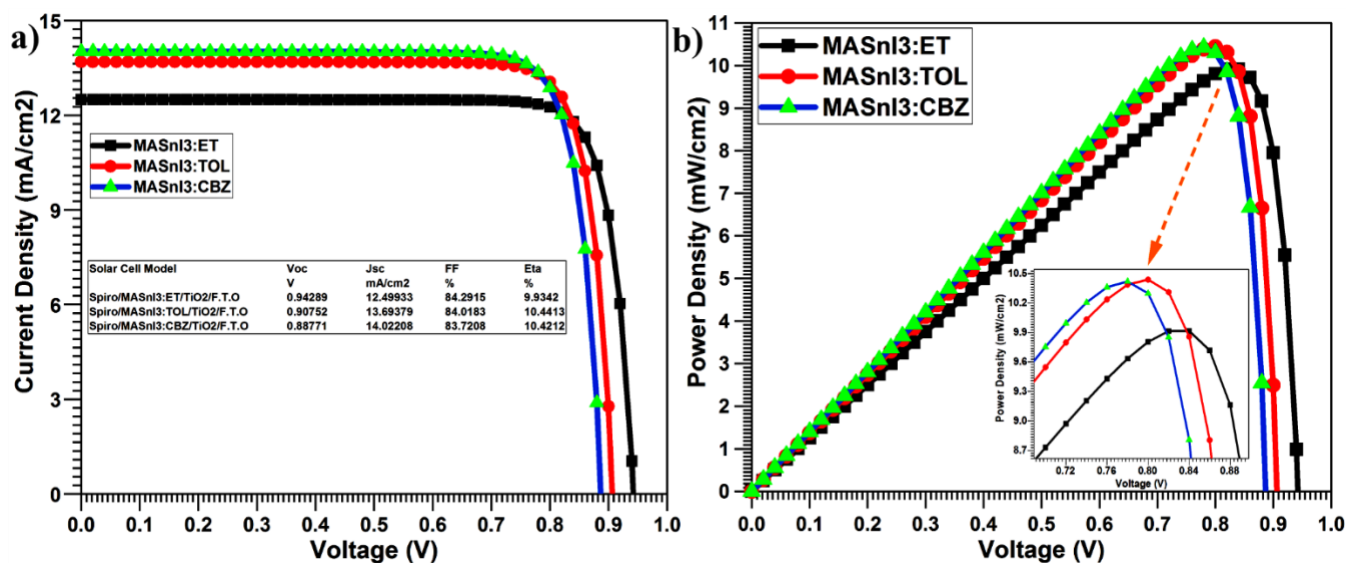


**Figure 6.** (a) J-V and (b) P-V characteristics curves of MASnI<sub>3</sub>-based solar cell.

Figures 2 (a) and (b) show the J-V and P-V curves for MASnI<sub>3</sub>, respectively, and demonstrate how the different antisolvents affect the results. Toluene has a positive

impact on the device; P-V angles deliver the highest power when using toluene as an antisolvent.

diethyl ether antisolvent-based MASnI<sub>3</sub> produced V<sub>oc</sub> of 0.94 V, J<sub>sc</sub> of 12.49 mA/cm<sup>2</sup>, FF of 84.29%, and Eta of 9.93% during the simulation of solar cells. We notice that diethyl ether is less effective because, chlorobenzene V<sub>oc</sub>, J<sub>sc</sub>, FF, and ETA were registered as 0.88 V, 14.02 mA/cm<sup>2</sup>, 83.72%, and 10.42%, respectively, which was good in comparison to when ET was used as antisolvent as shown in Table 3.

**Table 5.** Experimental Characteristics Parameters MASnI<sub>3</sub> of the based solar cell.

Solar Cell Model	V <sub>oc</sub>	J <sub>sc</sub>	FF	Eta
	V	mA/cm <sup>2</sup>	%	%
<b>Spiro-OMeTAD/MASnI<sub>3</sub>: ET/TiO<sub>2</sub>/FTO</b>	0.94	12.49	84.29	9.93
<b>Spiro-OMeTAD /MASnI<sub>3</sub>: TOL/TiO<sub>2</sub>/FTO</b>	0.90	13.69	84.01	10.44
<b>Spiro-OMeTAD /MASnI<sub>3</sub>: CBZ/TiO<sub>2</sub>/FTO</b>	0.88	14.02	83.72	10.42

In summary, TOL is the most profitable antisolvent because it gave excellent results compared to the other two antisolvents. With Toluene treatment for MASnI<sub>3</sub> films, we record V<sub>oc</sub>, J<sub>sc</sub>, FF, and ETA as 0.90 V, 13.69 mA/cm<sup>2</sup>, 84.01%, and 10.44%, respectively.

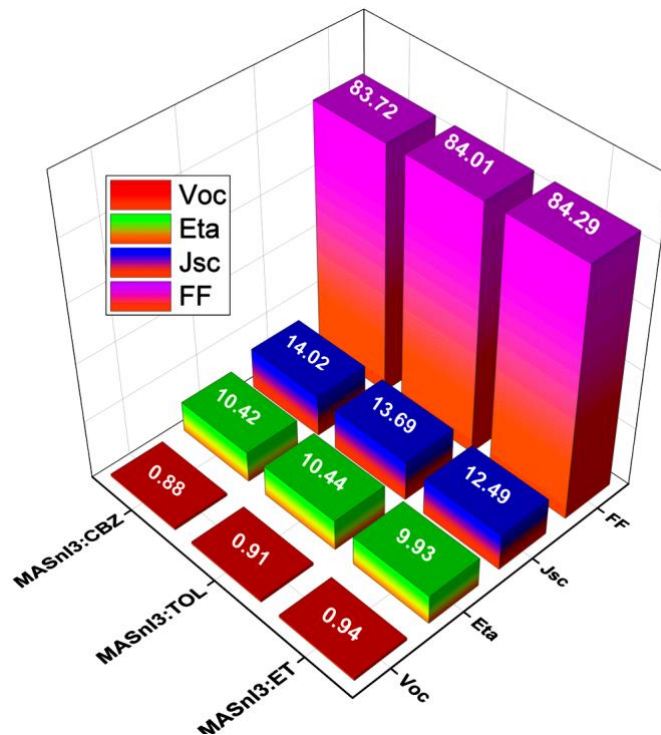


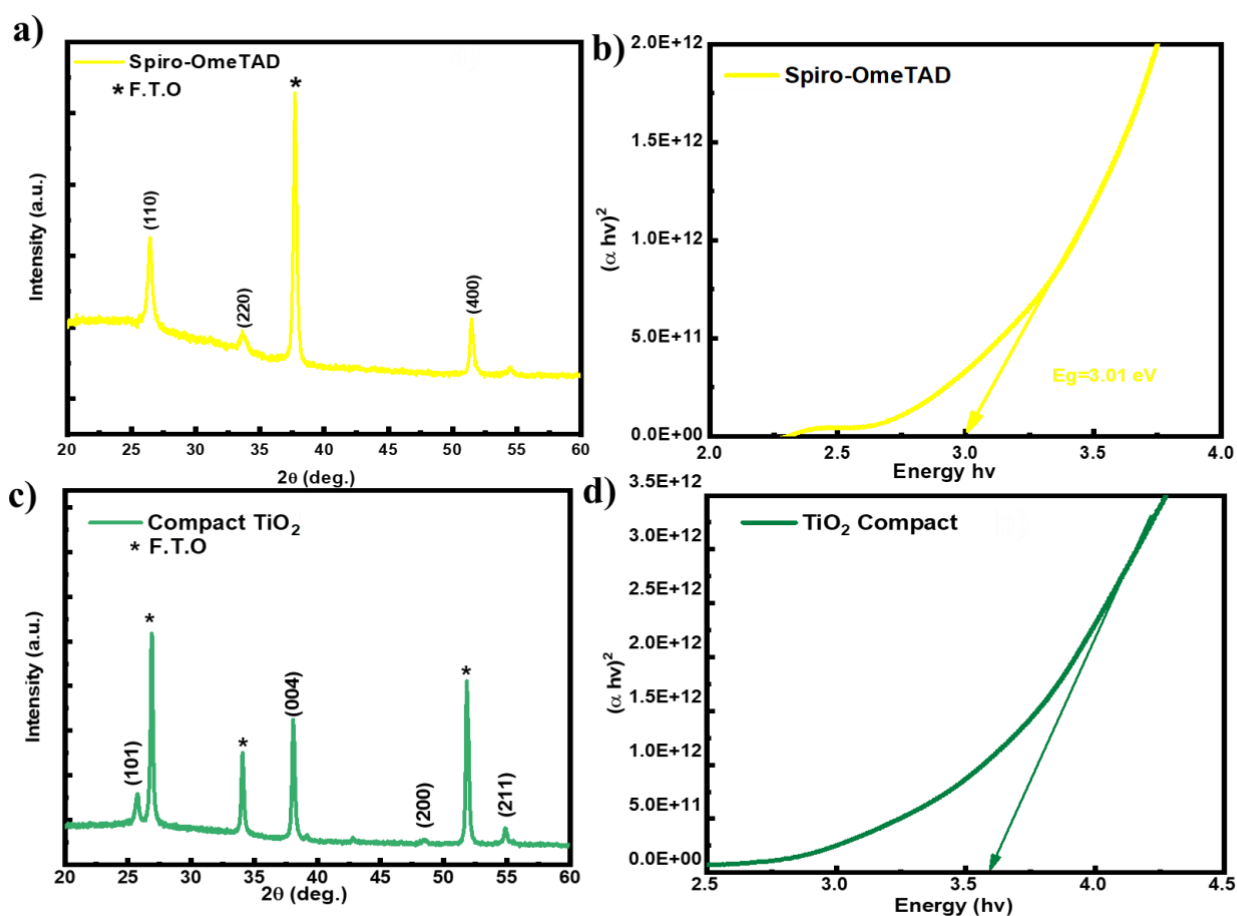
**Figure 7.** Characteristic parameters of MASnI<sub>3</sub>-based solar cell with the different antisolvents.

Here, in Figure 7, we compare the characteristic parameters of MASnI<sub>3</sub> solar cells based on different antisolvents used in the solution. We can observe that toluene would be the optimal antisolvent for preparing the MASnI<sub>3</sub> absorber layer as it gives us the best results of the characteristic parameters for the solar device.

## 6. Device Manufacture Spiro-OMeTAD/MASnI<sub>3</sub>/TiO<sub>2</sub>/FTO

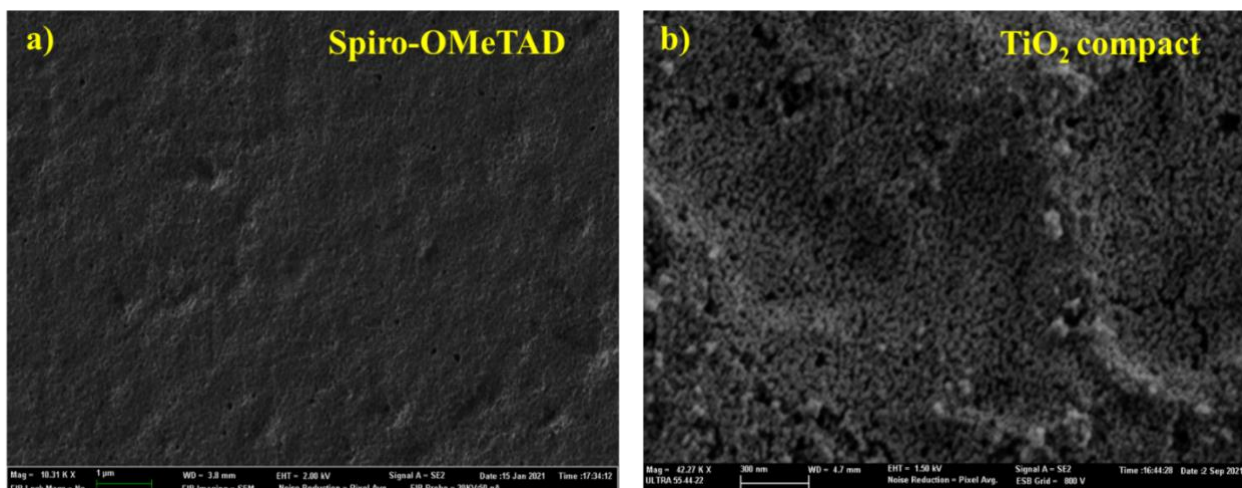
We report XRD analysis for the Spiro-OMeTAD film with characteristic peaks at (110), (220) and (400) (Figure 8 a). These results are in correspondence with previous studies [20]. When calculating the experimental bandgap after the absorbance characterization, we obtained 3.0 eV, which is the optimal bandgap, also previously reported [21].

For the compact TiO<sub>2</sub>, we obtained an XRD analysis with characteristic peaks at (101), (004), (200) and (211) (Figure 8 c). We found the same characteristic peaks when comparing these XRD spectra with the literature [22]. The absorption analysis for TiO<sub>2</sub> gave us an experimental bandgap of 3.6 eV (Figure 8 d).



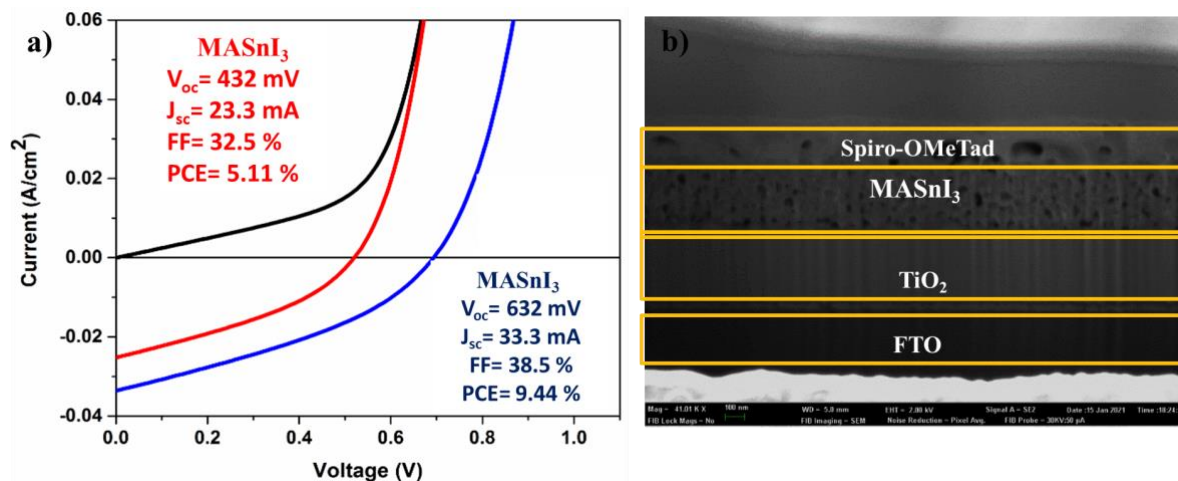
**Figure 8.** a) XRD Pattern of Spiro-OmeTAD film, b) bandgap spectra of Spiro-OmeTAD film, c) XRD Pattern of TiO<sub>2</sub> compact layer, d) bandgap spectra of TiO<sub>2</sub> compact layer.

Figure 9 shows SEM images of both Spiro-OmeTAD and TiO<sub>2</sub> layers. The SEM image of TiO<sub>2</sub> films shows smooth and homogenous surface. The Spiro-OmeTAD film show regular surface with no holes.



**Figure 9.** (a) SEM image of Spiro-OMeTAD film, (b) SEM image of TiO<sub>2</sub> compact layer.

Figure 10 illustrates the photovoltaic performance of MASnI<sub>3</sub>. J-V curves measurement. The prepared perovskite solar cell realized a remarkable PCE improvement from 5.11 % for MASnI<sub>3</sub>-chlorobenzene an open-circuit voltage (V<sub>oc</sub>) of 521.8 mV, short-circuit current (J<sub>sc</sub>) of 25.6 mA cm<sup>-2</sup>, and fill factor (FF) of 34.59 %. While, for PCE 9.44% for treated with Toluene, with V<sub>oc</sub> of 694.6 mV, J<sub>sc</sub> of 33.6 mA cm<sup>-2</sup> and FF of 38.09 %, which is significantly higher than MASnI<sub>3</sub> chlorobenzene based solar cell. It is possible that the use of toluene increases the quality of the film and stability which is helpful to increase the carrier concentration and decreases the electron-hole recombination, which enhances the photoconversion efficiency from 5.11% to 9.44%. The obtained results might be greater and contribute to stable and efficient photovoltaic device commercialization.



**Figure 10.** a) I-V performance of perovskite MASnI<sub>3</sub> (**Red colour**= Chlorobenzene and **blue colour** = toluene) b) cross-section of Lead-Free perovskite solar cell.

## 7. Conclusion

In this work, MASnI<sub>3</sub> thin films have been successfully prepared by the one-step spin coating technique. The effect that the different antisolvents diethyl ether, chlorobenzene, and toluene had on film properties was investigated using XRD, SEM, and optical analysis.

The XRD analysis revealed that all samples had an extraordinary (110) peak intensity by treating MASnI<sub>3</sub> film. The XRD results showed that the model toluene was applied superior crystallinity, reflected by the intensity of the (110) peak. This result was supported by AFM and SEM results, where the applying toluene led to increased grain size. Furthermore, the sample to which toluene was applied gave the highest absorbance. Our results suggest that using toluene to carry out the antisolvent quenching step in a one-step spin-coating method will lead to superior perovskite film and higher device efficiencies. Using SCAPS-1D software, we also find the effect of three different antisolvent on solar cell performance, like diethyl-ether, Chlorobenzene, and toluene, which gave the efficiencies of 9.93, 10.42, and 10.44%, respectively, hence concluding that Toluene is the well-optimized antisolvent for MASnI<sub>3</sub> absorber layer. Additionally, we produced the device FTO/TiO<sub>2</sub>/MASnI<sub>3</sub>/Spiro-OMeTAD/Au, with a remarkable photoconversion efficiency (PCE) of 9.11% on case of MASnI<sub>3</sub> film treated with toluene.

## References

- [1] Green, M. A., Emery, K., Hishikawa, Y., Warta, W., & Dunlop, E. D. (2015). Solar cell efficiency tables (Version 45). *Progress in photovoltaics: research and applications*, 23(1), 1-9.
- [2] Jeon, N. J., Na, H., Jung, E. H., Yang, T. Y., Lee, Y. G., Kim, G., ... & Seo, J. (2018). A fluorene-terminated hole-transporting material for highly efficient and stable perovskite solar cells. *Nature Energy*, 3(8), 682.
- [3] Quarti, C., Mosconi, E., Ball, J. M., D'Innocenzo, V., Tao, C., Pathak, S., ... & De Angelis, F. (2016). Methylammonium lead iodide's structural and optical properties across the tetragonal to cubic phase transition: implications for perovskite solar cells. *Energy & Environmental Science*, 9(1), 155-163.
- [4] Im, J. H., Kim, H. S., & Park, N. G. (2014). Morphology-photovoltaic property correlation in perovskite solar cells: One-step versus two-step deposition of  $\text{CH}_3\text{NH}_3\text{PbI}_3$ . *All Materials*, 2(8), 081510.
- [5] Carnie, M. J., Charbonneau, C., Davies, M. L., Troughton, J., Watson, T. M., Wojciechowski, K., ... & Worsley, D. A. (2013). A one-step low-temperature processing route for organolead halide perovskite solar cells. *Chemical Communications*, 49(72), 7893-7895.
- [6] Bi, D., Moon, S. J., Häggman, L., Boschloo, G., Yang, L., Johansson, E. M., ... & Hagfeldt, A. (2013). Using a two-step deposition technique to prepare perovskite ( $\text{CH}_3\text{NH}_3\text{PbI}_3$ ) for thin-film solar cells based on  $\text{ZrO}_2$  and  $\text{TiO}_2$  mesostructures. *RSC Advances*, 3(41), 18762-18766.
- [7] Chen, Q., Zhou, H., Hong, Z., Luo, S., Duan, H. S., Wang, H. H., ... & Yang, Y. (2013). Planar heterojunction perovskite solar cells via vapor-assisted solution process. *Journal of the American Chemical Society*, 136(2), 622-625.
- [8] Leyden, M. R., Ono, L. K., Raga, S. R., Kato, Y., Wang, S., & Qi, Y. (2014). High-performance perovskite solar cells by hybrid chemical vapor deposition. *Journal of Materials Chemistry A*, 2(44), 18742-18745.
- [9] Kong, W., Ye, Z., Qi, Z., Zhang, B., Wang, M., Rahimi-Iman, A., & Wu, H. (2015). Characterization of an abnormal photoluminescence behavior upon crystal-phase transition of perovskite  $\text{CH}_3\text{NH}_3\text{PbI}_3$ . *Physical Chemistry Chemical Physics*, 17(25), 16405-16411.
- [10] Guo, X., McCleese, C., Kolodziej, C., Samia, A. C., Zhao, Y., & Burda, C. (2016). Identification and characterization of the intermediate phase in hybrid organic-inorganic  $\text{MAPbI}_3$  perovskites. *Dalton Transactions*, 45(9), 3806-3813.
- [11] Xiao, Z., Dong, Q., Bi, C., Shao, Y., Yuan, Y., & Huang, J. (2014). Solvent annealing of perovskite-induced crystal growth for photovoltaic-device efficiency enhancement. *Advanced Materials*, 26(37), 6503-6509.




- [12] Luo, S., & Daoud, W. A. (2016). Crystal structure formation of  $\text{CH}_3\text{NH}_3\text{PbI}_{3-x}\text{Cl}_x$  perovskite. *Materials*, 9(3), 123.
- [13] Park, N. G. (2016). Crystal growth engineering for high-efficiency perovskite solar cells. *CrystEngComm*, 18(32), 5977-5985.
- [14] Zheng, X., Chen, B., Wu, C., & Priya, S. (2015). Room-temperature fabrication of  $\text{CH}_3\text{NH}_3\text{PbBr}_3$  by anti-solvent assisted crystallization approach for perovskite solar cells with fast response and small J-V hysteresis. *Nano Energy*, 17, 269-278.
- [15] Jeangros, Q., Duchamp, M., Werner, J., Kruth, M., Dunin-Borkowski, R. E., Niesen, B. & Hessler-Wyser, A. (2016). In situ TEM analysis of organic-inorganic metal-halide perovskite solar cells under electrical bias. *Nano Letters*, 16(11), 7013-7018.
- [16] Liu, D., Yang, J., & Kelly, T. L. (2014). Compact layer-free perovskite solar cells with 13.5% efficiency. *Journal of the American Chemical Society*, 136(49), 17116-17122.
- [17] Zhang, M., Yu, H., Lyu, M., Wang, Q., Yun, J. H., & Wang, L. (2014). Composition-dependent photoluminescence intensity and prolonged recombination lifetime of perovskite  $\text{CH}_3\text{NH}_3\text{PbBr}_{3-x}\text{Cl}_x$  films. *Chemical Communications*, 50(79), 11727-11730.
- [18] Choi, J. J., Yang, X., Norman, Z. M., Billinge, S. J., & Owen, J. S. (2013). Structure of methylammonium lead iodide within mesoporous titanium dioxide: active material in high-performance perovskite solar cells. *Nano letters*, 14(1), 127-133.
- [19] Halder, A., Chulliyil, R., Subbiah, A. S., Khan, T., Chattoraj, S., Chowdhury, A., & Sarkar, S. K. (2015). Pseudohalide ( $\text{SCN}^-$ )-doped  $\text{MAPbI}_3$  perovskites: A few surprises. *The journal of physical chemistry letters*, 6(17), 3483-3489.
- [20] Malinauskas, T., Tomkute-Luksiene, D., Sens, R., Daskeviciene, M., Send, R., Wonneberger, H., ... & Getautis, V. (2015). Enhancing thermal stability and lifetime of solid-state dye-sensitized solar cells via molecular engineering of the hole-transporting material spiro-OMeTAD. *ACS applied materials & interfaces*, 7(21), 11107-11116.
- [21] Zhang, J. Y., Boyd, I. W., O'sullivan, B. J., Hurley, P. K., Kelly, P. V., & Senateur, J. P. (2002). Nanocrystalline  $\text{TiO}_2$  films studied by optical, XRD and FTIR spectroscopy. *Journal of Non-Crystalline Solids*, 303(1), 134-138.
- [22] Hasan, M. M., Haseeb, A. S. M. A., Saidur, R., & Masjuki, H. H. (2008). Effects of annealing treatment on optical properties of anatase  $\text{TiO}_2$  thin films. *International Journal of Chemical and Biological Engineering*, 1(2), 92-96.



## Article

# Manufacture of High-Efficiency and Stable Lead-Free Solar Cells through Antisolvent Quenching Engineering

Amal Bouich <sup>1,2,3,\*</sup> , Julia Mari-Guaita <sup>1</sup>, Bernabé Mari Soucase <sup>1,\*</sup> and Pablo Palacios <sup>2,3</sup><sup>1</sup> Escuela Técnica Superior de Ingeniería del Diseño, Universitat Politècnica de València, 46022 València, Spain<sup>2</sup> Instituto de Energía Solar, ETSI Telecomunicación, Universidad Politécnica de Madrid, Ciudad Universitaria, s/n, 28040 Madrid, Spain<sup>3</sup> Departamento de Física Aplicada a las Ingenierías Aeronáutica y Naval, ETSI Aeronáutica y del Espacio, Universidad Politécnica de Madrid, Pz. Cardenal Cisneros, 3, 28040 Madrid, Spain

\* Correspondence: ambo1@doctor.upv.es (A.B.); bmari@fis.upv.es (B.M.S.)

**Abstract:** Antisolvent quenching has shown to significantly enhance several perovskite films used in solar cells; however, no studies have been conducted on its impact on MASnI<sub>3</sub>. Here, we investigated the role that different antisolvents, i.e., diethyl ether, toluene, and chlorobenzene, have on the growth of MASnI<sub>3</sub> films. The crystallinity, morphology, topography, and optical properties of the obtained thin films were characterized by X-ray diffraction (XRD), scanning electron microscopy (SEM), photoluminescence (PL) measurements, and UV-visible spectroscopy. The impact of the different antisolvent treatments was evaluated based on the surface homogeneity as well as the structure of the MASnI<sub>3</sub> thin films. In addition, thermal annealing was optimized to control the crystallization process. The applied antisolvent was modified to better manage the supersaturation process. The obtained results support the use of chlorobenzene and toluene to reduce pinholes and increase the grain size. Toluene was found to further improve the morphology and stability of thin films, as it showed less degradation after four weeks under dark with 60% humidity. Furthermore, we performed a simulation using SCAPS-1D software to observe the effect of these antisolvents on the performance of MASnI<sub>3</sub>-based solar cells. We also produced the device FTO/TiO<sub>2</sub>/MASnI<sub>3</sub>/Spiro-OMeTAD/Au, obtaining a remarkable photoconversion efficiency (PCE) improvement of 5.11% when using the MASnI<sub>3</sub> device treated with chlorobenzene. A PCE improvement of 9.44% was obtained for the MASnI<sub>3</sub> device treated with toluene, which also showed better stability. Our results support antisolvent quenching as a reproducible method to improve perovskite devices under ambient conditions.

**Keywords:** perovskite solar cell; MASnI<sub>3</sub>; antisolvent treatment; photoconversion efficiency; photochemical stability



Citation: Bouich, A.; Mari-Guaita, J.; Soucase, B.M.; Palacios, P.

Manufacture of High-Efficiency and Stable Lead-Free Solar Cells through Antisolvent Quenching Engineering. *Nanomaterials* **2022**, *12*, 2901. <https://doi.org/10.3390/nano12172901>

Academic Editors: Bouchta Sahraoui and Baizeng Fang

Received: 18 July 2022

Accepted: 21 August 2022

Published: 23 August 2022

**Publisher's Note:** MDPI stays neutral with regard to jurisdictional claims in published maps and institutional affiliations.



Copyright: © 2022 by the authors. Licensee MDPI, Basel, Switzerland.

This article is an open access article distributed under the terms and conditions of the Creative Commons Attribution (CC BY) license (<https://creativecommons.org/licenses/by/4.0/>).

## 1. Introduction

Solar energy is considered a basis to obtain clean and abundant energy; therefore it has become essential to take advantage of solar radiation as an energy source in the field of photovoltaics [1]. Recently, organic and inorganic perovskites, especially those based on methylammonium halides, have become attractive and promising research materials. Perovskite solar cells (PSC) showing power conversion efficiencies higher than 23% have been reported [2]. Perovskite materials also have remarkable optical and electronic properties, as they allow light to be absorbed in a wide wavelength for a long time, charge carriers to have a long diffusion length, and excitons to have small binding energy, which produces electrons and holes [3–5]. Furthermore, for perovskite thin film fabrication, a variety of techniques have been used, including one-step and two steps deposition [6], evaporation [7], and thermal deposition [8]. One-step deposition carried out via spin coating demonstrated an excellent capability to fabricate PSCs. Moreover, the PSCs showed homogeneous and compact thin films when fabricated using the spin coating technique. It has been shown that the morphology of perovskite thin films plays a vital role in device performance. Many



# Chapter 6: Investigation on the Stability and Efficiency of $\text{MaPbI}_3$ and $\text{MaSnI}_3$ Thin Films for Solar Cells

Authors: Julia Marí-Guaita<sup>a</sup>, Amal Bouich<sup>a</sup>, Muhammad Aamir Shafi<sup>c</sup>, Asmaa Bouich<sup>a, b</sup>, Bernabé Marí<sup>a, \*</sup>

<sup>a</sup>Institut de Disseny, Fabricació i Producció Automatitzada, Universitat Politècnica de València, València, Spain

<sup>b</sup>Ibn Tofail University, Kenitra, Morocco

<sup>c</sup>Department of Electrical Engineering, COMSATS University Islamabad, Pakistan

## Abstract

Hybrid organic-inorganic metal halides are considered as outstanding materials when used as the absorber layer in perovskite solar cells (PSCs) because of its efficiency, relieve of fabrication and low-cost materials. However, the content of lead (Pb) in the material may origin a dramatic after effect on human's health caused by its toxicity. Here, we investigate replacing the lead in  $\text{MAPbI}_3$  with tin (Sn) to show its influence on the growth of the film nucleation and stability of the solar device based on  $\text{MASnI}_3$ . By analysing the manufactured perovskite thin films by Scanning Electron Microscopy (SEM), Transmission Electron Microscopy (TEM), X-Ray Diffraction (XRD), UV-Visible Absorption, Photoluminescence (PL) and Atomic Force Microscopy (AFM), we report on the properties of the thin films when lead is replaced by tin. We report the simulation run for the case of  $\text{MAPbI}_3$ , where  $V_{oc}=0.856$  V,  $J_{sc}=25.65$  mA/cm<sup>2</sup>, FF= 86.09% and  $\eta=18.91\%$ ; and for  $\text{MASnI}_3$ ,  $V_{oc}=0.887$  V,  $J_{sc}=14.02$  mA/cm<sup>2</sup>, FF=83.72% and  $\eta=10.42\%$ . In perovskite-based devices using  $\text{MASnI}_3$  as absorber, it was found to be more stable despite of its lower efficiency, which could be improved by enhancing the bandgap alignment of  $\text{MaSnI}_3$ . The results of this paper also allow the development of a new, reliable production system for PSCs.

## 1. Introduction

Perovskite materials possess excellent optical and electrical properties, such as a direct bandgap ranging from 1.5 to 2.3 eV and the potential to transport electrons and holes [1-3]. For manufacturing perovskite thin films with good morphology and high quality, various low-cost techniques have been used. Among these techniques, spin coating with one-step process is usually used since it is easy to control and quick to produce [4, 5]. Also, two-step process is widely used due to its ease of control for the preparation of perovskite thin layers [6]. Other PSCs manufacturing techniques are two-step vapor-assisted deposition, which is advantageous for controlling the thin film morphology,

thickness, and grain size [7] and thermal vapor deposition normally used to manufacture films with consistent thickness.

Indeed, the highest conversion efficiency in PSCs is reached when MAPbI<sub>3</sub> is used as absorber. Moreover, the content of lead (Pb) in the material may origin a dramatic after effect on human's health caused by its toxicity. Therefore, the required study of substituting the lead in MAPbI<sub>3</sub> by tin (Sn) is highly suitable and must be studied. In the paper, we report on the influence on the growth of the film nucleation and stability of the solar device based on MASnI<sub>3</sub> perovskite (instead of MAPbI<sub>3</sub> absorbers), having elaborated both absorbers with the same one-step deposition technique. This technique exhibits wide-scale manufacturing for PSCs with high performance. Typically, the fabrication of the device is associated with the regulation of the surface shape and the capability to be developed scaled-up. The surface morphology has shown to be highly controllable, and that it is the primary factor influencing the efficiency of PSCs. For this reason, many techniques and treatments for the PSCs have been revised in order to improve the surface uniformity and the perovskite crystal formation.

In this work, we looked at the impact of replacing Pb by Sn on the properties of perovskite MAPbI<sub>3</sub> thin film. We report complex change of the device by observing the morphology and the composition of the films. The obtained perovskite devices were characterized by XRD, SEM, AFM, TEM, PL, and UV-Visible absorption analysis to inquire into the electrical and optical properties of the deposited films and the performance of solar cells which was estimated by SCAPS simulator [8].

## 2. Perovskite Manufacture

Perovskite absorbers ABX<sub>3</sub>, where A = Methylammonium (MA), B = (Pb or Sn) and X=Iodide (I), were manufactured employing different materials purchased from Sigma-Aldrich and Alfa Caesar. Specifically, Methylammonium iodide (MAI), thin II iodide 99% (SnI<sub>2</sub>) and lead iodide (PbI<sub>2</sub>) were used as precursors, and N-dimethylformamide (DMF) and Dimethyl Sulfoxide (DMSO) were used as solvents.

First, the prepared solutions of MAPbI<sub>3</sub> and MASnI<sub>3</sub> were dropped onto fluorine-dope tin oxide (FTO) glass substrates. The FTO glass was spun at 4000 rpm for 50 s during the dripping of the perovskite solution and the addition of toluene as antisolvent. Later, the samples were annealed at 60 °C for 5 minutes followed by an annealing at 100 °C for 10 minutes. **Figure 1** shows a diagram of the elaboration process carried out.

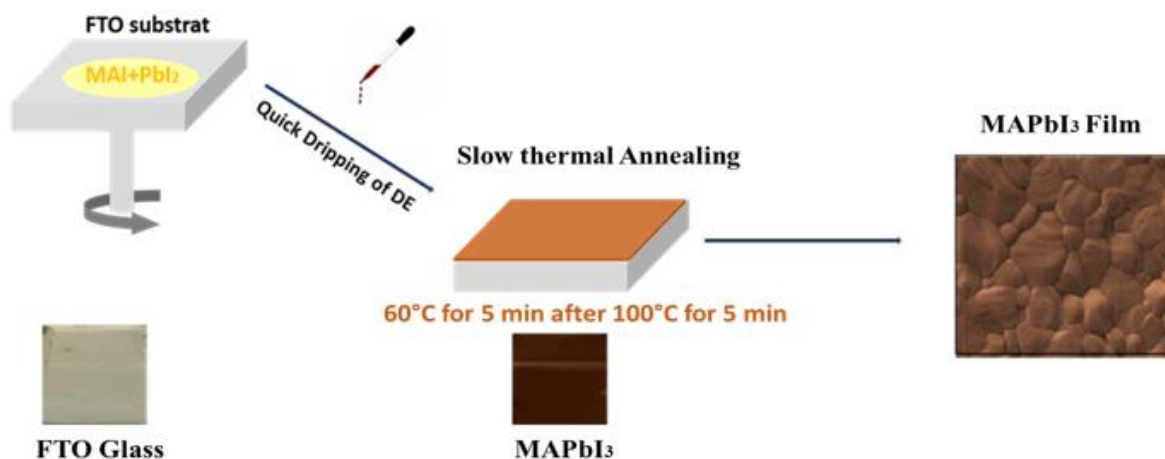


**Figure 1.** Elaboration process of the MAPbI<sub>3</sub> and MASnI<sub>3</sub> thin films.

### 3. Characterization techniques

The structural properties of the thin films were examined by XRD with RIGAKU Ultima IV diffractometer using Cu  $\alpha$  radiation ( $\lambda = 1.5418 \text{ \AA}$ ). SEM was used to examine the surface morphology of the perovskite layers using 1.5 kV at different magnifications. AFM measures were performed by using Nano Surf with Voltage cell from -1.5V–1.5V at a scan rate of 0.5Hz. TEM (JEO-JEM-1010) analysis was carried out with 2.5 kV at different magnifying toons. UV-visible absorption analysis was made with a Si-CCD and PL emission were excited with a 405 nm semiconductor laser. The output parameters of the solar cell, namely in the short circuit current density ( $J_{sc}$ ), the open circuit voltage ( $V_{oc}$ ), the form factor (FF) and the efficiency ( $\eta$ ), were assessed by SCAPS simulator.

### 4. Results and discussion

XRD scanning of MAPbI<sub>3</sub> and MASnI<sub>3</sub> thin films (**Figure 2**) reveals various diffractions peaks located at 14°, 28° and 52° matching the characteristics peaks of the perovskite materials; (110), (220) and (303) respectively. Previously published structures of MAPbI<sub>3</sub> [9] are in good agreement with the patters of this work. Furthermore, it was observed that the replacement of Pb by Sn lead to an increase of the intensity of the peak (110). All perovskite films form a tetragonal crystal structure with the space group I4/mcm.

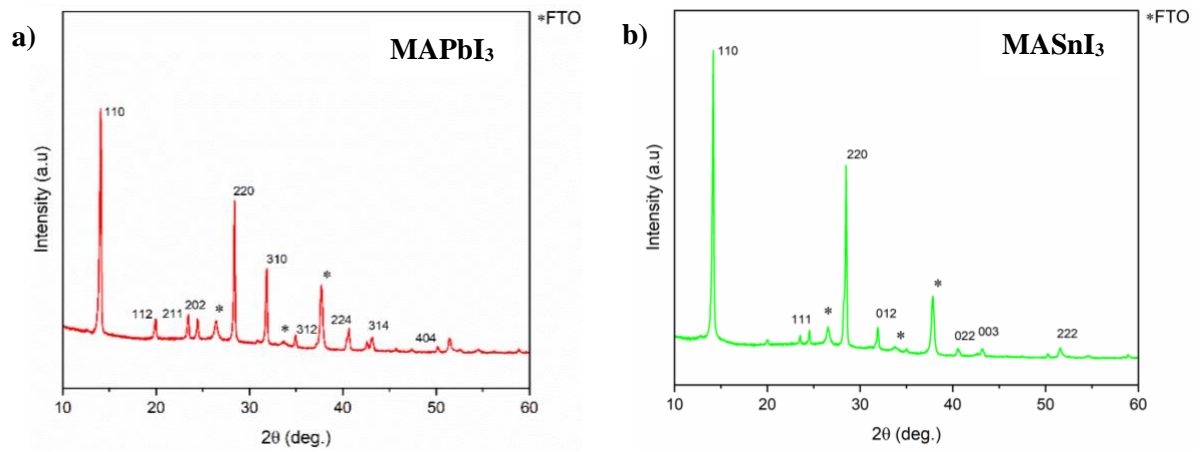


**Figure 2.** XRD patterns of MAPbI<sub>3</sub> and MASnI<sub>3</sub>.

The (110) XRD peak is wider for the MASnI<sub>3</sub> than for MAPbI<sub>3</sub> as revealed by the values of FWHM for this XRD peak (FWHM (110) = 0.23 for MASnI<sub>3</sub> and FWHM (110) = 0.13 for MAPbI<sub>3</sub>), which means bigger crystallite sizes for MAPbI<sub>3</sub>, according to the well-known Scherrer equation [10].

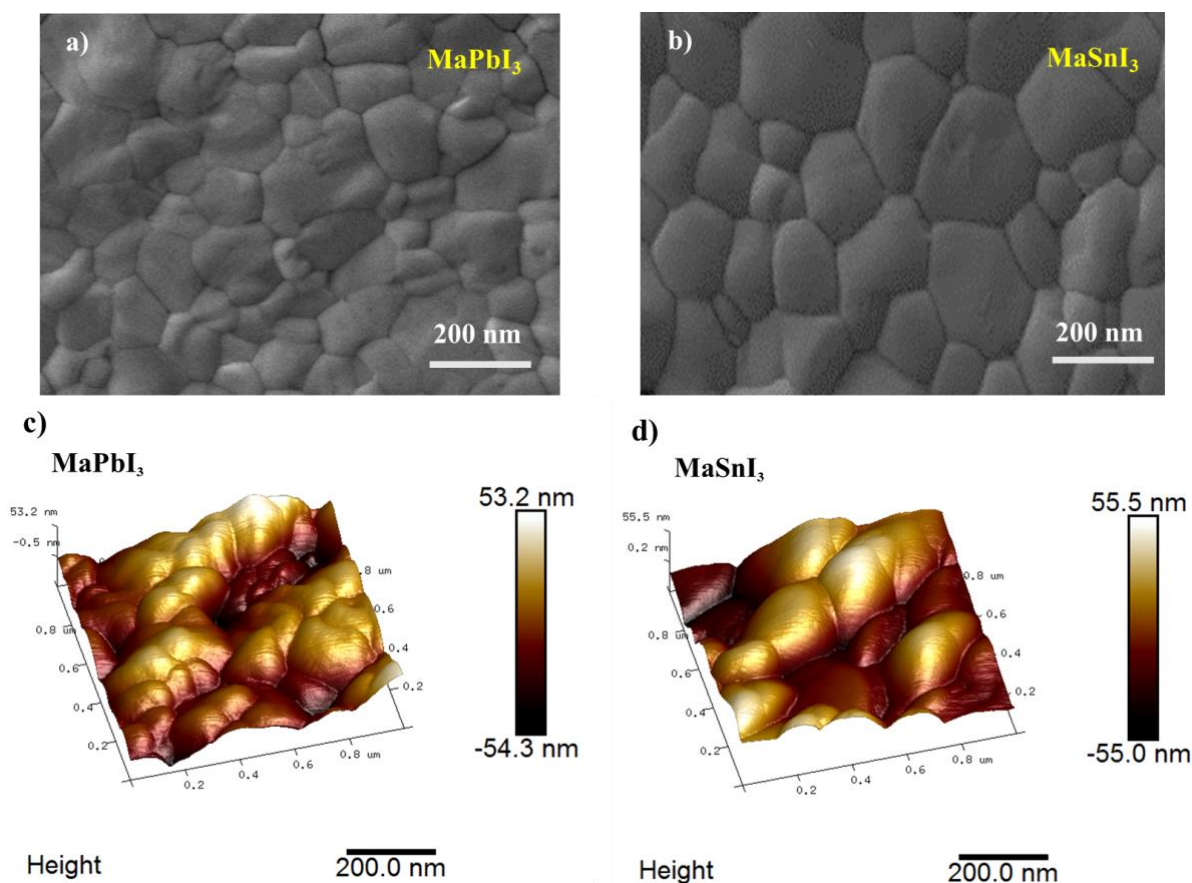
The calculated grain size, dislocation density, lattice strain and effective lattice strain data are represented in Table 1. The grain size for MASnI<sub>3</sub> (403 nm) thin films was found to have a substantial bigger grain size than MAPbI<sub>3</sub>, which was 302 nm. So, according to XRD and AFM analysis, when Pb is replaced by Sn, grain sizes increases even if crystallite sizes decrease. Further, dislocation density and effective lattice strain have been calculated to have an idea about scarcity and deformations of the grains in the film.

**Table 1:** The structural parameters of MAPbI<sub>3</sub> and MaSnI<sub>3</sub> thin films.

Sample.ID	Grain Size (nm)	Roughness (nm)	Dislocation density (10 <sup>-05</sup> nm <sup>-1</sup> )	Lattice strain (ε)
MaSnI <sub>3</sub>	403	46.7	0.62	0.39
MaPbI <sub>3</sub>	302	37.0	1.11	0.37

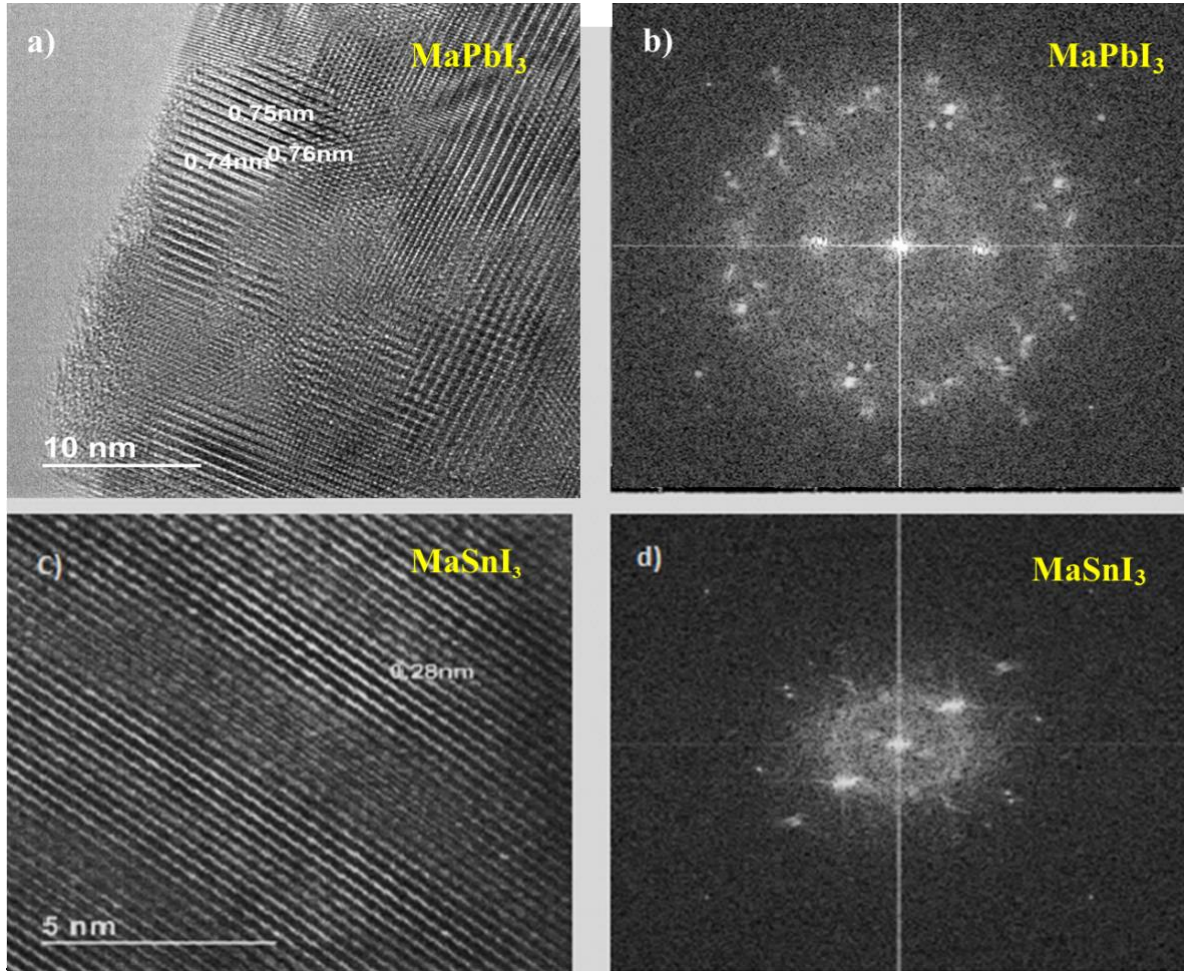


Figure 3 a) and b) shows SEM images of  $\text{MAPbI}_3$  and  $\text{MASnI}_3$ , the Surface morphology of both thin films was smooth and contained random grain boundaries. Furthermore, the  $\text{MASnI}_3$  showed improvement of the surface morphology like previously reported investigations [11, 12]. It can be clearly observed from the homogeneity of surface that  $\text{MASnI}_3$  produced have large grain size around 403 nm where  $\text{MAPbI}_3$  film, the grain size is about 302 nm. Also, the addition of Antisolvent toluene, which evaporates the solvent and therefore creates supersaturation to speed up crystallization process, resulted in excellent film development. Moreover, temperature annealing treatment had a significant impact on the surface of the films. Results indicate that when annealing temperature rises, the crystal as well as the grain size grow considerably. Figures 3 c) and d) show the AFM analysis of  $\text{MAPbI}_3$  and  $\text{MASnI}_3$  over a  $2\mu\text{m} \times 2\mu\text{m}$  region. Computed roughness of  $\text{MAPbI}_3$  was 37.0 nm when Pb was replaced by Sn, roughness was 46.7 nm (Table 1). The surface of  $\text{MASnI}_3$  is rougher due to huge size of hills and troughs.



**Figure 3.** SEM images of a)  $\text{MaPbI}_3$  b)  $\text{MASnI}_3$ , AFM images of c)  $\text{MaPbI}_3$ , d)  $\text{MASnI}_3$ .

TEM examination of  $\text{MASnI}_3$  and  $\text{MAPbI}_3$  thin films with lattice fringe spacing of 0.28 nm and 0.75 nm, respectively, corresponding to (110) or (220) of the tetragonal perovskite phase are shown in Figures 3 a) and c). Figure 3 exhibits the selected area of electron diffraction (SAED) spectrum and revealed that the  $\text{MAPbI}_3$  and  $\text{MASnI}_3$  thin films are polycrystalline, validated findings [13,15].



**Figure 4.** a, c) HRTEM images of  $\text{MAPbI}_3$  and  $\text{MASnI}_3$ , respectively, b, d) SAED of  $\text{MAPbI}_3$  and  $\text{MASnI}_3$ , respectively.

PL measurement was recorded in the range of 500-1100 nm as represented in Figure 6. The PL peak intensity in the region of 700-900 nm is in good agreement with previously reported study of  $\text{MAPbI}_3$  [16]. The measured intensity of the PL peak in  $\text{MAPbSn}_3$  films is about 30% higher than in  $\text{MAPbI}_3$  films.

It is suggested that the tin can be placed at the optimal level for absorbing the light. This finding also boosts the enhancement crystallinity of the perovskite thin film. The UV-visible absorption spectrum of  $\text{MAPbI}_3$  and  $\text{MASnI}_3$  were obtained between 400 nm and 900 nm. The optical bandgap was calculated through the Tauc plot for the absorbance spectrum, from the equation  $(Ah\nu)^2 = B(h\nu - E_g)$ . An optical bandgap of 1.60 eV and 1.62

were found for MAPbI<sub>3</sub> and MASnI<sub>3</sub> films respectively (Figure 6 c, d) [17,19]. Table 2 summarizes the optical bandgap and PL emission peaks according to PL and UV-visible absorption measurements. The energy difference between the edge of the optical absorption and the energy of the PL emission, known as Stokes shift, is found to be higher for MASnI<sub>3</sub> (40 meV) than for MAPbI<sub>3</sub> (10 meV), meaning that the bottom of the conduction band is more filled with electrons in MASnI<sub>3</sub> films.

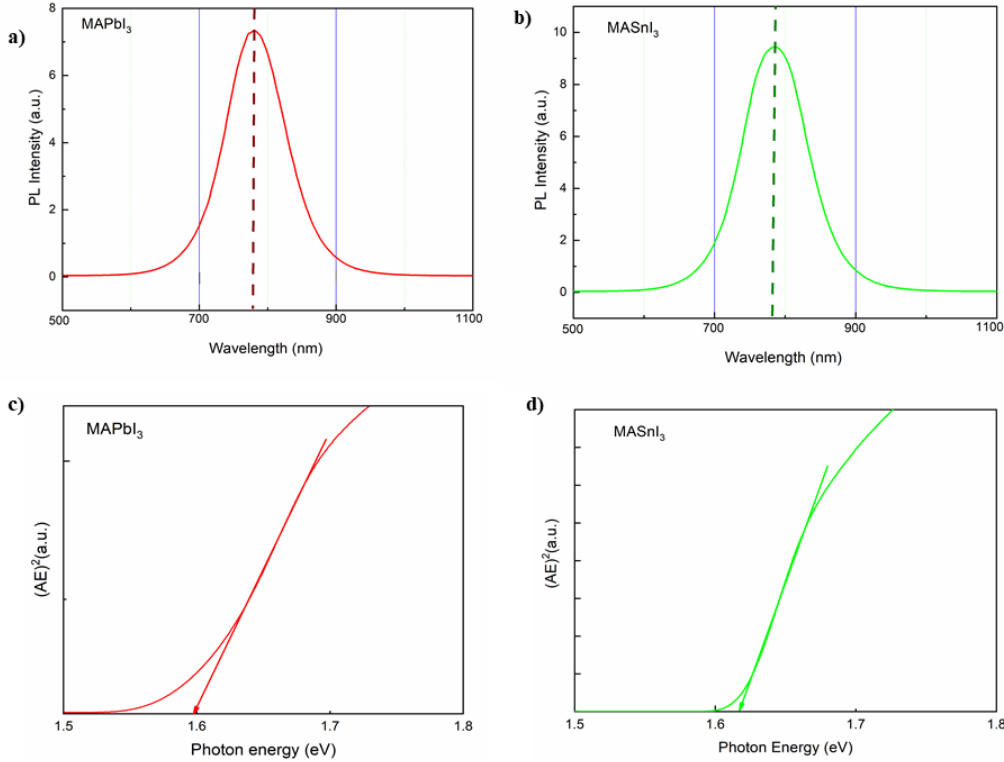


**Figure 6.** a) PL emission for MAPbI<sub>3</sub> perovskite thin films, b) PL emission for MaPbI<sub>3</sub> perovskite thin films, c) Optical bandgap of MAPbI<sub>3</sub>, d) Optical bandgap of MASnI<sub>3</sub>.

**Table 2:** PL and optical bandgap for MAPbI<sub>3</sub> and MASnI<sub>3</sub>

Sample.ID	PL		Optical absorption		Stokes shift (meV)
	$\lambda$ (nm)	E <sub>g</sub> (eV)	$\lambda$ (nm)	E <sub>g</sub> (eV)	
MaPbI <sub>3</sub>	780	1.59	775	1.60	10
MaSnI <sub>3</sub>	786	1.58	765	1.62	40

## 5. Degradation study

Environmental components like oxygen and humidity have a significant impact on photovoltaic stability of perovskite solar devices. The degradation mechanism of the of Methylammonium-based perovskites when exposed to the environment, has been

attributed to a reduction of these compounds in  $\text{PbI}_2$ ,  $\text{CH}_3\text{NH}_2$  and HI. In order to evaluate the degradation of  $\text{MAPbI}_3$  and  $\text{MaSnI}_3$  samples, we performed XRD, SEM and PL measurements on fresh and 4 weeks aged samples, kept under 60% of humidity and dark environment (Figure 7).

For the 4 weeks aged  $\text{MAPbI}_3$  samples, XRD patterns reveal lesser intensity of characteristic peaks (Figure 7.a) and a reduction of the intensity of PL emission (Figure 7.c). In the case of 4 weeks aged  $\text{MASnI}_3$  samples, both XRD peaks and PL emission decreases in intensity, but this reduction in intensity is minor for  $\text{MASnI}_3$  than for  $\text{MAPbI}_3$  samples (Figure 7.d and 7.e). This fact means that  $\text{MASnI}_3$  samples are more stable than  $\text{MAPbI}_3$  ones. Similar results are reported in literature [20, 24]. Further, SEM images (Figures 7.b and 7.e) support this finding. New grain boundaries, as presented in Figures 7.b, appear in aged  $\text{MAPbI}_3$  films. In the case of aged  $\text{MASnI}_3$  films, some new defects consisting of pinholes and changes in the surface morphology with respect no fresh samples (Figure 7.e) are observed in SEM images. As a result, the degradation process seems to be different for both types of films.

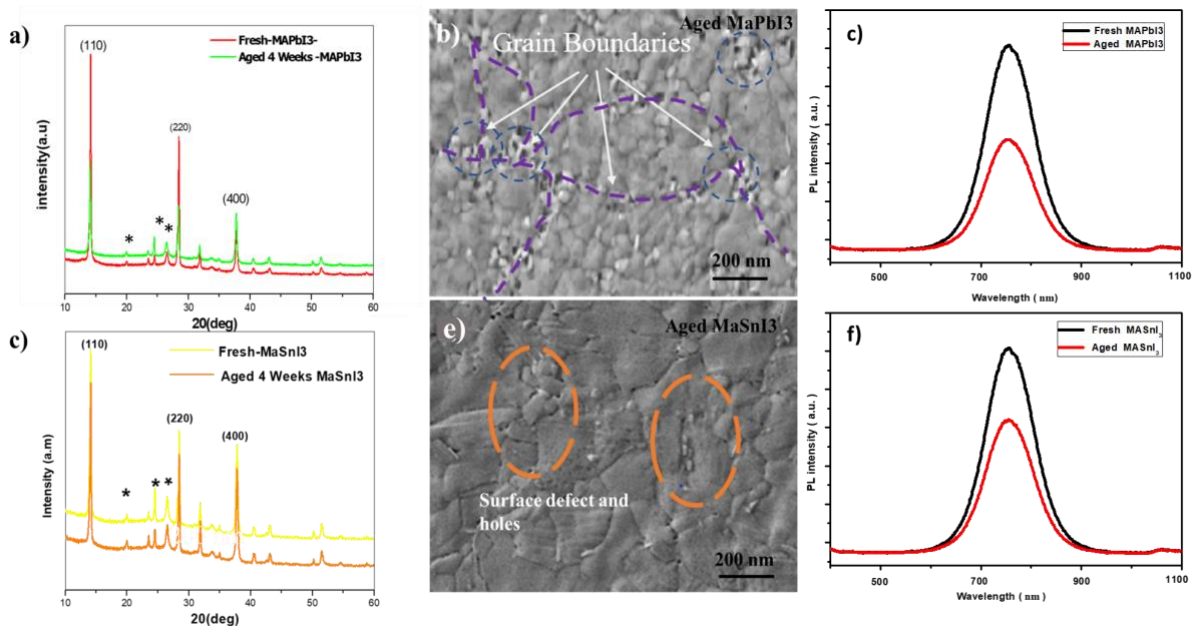


**Figure 7.** Degradation study of  $\text{MAPbI}_3$  (a) XRD pattern fresh and aged  $\text{MAPbI}_3$  samples after 4 weeks b) SEM image of Aged  $\text{MAPbI}_3$  (c) PL emission of aged fresh and aged  $\text{MAPbI}_3$  samples. Degradation study of  $\text{MASnI}_3$  (a) XRD pattern fresh and aged  $\text{MASnI}_3$  samples after 4 weeks b) SEM image of Aged  $\text{MASnI}_3$  (c) PL emission of aged fresh and aged  $\text{MASnI}_3$  samples.

## 6. Device Manufacture and Numerical Simulation

For the study of the Solar Cell performance, we performed the simulation of MAPbI<sub>3</sub> and MASnI<sub>3</sub> based Perovskites solar cells using SCAPS simulator software. The structure of solar '*Spiro OMeTAD/MA(Pb/Sn)I<sub>3</sub>/TiO<sub>2</sub>/FTO*' used in the simulation is shown in the following diagram (Figure 8).

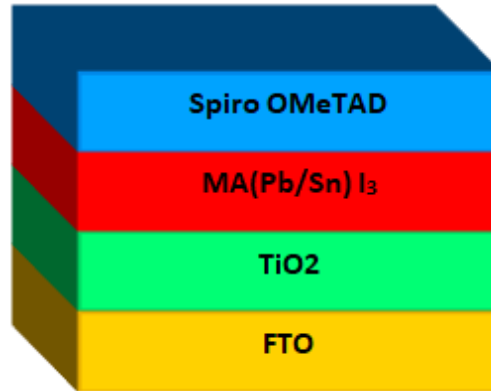


**Figure 8.** Schematic diagram of proposed solar used in SCAPS.

The simulation was run two times for '*OMeTAD/MAPbI<sub>3</sub>/TiO<sub>2</sub>/FTO*' and '*OMeTAD/MASnI<sub>3</sub>/TiO<sub>2</sub>/FTO*' proposed models separately [25,26]. Figure 9 and Figure 10 show the J-V and P-V characteristics curves, and from these curves we observed that MASnI<sub>3</sub> based solar cell is less efficient as compared to MAPbI<sub>3</sub> based solar cell. The bandgap of MAPbI<sub>3</sub> is more favourable for the light absorption as compared to other one.

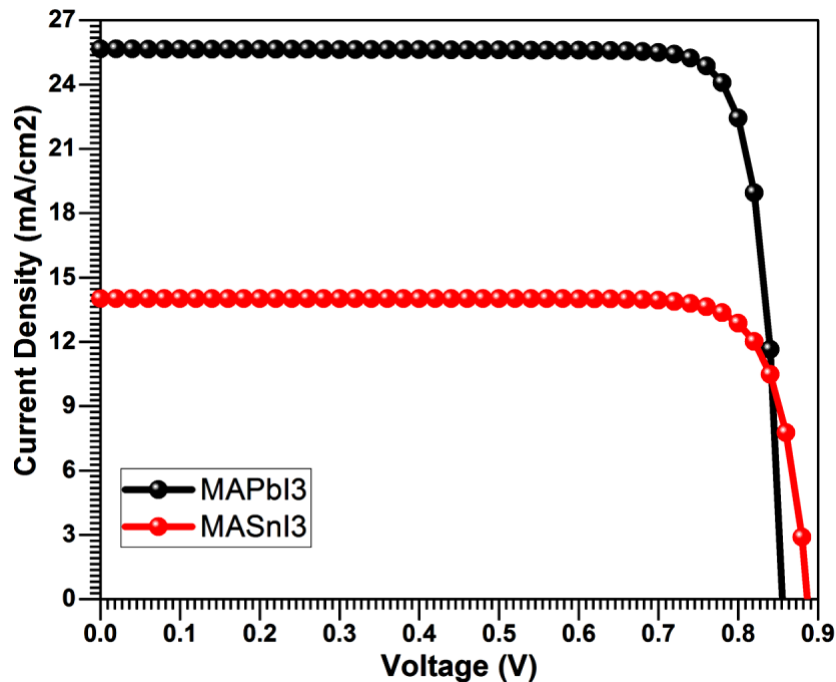


**Figure 9.** J-V characteristics curve for both MAPbI<sub>3</sub> and MASnI<sub>3</sub>

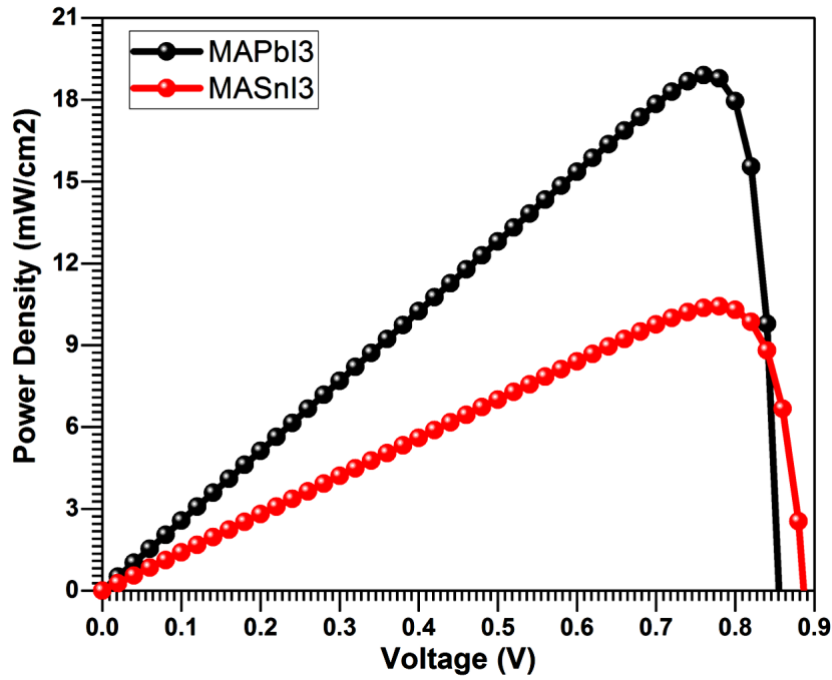


**Figure 10.** P-V characteristics curve for both MAPbI<sub>3</sub> and MASnI<sub>3</sub>

**Table 3:** Characteristics Parameters of MAPbI<sub>3</sub> and MASnI<sub>3</sub> obtained by simulation

Absorber	Voc	Jsc	FF	ETA
	V	mA/cm <sup>2</sup>	%	%
MAPbI <sub>3</sub>	0.856	25.65	86.09	18.91
MASnI <sub>3</sub>	0.888	14.02	83.72	10.42

The results of simulation are summarized in **Table 3**, where the photovoltaic characteristic parameters; Voc (open circuit voltage), Jsc (short circuit current density), FF (fill factor) and ETA (conversion efficiency) are shown. When the simulation was run for the case of MAPbI<sub>3</sub>, we find the Voc of 0.856 V, Jsc of 25.65 mA/cm<sup>2</sup>, FF of 86.09% and ETA of 18.91%. For MASnI<sub>3</sub> we report Voc of 0.888 V, Jsc of 14.02 mA/cm<sup>2</sup>, FF of 83.72% and ETA of 10.42%. It is worthy to notice that there is about 9% difference in the efficiencies of both devices. For Sn-based PSCs, this efficiency could be improved by enhancing the bandgap alignment of MASnI<sub>3</sub> with respect the hole transport layer and by adjusting film thickness.

In order to better show the differences of the photovoltaic parameters of MAPbI<sub>3</sub> and MASnI<sub>3</sub>, a bar graph displaying the four photovoltaic parameters for both proposed

devices are plotted in Figure 11. This comparison shows well-defined difference between both devices' parameters.

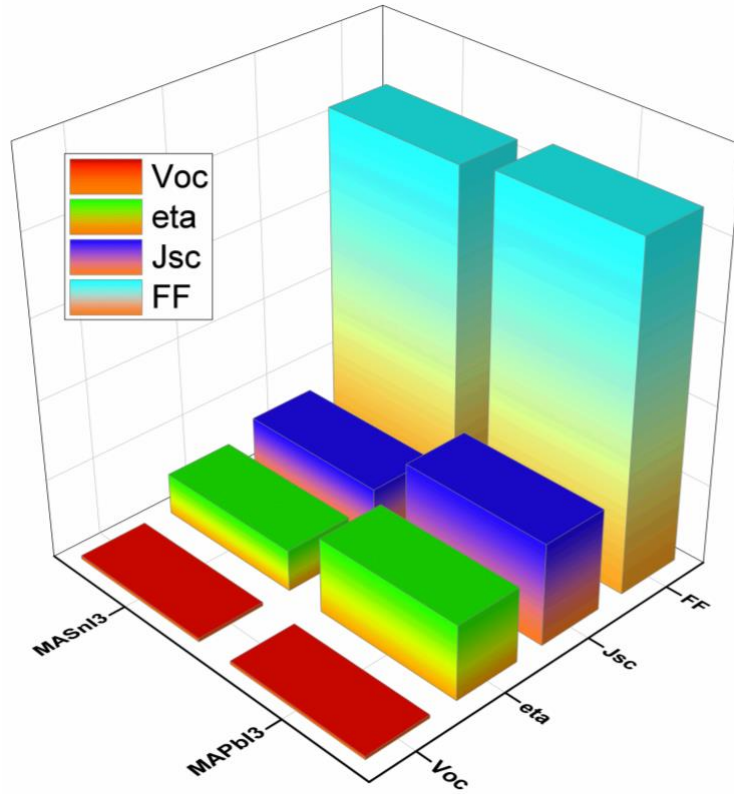


**Figure.11:** Graphical Comparison of Characteristics Parameters of MAPbI<sub>3</sub> and MASnI<sub>3</sub>.

## 7. Conclusion

In summary, the use of Sn in spite of Pb to increase the stability and decrease of toxicity of perovskite solar cells has been demonstrated. Results show a higher intensity of characteristic peaks of perovskite when using Sn. Replacement of Pb by Sn has a significant impact on the crystallization process of perovskite materials and produces an increase in the grain size of the perovskite thin film, as seen by SEM pictures. The fact that Sn rises the grain size may result in an increase in the light absorption of the perovskite layer. Optimizing the inclusion of Sn in perovskite-based solar cells can significantly enhance stability, according to our research. Simulation was run for both films prepared. On the one hand, for MAPbI<sub>3</sub>, we obtained Voc = 0.856 V, Jsc = 25.65

mA/cm<sup>2</sup>, FF = 86.09% and ETA = 18.91%. On the other hand, for MASnI<sub>3</sub>, we calculated Voc = 0.888 V, Jsc = 14.02 mA/cm<sup>2</sup>, FF = 83.72% and ETA = 10.42%. Here, we report that there is around 9% difference in efficiencies of both devices. But, in case of Sn-based perovskite, this efficiency could be enhanced by improving the bandgap alignment of the material.

## References

- [1] Bouich, A., Ullah, S., Ullah, H., Mollar, M., Marí, B., & Touhami, M. E. (2020). Electrodeposited CdZnS/CdS/CIGS/Mo: characterization and solar cell performance. *JOM*, 72(2), 615-620.
- [2] Jeon, N. J., Na, H., Jung, E. H., Yang, T. Y., Lee, Y. G., Kim, G., ... & Seo, J. (2018). A fluorene-terminated hole-transporting material for highly efficient and stable perovskite solar cells. *Nature Energy*, 3(8), 682.
- [3] Bouich, A., Ullah, S., Marí, B., Atourki, L., & Touhami, M. E. (2021). One-step synthesis of FA<sub>1-x</sub>GA<sub>x</sub>PbI<sub>3</sub> perovskites thin film with enhanced stability of alpha (α) phase. *Materials Chemistry and Physics*, 258, 123973.
- [4] Im, J. H., Kim, H. S., & Park, N. G. (2014). Morphology-photovoltaic property correlation in perovskite solar cells: One-step versus two-step deposition of CH<sub>3</sub>NH<sub>3</sub>PbI<sub>3</sub>. *Apl Materials*, 2(8), 081510.
- [5] Carnie, M. J., Charbonneau, C., Davies, M. L., Troughton, J., Watson, T. M., Wojciechowski, K., ... & Worsley, D. A. (2013). A one-step low temperature processing route for organolead halide perovskite solar cells. *Chemical communications*, 49(72), 7893-7895.
- [6] Bi, D., Moon, S. J., Häggman, L., Boschloo, G., Yang, L., Johansson, E. M., ... & Hagfeldt, A. (2013). Using a two-step deposition technique to prepare perovskite (CH<sub>3</sub>NH<sub>3</sub>PbI<sub>3</sub>) for thin film solar cells based on ZrO<sub>2</sub> and TiO<sub>2</sub> mesostructures. *RSC Advances*, 3(41), 18762-18766.
- [7] Chen, Q., Zhou, H., Hong, Z., Luo, S., Duan, H. S., Wang, H. H., ... & Yang, Y. (2013). Planar heterojunction perovskite solar cells via vapor-assisted solution process. *Journal of the American Chemical Society*, 136(2), 622-625.
- [8] Bouich, A., Hartiti, B., Ullah, S., Ullah, H., Touhami, M. E., Santos, D. M. F., & Mari, B. (2019). Experimental, theoretical, and numerical simulation of the performance of CuIn<sub>x</sub>Ga<sub>1-x</sub>S<sub>2</sub>-based solar cells. *Optik*, 183, 137-147.
- [9] Kong, W., Ye, Z., Qi, Z., Zhang, B., Wang, M., Rahimi-Iman, A., & Wu, H. (2015). Characterization of an abnormal photoluminescence behavior upon crystal-phase



transition of perovskite  $\text{CH}_3\text{NH}_3\text{PbI}_3$ . *Physical Chemistry Chemical Physics*, 17(25), 16405-16411.

[10] Holzwarth, U., & Gibson, N. (2011). The Scherrer equation versus the Debye-Scherrer equation. *Nature nanotechnology*, 6(9), 534-534.

[11] Xiao, Z., Dong, Q., Bi, C., Shao, Y., Yuan, Y., & Huang, J. (2014). Solvent annealing of perovskite-induced crystal growth for photovoltaic-device efficiency enhancement. *Advanced Materials*, 26(37), 6503-6509.

[12] Luo, S., & Daoud, W. A. (2016). Crystal structure formation of  $\text{CH}_3\text{NH}_3\text{PbI}_{3-x}\text{Cl}_x$  perovskite. *Materials*, 9(3), 123.

[13] Park, N. G. (2016). Crystal growth engineering for high efficiency perovskite solar cells. *CrystEngComm*, 18(32), 5977-5985.

[14] Zheng, X., Chen, B., Wu, C., & Priya, S. (2015). Room temperature fabrication of  $\text{CH}_3\text{NH}_3\text{PbBr}_3$  by anti-solvent assisted crystallization approach for perovskite solar cells with fast response and small J-V hysteresis. *Nano Energy*, 17, 269-278.

[15] Jeangros, Q., Duchamp, M., Werner, J., Kruth, M., Dunin-Borkowski, R. E., Niesen, B. & Hessler-Wyser, A. (2016). In situ TEM analysis of organic-inorganic metal-halide perovskite solar cells under electrical bias. *Nano letters*, 16(11), 7013-7018.

[16] Liu, D., Yang, J., & Kelly, T. L. (2014). Compact layer free perovskite solar cells with 13.5% efficiency. *Journal of the American Chemical Society*, 136(49), 17116-17122.

[17] Zhang, M., Yu, H., Lyu, M., Wang, Q., Yun, J. H., & Wang, L. (2014). Composition-dependent photoluminescence intensity and prolonged recombination lifetime of perovskite  $\text{CH}_3\text{NH}_3\text{PbBr}_{3-x}\text{Cl}_x$  films. *Chemical Communications*, 50(79), 11727-11730.

[18] Choi, J. J., Yang, X., Norman, Z. M., Billinge, S. J., & Owen, J. S. (2013). Structure of methylammonium lead iodide within mesoporous titanium dioxide: active material in high-performance perovskite solar cells. *Nano letters*, 14(1), 127-133.

[19] Halder, A., Chulliyil, R., Subbiah, A. S., Khan, T., Chattoraj, S., Chowdhury, A., & Sarkar, S. K. (2015). Pseudohalide (SCN<sup>-</sup>)-doped  $\text{MAPbI}_3$  perovskites: A few surprises. *The journal of physical chemistry letters*, 6(17), 3483-3489.

[20] Xie, Z., Sun, S., Yan, Y., Zhang, L., Hou, R., Tian, F., & Qin, G. G. (2017). Refractive index and extinction coefficient of  $\text{NH}_2\text{CH}_2\text{NH}_2\text{PbI}_3$  perovskite photovoltaic material. *Journal of Physics: Condensed Matter*, 29(24), 245702.

[21] Homes, C. C., Vogt, T., Shapiro, S. M., Wakimoto, S., & Ramirez, A. P. (2001). Optical response of high-dielectric-constant perovskite-related oxide. *Science*, 293(5530), 673-676.

- [22] Abdelmageed, G., Jewell, L., Hellier, K., Seymour, L., Luo, B., Bridges, F., ... & Carter, S. (2016). Mechanisms for light induced degradation in MAPbI<sub>3</sub> perovskite thin films and solar cells. *Applied Physics Letters*, 109(23), 233905.
- [23] Li, J., Dong, Q., Li, N., & Wang, L. (2017). Direct Evidence of Ion Diffusion for the Silver-Electrode-Induced Thermal Degradation of Inverted Perovskite Solar Cells. *Advanced Energy Materials*, 7(14), 1602922.
- [24] Bouich, A., Mari, B., Atourki, L., Ullah, S., & Touhami, M. E. (2021). Shedding Light on the Effect of Diethyl Ether Antisolvent on the Growth of CH<sub>3</sub>NH<sub>3</sub>PbI<sub>3</sub> Thin Films. *JOM*, 73(2), 551-557.
- [25] Wu, X., Wang, H., Song, Y., Ma, X., Zeng, Z., Wu, J., & Liu, Y. (2021). Improving the Performance of Organic Lead-tin Laminated Perovskite Solar Cells From the Perspective of Device Simulation.
- [26] Alipour, H., & Ghadimi, A. (2021). Optimization of lead-free perovskite solar cells in normal-structure with WO<sub>3</sub> and water-free PEDOT: PSS composite for hole transport layer by SCAPS-1D simulation. *Optical Materials*, 120, 111432.

# Investigation on the Stability and Efficiency of MAPbI<sub>3</sub> and MASnI<sub>3</sub> Thin Films for Solar Cells

Julia Marí-Guaita, Amal Bouich, Muhammad Aamir Shafi, Asmaa Bouich, and Bernabé Marí\*

Hybrid organic–inorganic halides are considered as outstanding materials when used as the absorber layer in perovskite solar cells (PSCs) because of its efficiency, relieve of fabrication and low-cost materials. However, the content of lead (Pb) in the material may origin a dramatic after effect on human's health caused by its toxicity. Here, we investigate replacing the lead in MAPbI<sub>3</sub> with tin (Sn) to show its influence on the growth of the film nucleation and stability of the solar device based on MASnI<sub>3</sub>. By analysing the manufactured perovskite films by scanning electron microscopy (SEM), transmission electron microscopy (TEM), X-ray diffraction (XRD), UV–visible absorption, photoluminescence (PL) and atomic force microscopy (AFM), the properties of the thin films when lead is replaced by tin are reported. The simulation run for the case of MAPbI<sub>3</sub> is reported, where  $V_{oc} = 0.856$  V,  $J_{sc} = 25.65$  mA cm<sup>-2</sup>, FF = 86.09%, and ETA = 18.91%, and for MASnI<sub>3</sub>,  $V_{oc} = 0.887$  V,  $J_{sc} = 14.02$  mA cm<sup>-2</sup>, FF = 83.72%, and ETA = 10.42%. In perovskite-based devices using MASnI<sub>3</sub> as absorber, it was found to be more stable despite of its lower efficiency, which could be improved by enhancing the bandgap alignment of MaSnI<sub>3</sub>. The results of this paper also allow the development of a new, reliable production system for PSCs.

various low-cost techniques have been used. Among these techniques, spin coating with one-step process is usually used as it is easy to control and quick to produce.<sup>[4,5]</sup> Also, the two-step process is widely used due to its ease of control for the preparation of perovskite thin layers.<sup>[6]</sup> Other PSCs' manufacturing techniques are the two-step vapor-assisted deposition, which is advantageous for controlling the thin film morphology, thickness, and grain size,<sup>[7]</sup> and thermal vapor deposition normally used to manufacture films with consistent thickness.

Indeed, the highest conversion efficiency in PSCs is reached when MAPbI<sub>3</sub> is used as an absorber. Moreover, the content of lead (Pb) in the material may lead to a dramatic aftereffect on human health caused by its toxicity. This is why the required study of substituting the lead in MAPbI<sub>3</sub> by tin (Sn) is highly suitable and must be done. In the article, we report on the influence on the growth of film nucleation and stability of the solar

device based on MASnI<sub>3</sub> perovskite (instead of MAPbI<sub>3</sub> absorbers), having elaborated both absorbers with the same one-step deposition technique. This technique exhibits wide-scale manufacturing for PSCs with high performance. Typically, the fabrication of the device is associated with the regulation of the surface shape and the capability to be developed scaled-up. The surface morphology has shown to be highly controllable and that it is the primary factor influencing the efficiency of PSCs. For this reason, many techniques and treatments for PSCs have been revised to improve the surface uniformity and the perovskite crystal formation.

In this work, we looked at the impact of replacing Pb by Sn on the properties of perovskite MAPbI<sub>3</sub> thin film. We report complex changes of the device by observing the morphology and the composition of the films. The obtained perovskite devices were characterized by X-ray diffraction (XRD), scanning electron microscopy (SEM), atomic force microscopy (AFM), transmission electron microscopy (TEM), photoluminescence (PL), and UV–vis absorption analysis to inquire into the electrical and optical properties of the deposited films and the performance of solar cells which were estimated by SCAPS simulator.<sup>[8]</sup>


## 1. Introduction

Perovskite materials possess excellent optical and electrical properties, such as a direct bandgap ranging from 1.5 to 2.3 eV and the potential to transport electrons and holes.<sup>[1–3]</sup> For manufacturing perovskite thin films with good morphology and high quality,

J. Marí-Guaita, A. Bouich, A. Bouich, B. Marí  
Institut de Disseny, Fabricació i Producció Automatizada  
Universitat Politècnica de València  
València 46022, Spain  
E-mail: bmari@fis.upv.es

A. Bouich  
Department of Computer Science Engineering  
Ibn Tofail University  
Kenitra 14000, Morocco

M. A. Shafi  
Department of Electrical Engineering  
COMSATS University Islamabad  
Islamabad 45550, Pakistan

 The ORCID identification number(s) for the author(s) of this article can be found under <https://doi.org/10.1002/pssa.202100664>.

© 2022 The Authors. physica status solidi (a) applications and materials science published by Wiley-VCH GmbH. This is an open access article under the terms of the Creative Commons Attribution License, which permits use, distribution and reproduction in any medium, provided the original work is properly cited.

DOI: 10.1002/pssa.202100664

## 2. Perovskite Manufacture

Perovskite absorbers ABX<sub>3</sub>, where A = methylammonium (MA), B = (Pb or Sn), and X = Iodide (I), were manufactured employing different materials purchased from Sigma-Aldrich and Alfa



## Chapter 7: Conclusion

### General conclusion

At the end of each article there is the corresponding specific conclusion. Here, the general conclusions of the research are presented.

1. Characterization techniques have been fundamental for deep study of the optoelectronic properties of the thin films. X-ray diffraction technique made possible to study the presence of perovskite material in the samples and demonstrate the crystalline structure. UV-visible absorption and photoluminescence analysis are both important characterization techniques to evaluate the optoelectronic properties and light absorption coefficient of the devices. AFM and FE-SEM analysis techniques are also fundamental understanding the morphology of the grains the surface of the films.
2. SCAPS-1D simulation work is remarkable in the investigation of solar cells materials as it makes possible to calculate the fundamental parameters of a solar device regarding the composition choice for the absorber layer.
3. The use of doping with certain materials demonstrated to increase the stability of the perovskite materials. Also, doping by substituting a part of Pb in the composition of the perovskite leads to a less toxic device.
4. The importance of the manufacturing process is decisive in technology of solar cells and the proper commercialization of perovskite solar cells. The synthesis of the films requires, therefore certain features such ease of fabrication and low-cost techniques. During the manufacture, the step of the antisolvent addition can influence the properties of the solar device
5. Techniques for enhancing the stability of the perovskite solar cells have a direct influence in the growth of the film nucleation and light absorption. However, loss of efficiency will ideally be insignificant.

### Suggested further studies

Further studies are required for the technology of hybrid perovskites. It has been demonstrated in numerous studies that HOPs have great potential for solar cell applications. However, we are still facing several challenges, such as stability and toxicity, that hopefully will be overcome. Composition and manufacture of the films is determinant for proper research in the matter, and thus, obtaining good performance of solar cells. Inkjet printing is an emerging technology that allows to control easily all the

parameters regarding the synthesis process. Also, it is probably the technology that will make possible the scale up of the devices warranting a low cost of fabrication.

In summary, the work can be continued implementing the innovative technique of the inkjet printing in the manufacture of solar cells and testing many other compounds involved including doping, mixed perovskites, antisolvent engineering, etc.

## Annex: Detailed publications and conferences during PhD period

### Publications

Marí-Guaita, Julia; Bouich, Amal; Muhammad Aamir Shafi; Aasma Bouich; Marí, B.. (2022) *Investigation on the stability and efficiency of MAPbI<sub>3</sub> and MASnI<sub>3</sub> thin films for Solar Cells*. *Physica Status Solidi (A)*, 221664 (219), 10.1002/pssa.202100664

Marí-Guaita, Julia; Bouich, Amal; Marí, B.. (2022) *Stability Improvement of Methylammonium Lead Iodide Perovskite Thin Films by Bismuth Doping*. *JOM Journal of the Minerals, Metals and Materials Society*. <https://doi.org/10.1007/s11837-022-05347-4>.

Marí-Guaita, Julia; Bouich, Amal; Marí, B. (2021) *Shedding Light on Phase Stability and Surface Engineering of Formamidinium Lead Iodide (FAPbI<sub>3</sub>) Thin Films for Solar Cells*. *Engineering Proceedings*, 1 (12), 1 - 4. 10.3390/engproc2021012001

Bouich, Amal; Marí-Guaita, Julia; Marí, B. (2022) *Optimization of electrodeposition time on the properties of Cu<sub>2</sub>ZnSnS<sub>4</sub> thin films for thin film solar cell applications*. *Optical and Quantum Electronics*. 10.21203/rs.3.rs-963102/v1

Bouich, Amal; Marí-Guaita, Julia; Marí, B.. (2022) *Effect of Deposition Cycles on the Properties of ZnO Thin Films Deposited by Spin Coating Method for CZTS-based Solar Cells*. *Optik - International Journal for Light and Electron Optics*, <https://doi.org/10.1016/j.ijleo.2022.168854>.

Bouich, Amal; Marí-Guaita, Julia; Marí, B.; Palacios, Pablo. (2022) *Tetrabutylammonium-Doped Methylammonium lead iodide: high quality and stable perovskite thin films*. *Frontiers in Energy Research*. 10.3389/fenrg.2022.840817

Bouich, Amal; Marí-Guaita, Julia; Marí, B.; Muhammad Aamir Shafi. (2022) *Effect of Deposition Cycles on the Properties of ZnO Thin Films Deposited by Spin Coating Method for CZTS-based Solar Cells*. *Optik - International Journal for Light and Electron Optics*. 10.1016/j.ijleo.2022.168854

Marí-Guaita, Julia; Gallego-Parra, Samuel; Sans-Tresserras, Juan Ángel; Velázquez, M.; Rodríguez-Hernández, P.; Muñoz, A.; Manjón, Francisco-Javier. (2021) *Lattice dynamics study of (Gd<sub>1-x</sub>Yb<sub>x</sub>)<sup>(2)</sup>O<sup>-3</sup>(x=0.11) at high pressure*. *Journal of Alloys and Compounds* (871)1 - 9. 10.1016/j.jallcom.2021.159525

Bouich, Amal; Marí-Guaita, Julia; Aasma Bouich; Guaita-Pradas, Inmaculada; Marí, B.. (2022) *Towards Manufacture Stable Lead Perovskite APbI3 (A = Cs, MA, FA) Based Solar Cells with Low-Cost Techniques*. Engineering Proceedings. 10.3390/engproc2021012081

Bouich, Amal; Marí-Guaita, Julia; Marí, B.; Palacios, Pablo. (2022) *Manufacture of High-Efficiency and Stable Lead-Free Solar Cells through Antisolvent Quenching Engineering*. Nanomaterials. 10.3390/nano12172901

Bouich, Amal; Marí-Guaita, Julia; Marí, B.; Khattak, Yousaf Hameed; Baig, Faisal; Palacios, Pablo. (2022) *Investigation of the Surface Coating, Humidity Degradation, and Recovery of Perovskite Film Phase for Solar-Cell Applications*. Nanomaterials. <https://doi.org/10.3390/nano12173027>

García Manrique, Juan Antonio; Marí, B.; A. Ribes-Greus; Monreal Mengual, Lluçia; Teruel Juanes, Roberto; Gascón Martínez, María Llanos; Marí-Guaita, Julia. (2019) *Study of the Degree of Cure through Thermal Analysis and Raman Spectroscopy in Composite-Forming Processes*. Materials, 23 (12), 3991 - 4003. 10.3390/ma12233991

### **Book chapters**

Feriel Bouhjar, Derbali Lofti, Júlia Marí Guaita; Anuj Mittal; Chapter: *Development of metal oxide heterostructures for hydrogen production in Metal Oxide-Based Heterostructures. Fabrication and Applications*. ISBN: 9780323852418 Elsevier (2022)

### **Conferences**

Marí-Guaita, Julia; Bouich, Amal; Marí, B. (2022). *Boosting the Performance of Cesium Lead Bromide Perovskites doped with Bismuth for Solar Cell Applications*. EN 10th European Conference on Renewable Energy Systems (ECRES 2022). Istanbul, Turkey. – Poster

Marí-Guaita, Julia; Bouich, Amal; Marí, B. (2021). *Comparative Study of Methylammonium Lead Iodide (MaPbI3) and Methylammonium Tin Iodide (MASnI3) Absorber Layers for Solar Cells*. EN E-MRS Fall Meeting 2021. Online. – Oral presentation

Bouich, Amal; Ullah, Shafi; Marí-Guaita, Julia; Marí, B. (2021). *Towards high crystallinity and stable MASnI3 perovskite films treated with different antisolvents*. EN Ninth European Conference on Renewable Energy Systems (ECRES 2021). Online. – Oral presentation



Bouich, Amal; Ullah, Shafi; Marí-Guaita, Julia; Stewart, Alexander Wyn; Marí, B.; Ebn Touhami, Mohamed (2021). *The investigation on the surface Coating and the Stability of CsPbI<sub>3</sub>, FAPbI<sub>3</sub> and MAPbI<sub>3</sub> perovskite thin films for solar cells*. EN E-MRS Fall Meeting 2021. Online. – Oral presentation.

Bouich, Amal; Marí-Guaita, Julia; Guaita-Pradas, Inmaculada; Marí, B. (2021). *Towards manufacture stable lead Perovskite APbI<sub>3</sub> (A= Cs, MA, FA) based solar cells with low-cost techniques*. En 1st International Conference on Energy, Power and Environment (ICEPE 2021). Gujrat, Pakistan. – Oral presentation

Bouich, Amal; Ullah, Shafi; Marí-Guaita, Julia; Stewart, Alexander Wyn; Marí, B.; Ebn Touhami, Mohamed (2021). *The investigation on the surface Coating and the Stability of CsPbI<sub>3</sub>, FAPbI<sub>3</sub> and MAPbI<sub>3</sub> perovskite thin films for solar cells*. EN E-MRS Fall Meeting 2021. Online.

Marí-Guaita, Julia; Bouich, Amal; Marí, B.; Ullah, Shafi; ISNI 0000 0004 4940 548x (2021). *Modulation of the Crystallization in MaPbI<sub>3</sub> Perovskite Films: Studying the impact of Different Antisolvents*. EN The 11th International Conference on Image Processing, Wavelet and Applications (IWW2021). Online. – Oral presentation.

Marí-Guaita, Julia; Bouich, Amal; Marí, B. (2021). *Shedding light on phase stability and surface engineering of formamidinium lead iodide thin films for solar cells*. EN 1st International Conference on Energy, Power and Environment (ICEPE 2021). Gujrat, Pakistan. – Oral presentation

Marí-Guaita, Julia; Gallego-Parra, Samuel; Sans-Tresserras, Juan Ángel; Manjón, Francisco-Javier; M. Velazquez; Ph. Veber ... Alfonso Muñoz (2020). *Experimental study of lattice dynamics in Yb<sup>3+</sup>:Gd<sub>2</sub>O<sub>3</sub> under high pressure*. EN 58th European High Pressure Research Group Meeting (EHPRG 2020). (150 - 151). Puerto de la Cruz, Spain. – Poster

Ullah, Shafi; Bouich, Amal; Marí-Guaita, Julia; Ullah, Hanif; Marí, B. (2021). *Bandgap alignment of buffer CdS toward ZnO Window layer for thin-film application*. The 11th International Conference on Image Processing, Wavelet and Applications (IWW2021). Online. – Oral presentation.